PHOTON ABSORPTION, COLOR DETECTION, AND CHROMATIC INDUCTION

BY

SHAHRAM PEYVANDI

A dissertation submitted to the

Graduate School–Newark

Rutgers, The State University of New Jersey

in partial fulfillment of the requirements

for the degree of

Doctor of Philosophy

Graduate Program in Psychology

written under the direction of

Alan L. Gilchrist

and approved by

_____

_____

_____

_____

_____

Newark, New Jersey

May, 2017

ABSTRACT OF THE DISSERTATION

Photon Absorption, Color Detection, and Chromatic Induction

by Shahram Peyvandi

Dissertation Director: Alan L. Gilchrist

Due to the quantum nature of light, when a population of identical photoreceptors in the retina, or identical pixels in a digital sensor, is exposed repeatedly to uniform light, there is both spatial and temporal variation in absorbed light. We have derived the histogram of the expected number of cells absorbing each specific level of energy, the variance of which quantifies the spatial variation in absorption by cells. Moreover, the actual histogram varies across identical trials of exposure. We quantified this temporal variation by the variance of the number of cells at a given energy level, showing that the temporal variation has a unimodal distribution, and is reciprocally related to the spatial variation.

The proposed model predicts that, due, not to higher-order visual mechanisms, but rather to low-level vision and the quantum nature of light, stimulating cone cells with uniform colored light produces a distribution of responses in cone excitation space (rather than a point) and these reproduce MacAdam's (1942)

classic measurements of the variability of color matches. We measured the temporal dynamics of human color detection when a target is briefly presented on an equiluminant neutral surround. Our results showed that momentary-produced signals of varying luminance in the adapting field are affected by an instantaneous neuronal mechanism rather than a slow cone adaptation, suggesting that the detection threshold is limited by fluctuations of a Poisson nature in the postreceptoral stage. Our model predicts that the signal to noise ratio in a response channel remains the same, regardless of luminance, so long as the state of equilibrium in this channel is constant.

A neutral disk appears slightly greenish when surrounded by a large red field, illustrating chromatic induction. When observers' heads were placed inside a special ganzfeld apparatus, they saw a 3 degree, physically neutral disk surrounded by a saturated red area that filled the remainder of the visual field and they adjusted the color of the disk to make it appear neutral. We found that chromatic induction increases non-linearly with surround saturation but falls-off with highly saturated surrounds, suggesting two antagonistic processes, an adaptation-related component and an additive process exerted by surround color.

Acknowledgements

I would like to acknowledge my advisor, Alan Gilchrist, who supported me during my PhD research at Rutgers University. I am also grateful to the members of my committee, Vebjørn Ekroll, Bart Krekelberg, Elizabeth Bonawitz, Mauricio Delgado, for their help at several stages of my research. I would like to thank Stephen Hanson for his valuable feedback on the work. I would also like to thank Ellen Halpern for her help in statistical analysis of the data. I would like to acknowledge all the research assistants in our lab, Christhian Altamirano, Katarina Jevtic, Raziye Akbulut, Sophia Bautista, and Dejan Jovcevski for their invaluable help in conducting visual experiments. In addition, I would like to express my gratitude to James Tornes and Manjunath Somayaji from ON Semiconductor for providing us with an imaging sensor, and Sunex, Inc. for providing the spectral transmittance of the lens. I would like to thank the all anonymous students at Rutgers University-Newark for their participation in my experiments. I also acknowledge support by National Science Foundation (NSF) (BCS-1230793). Finally, I am indebted to my wife, Elham, and my daughter, Parmys, for supporting me throughout my study.

Dedication

This dissertation is dedicated to my beloved wife, ELHAM, and my dearest daughter, PARMYS, who supported me in every single moment of this journey.

Table of Contents

List of Tables

List of Figures

Chapter 1
Introduction

The human eye is a complex sensory system receiving environmental information in the form of stimulating light reflected or emitted from objects. The pattern of light that reaches the eye and strikes the retina comes from the interaction of light and objects in our environment. It provides information about objects, including their surface color, a fundamental property of objects. The visual processing of color starts with the stimulation of photoreceptor cells in the retina by light energy. The signals from retinal stimulation are then passed on to the cortical stage further processes. Figure 1.1 illustrates the image formation on the retina when a reflecting object is illuminated by a light source.

1.1 Research Scope

Understanding the processes of color in the human visual system requires the study of multiple hierarchical stages through which the information contained in the light from the environmental is processed by the visual system. Visual processing begins in the retina with two main levels of processing. These are a primary receptoral level and a secondary postreceptoral stage. In order to allow a better assessment of subsequent perceptual computation, the goal is to clarify what aspects of color vision can be attributed to such early low-vision processing.

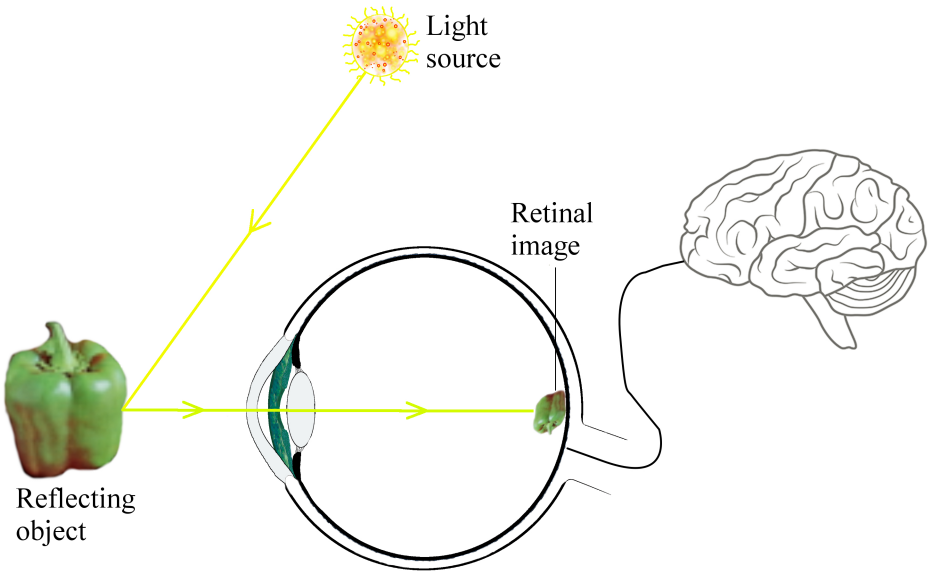

Figure 1.1: The electromagnetic radiation stimulates retinal photoreceptors and initiates responses in the cells. The retinal signals are transformed to the cortical stage.

1.1.1 Photon Absorption by Photoreceptor Cells

Neuronal signals from stimulated retinal cells are the very early information utilized by the human visual system for color detection and discrimination. In Chapter 3, we aim to characterize the spatiotemporal variation of absorbed energy by a population of photoreceptor cells. We used the properties of this characterization in Chapter 4 to better understand the mechanisms behind color detection.

1.1.2 Color Detection

In Chapter 4, we aim to understand the retinal factors that limit the performance of color detection behavior. More specifically, the goal is to find out whether color detection is a noise-limited behavior or not. If so, we aim to determine the source of noise in the retina, its response to light, and its impact on color detection behavior.

1.1.3 Chromatic Induction

In Chapter 5, we analyze behaviorally chromatic induction in a simple center-surround stimulus. We aim to determine the role of temporal adaptation on chromatic induction. The temporal adaptation is an early-retinal-stage mechanism. To understand processes beyond the receptoral level, we also investigate a non-linear effect of an inducing surround on an infield target.

Chapter 2
Fundamental of Color Theories

In this chapter, we first review the fundamental principles of radiant energy and definitions of radiometric and photometric quantities that are central to physical specifications of the stimulating radiation. Then, we describe the anatomical structure of the human eye, microscopic elements of the retina, and photoreceptor cells. Finally, we explain the principles of retinal stimulation, light absorption in a photoreceptor cell and quantitative representation of color.

2.1 Electromagnetic Radiation

The electromagnetic radiation is a radiant energy propagating through space in the form of light waves. Monochromatic radiation is radiant energy of a single frequency. Due to the quantum nature of light, emission and absorption of light energy occur in discrete quantal units called photons (Planck, 1900; Einstein, 1907). The energy of constituent photon, E, with frequency ν is specified by the Planck-Einstein relation,

$$\mathrm{E} = h\nu = h\frac{c}{\lambda}, \qquad [\mathrm{J}] \quad (2.1)$$

in which $h = 6.626\,075\,5 \times 10^{-34}\,\mathrm{J\,s}$ is the Planck constant, $c \simeq 3 \times 10^{-8}\,\mathrm{m\,s^{-2}}$ is the speed of light, and λ is wavelength of the radiation. The electromagnetic radiation spectrum encompasses a broad range of possible frequencies and the human eye is sensitive to a tiny portion of this range, namely from 360 to 780 nm.

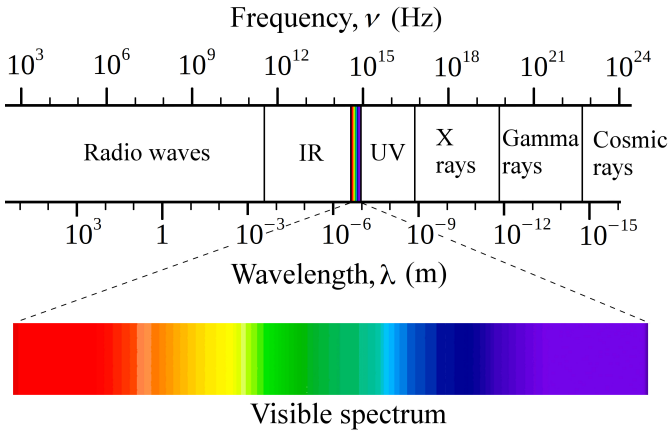

Figure 2.1: The electromagnetic radiation spectrum is a broad range of frequencies. The human eye is mainly sensitive to a very small region of wavelength.

Figure 2.1 shows the electromagnetic radiation in terms of frequency and wavelength, and the range of frequencies to which the human eye is sensitive (the visible spectrum). Although, in a common setting, the visible spectrum mainly refers to a wavelength range of easily visible lights, sufficiently intense radiations beyond the nominal range of 0.36 to 0.78 µm are also visible to the human eyes (Nutting, 1912; Goodeve, 1936; Griffin, Hubbard, & Wald, 1947; Lau & Leo, 1948; Brindley, 1955).

2.2 Radiometry

The fundamental concepts of radiometric quantities explained here are mainly taken from the book by McCluney (1994). Radiation of light is the propagation of light energy, emitted or reflected from a surface, through the space. The radiant energy, P, is the quantity of electromagnetic energy measured in joule, emanating from or propagating onto a surface. The radiant flux in watt (W) is the quantity of energy flowing from or through a surface region per unit time and is defined

by the rate of radiant energy,

$$\Phi = \frac{\mathrm{d}P}{\mathrm{d}t}. \qquad [\mathrm{J\,s^{-1}}] \quad (2.2)$$

Irradiance,

$$E = \frac{\mathrm{d}\Phi}{\mathrm{d}S}, \qquad [\mathrm{W\,m^{-2}}] \quad (2.3)$$

is the density of radiant flux incident on a point of a surface. Throughout the thesis, the term irradiance is also used for radiant exitance, referring to the area density of radiant flux leaving a point on a surface, with no violation of mathematical relation. Radiance, I, is the radiant flux per unit solid angle emanating from or flowing through a surface element in a given direction, per unit area of the surface element, $\mathrm{d}S$, perpendicular to the direction, defined by,

$$I = \frac{\mathrm{d}^2\Phi}{\mathrm{d}\omega\,\mathrm{d}S} = \frac{\mathrm{d}^2\Phi}{\mathrm{d}\omega\,\mathrm{d}S_0\cos\theta}, \qquad [\mathrm{W\,sr^{-1}\,m^{-2}}] \quad (2.4)$$

where, $\mathrm{d}\omega$ is the element of solid angle in steradian (sr) (Nicodemus & Kostkowski, 1976). Components of Eq. (2.4) are shown in Figure 2.2.

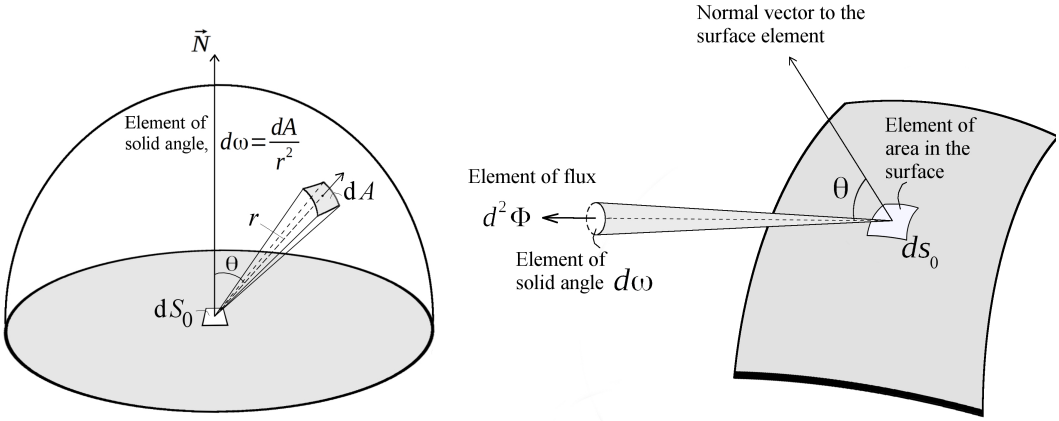

Figure 2.2: (a) The element of solid angle, $\mathrm{d}\omega$, subtended by the surface element, $\mathrm{d}A$. (b) Illustration of the radiant flux emitted from a surface element, $\mathrm{d}S_0$, confined to the element of solid angle, $\mathrm{d}\omega$, oriented at the angle of θ to the normal vector of the surface element.

The radiometric quantities in Eqs (2.2)-(2.4) are functions of wavelength of the

electromagnetic radiation. Incorporating wavelength into a radiometric quantity gives the spectral density function of the quantity. For x being a radiometric quantity, the spectral density of x is,

$$x_\lambda = \frac{\mathrm{d}x}{\mathrm{d}\lambda}. \tag{2.5}$$

Based on Eq. (2.5), therefore, we can define the spectral radiant flux, Φ_λ in $\mathrm{W\,nm^{-1}}$, the spectral irradiance, E_λ in $\mathrm{W\,m^{-2}\,nm^{-1}}$, and the spectral radiance, Φ_λ in $\mathrm{W\,sr^{-1}\,m^{-2}\,nm^{-1}}$ (Nicodemus & Kostkowski, 1976).

Example 2.1. The Planck function for a blackbody radiation (Pais, 1979),

$$B_\lambda(T) = \frac{2hc^2}{\lambda^5}\frac{1}{\exp(\frac{hc}{\lambda K_B T}) - 1},\ [\mathrm{W\,sr^{-1}\,m^{-2}\,m^{-1}}] \tag{2.6}$$

relates the intensity of a monochromatic radiation to the temperature of the blackbody and emission wavelength, λ. In Eq. (2.6), $B_\lambda(T)$ is the spectral radiance, Planck constant $h = 6.626\,075\,5 \times 10^{-34}\,\mathrm{J\,s}$, the speed of light $c \simeq 3 \times 10^{-8}\,\mathrm{m\,s^{-2}}$, Boltzmann constant $K_B = 1.380\,648\,52 \times 10^{-23}\,\mathrm{J\,K^{-1}}$, λ (m) is wavelength, and T is temperature in Kelvin (K). Figure 2.3 shows the radiance spectrum of a blackbody at 6500 K within the wavelength range of 0.3 to 0.8 µm.

2.3 Photometry

Photometric quantities are physiologically-relevant values determined by incorporating factors of brightness perception of the standard human observer into the respective radiometric quantities. The human perception of brightness in photometry is defined by the relative sensitivity of the average human observers to lights of different wavelengths. At low light where rod cells are mainly operative, the standard observer's spectral sensitivity for the brightness perception is defined by the scotopic luminous efficiency function (Wald, 1945; Crawford,

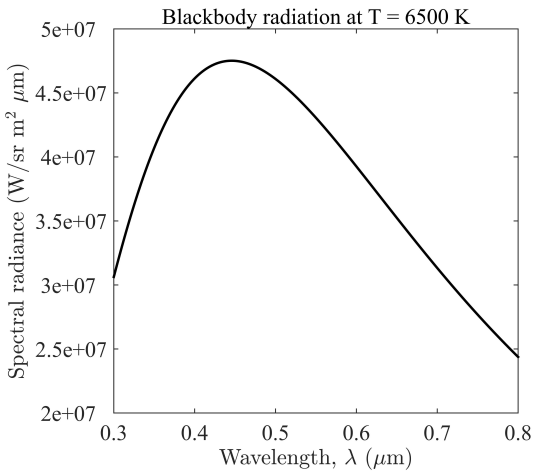

Figure 2.3: The spectral radiance function of a blackbody at 6500 K in the wavelength range of 0.3 to 0.8 µm.

1949). At higher intensities where cones are normally operative, the sensitivity is given by the photopic luminous efficiency function (Judd, 1951; Vos, 1978). An improved version of the photopic luminous efficiency function was also suggested by Sharpe, Stockman, Jagla, and Jägle (2005). The CIE photopic luminous efficiency function, $V(\lambda)$, modified by Judd and Vos as well as the CIE scotopic luminous efficiency function, $V(\lambda)$, are shown in Figure 2.4.

In principle, a photometric quantity can be converted from the corresponding radiometric quantity presented in Eqs (2.2)-(2.4). The illuminance is defined by,

$$E_V = K_m \int_{360}^{780} E_\lambda V_\lambda \, \mathrm{d}\lambda \qquad [\mathrm{lm\,m^{-2}}] \quad (2.7)$$

in which, $K_m = 683.002\,\mathrm{lm\,W^{-1}}$ is a constant determining the maximum photopic luminous efficacy of a monochromatic light at 550 nm. The luminance of a Lambertian surface can be derived by,

$$L_V = \frac{E_V}{\pi}. \qquad [\mathrm{cd\,m^{-2}}] \quad (2.8)$$

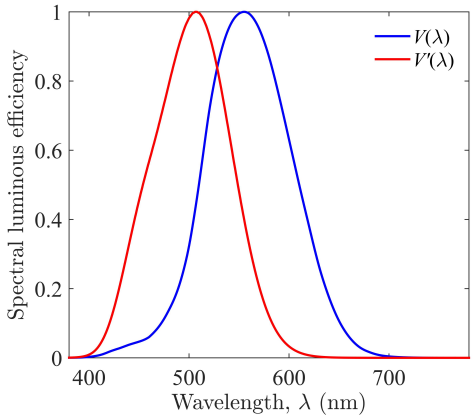

Figure 2.4: The CIE spectral luminous efficiency functions, $V(\lambda)$ and $V'(\lambda)$ (Wyszecki & Stiles, 1982).

2.4 Interactions of Light and Objects

The electromagnetic radiant energy interacts with objects through absorption and scattering processes. When an object is exposed to a radiation, the radiant energy of the impinging light is either transmitted through, absorbed within, or reflected by the object. In a general term, the spectral reflectance, transmittance, and absorbance of an object is defined by,

$$\frac{\Phi_\lambda}{\Phi_{\lambda,i}}, \tag{2.9}$$

that is the fraction of the incident radiation, $\Phi_{\lambda,i}$, up on the object that is reflected back, transmitted through or absorbed within the object.

According to the Beer-Lambert-Bouguer law (Swinehart, 1962), the linear attenuation of the intensity of a monochromatic radiation after passing through a material containing absorbing molecules with the number concentration, C_n, is expressed by,

$$-\frac{\mathrm{d}I}{I_x} = \sigma_\lambda \, C_n \, \mathrm{d}x \,, \tag{2.10}$$

where, σ_λ is the collecting area of absorbers for capturing a photon of wavelength λ, and $\mathrm{d}I$ is the differential flux of wavelength λ absorbed within the thickness

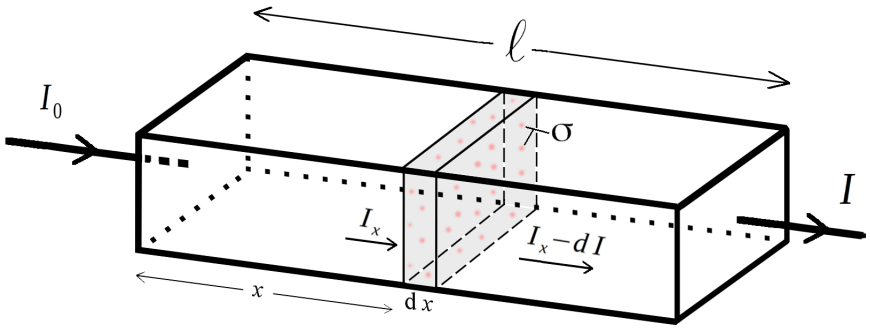

Figure 2.5: The intensity of the flux, I_0, is attenuated by passing through a material of length, ℓ. The differential flux, $\mathrm{d}I$, absorbed within the thickness element, $\mathrm{d}x$, is linearly related to the concentration of absorbing molecules with the cross section σ for collecting a photon of a particular wavelength.

element, $\mathrm{d}x$. The components of Eq. (2.10) are illustrated in Figure (2.5). Solving Eq.(2.10),

$$\int_{I_0}^{I} \frac{\mathrm{d}I}{I_x} = -\int_0^{\ell} \sigma_\lambda \, C_n \, \mathrm{d}x \,, \tag{2.11}$$

for the path length, ℓ, along which the flux is traveling through the material, we find the ratio of the transmitted flux density, I, to the incident flux density, I_0,

$$\tau_\lambda = \frac{I}{I_0} = 10^{-\ell D_\lambda} \tag{2.12}$$

in which,

$$D_\lambda = \frac{\mathrm{N_A}\,\sigma_\lambda}{2303} C_m, \qquad [\mathrm{m}^{-1}] \tag{2.13}$$

is the spectral absorptivity (specific absorbance coefficient), defined as the absorbance per unit path length, ℓD_λ is the spectral absorbance, and τ_λ is the spectral transmittance (Mielenz, 1976). In Eq. (2.13), $\mathrm{N_A} = 6.022\,141\,29 \times 10^{23}\,\mathrm{mol}^{-1}$ is Avogadro's number, and C_m ($\mathrm{mol\,l}^{-1}$) is the molar concentration of absorbers.

2.5 The Eye

Color perception is mediated by interpretation of the signals received to the brain when photoreceptor cells in the retina are stimulated by the electromagnetic radiation reflected or emitted from an object. The human eye is an approximately spherical organ with a diameter of about 24 mm and the retina is an inner layer within the eye with millions of light-sensitive cells of two types, the rods and cones (Polyak, 1941; Wyszecki & Stiles, 1982). The schematic diagram and anatomical parts of the human eye as well as the microscopic structure of the retina are illustrated in Figure 2.6. In the following sections, we review the fundamental components of the human eye and retina that are required for understanding retinal stimulation.

2.5.1 Pupil

The pupil of human eyes is a round-shaped opening (Land, 2006) in the middle of the iris which responds to several stimulations, including the light intensity, by contraction and dilation (Loewenfeld, 1999). The pupil diameter changes from about 2 to 8 mm with changing the level of the field luminance (Wyszecki & Stiles, 1982, p. 105-107). There have been numerous efforts to relate the pupil diameter with the stimulus luminance (Moon & Spencer, 1944; de Groot & Gebhard, 1952; Le Grand, 1968; Trezona, 1983; Pokorny & Smith, 1997). Watson and Yellott (2012) also proposed a unified equation for calculating the average pupil size from the stimulus intensity. According to Pokorny and Smith (1997), the average of pupil size can be estimated from the luminance, L_V ($\mathrm{cd\,m^{-2}}$), of a stimulus by,

$$d_p = 5 - 3\tanh(0.4\log L_V), \qquad [\mathrm{mm}] \quad (2.14)$$

in which d_p is the pupil diameter.

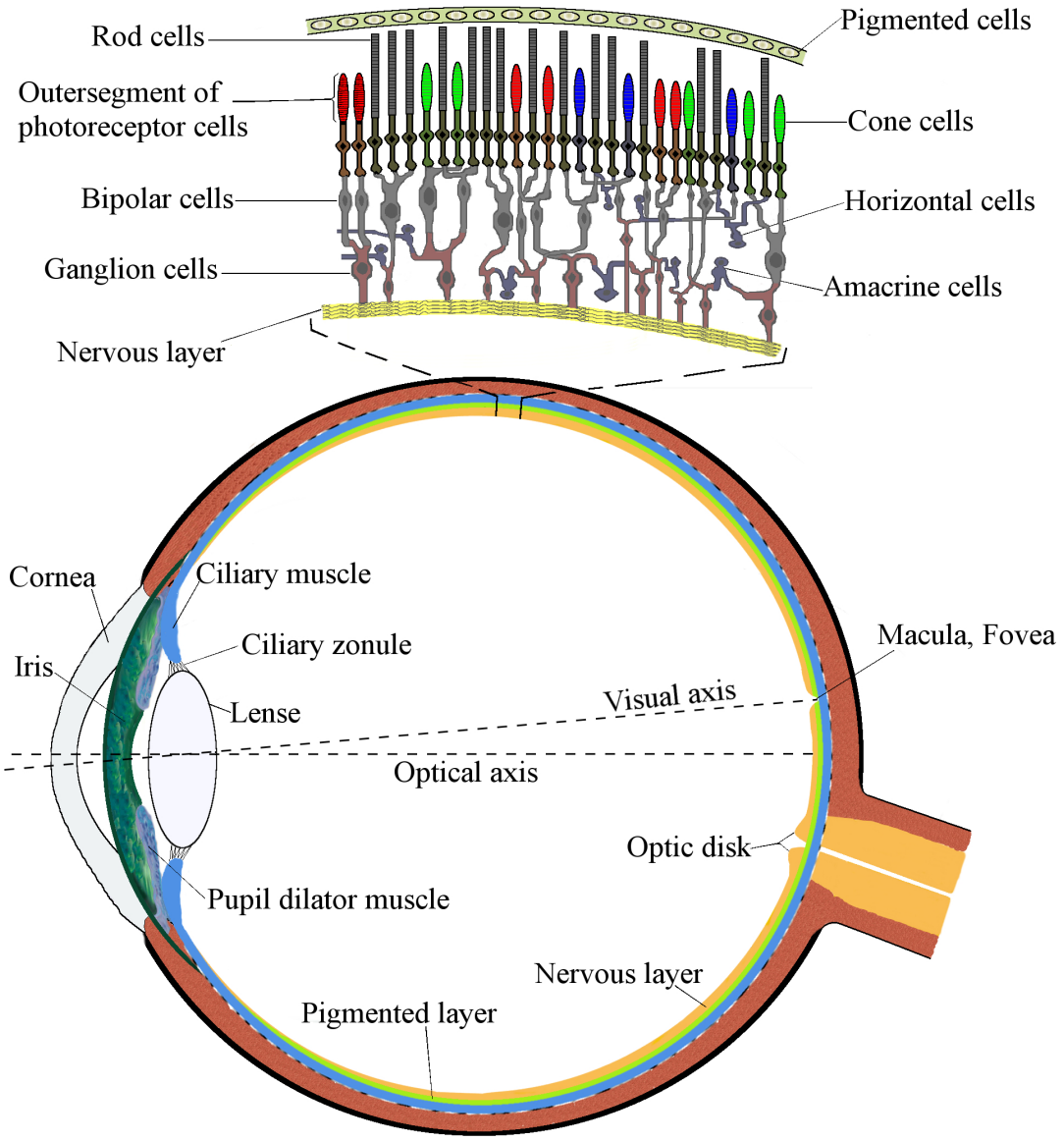

Figure 2.6: The schematic anatomical structure of the human eye is presented together with the microscopic elements of the retina. The rod and cone cells in the retina are stimulated by the light from an object after passing through the cornea, lens, optic media, and the macula, which all modify the spectral stimulus radiation before reaching the retina. The electrical responses in retinal photoreceptors are triggered by absorption of photons in the outersegment of a cell. The photoreceptor signals, with different convergence rate, are connected to a network of bipolar and horizontal cells. The signals from bipolar and horizontal cells are then transformed to the ganglion cells directly or indirectly by amacrine cells. The signals processed within the network of the ganglion cells are projected into the primary visual cortex (Polyak, 1941; Kaiser & Boynton, 1996; Shevell, 2003).

2.5.2 Pre-retinal Filtering

The spectral radiation of an external stimulus is modified by scattering and absorption in different components of the eye as it passes through the cornea, lens, optic media, and the macula before reaching the retina. This process is called pre-retinal filtering (van de Kraats, Berendschot, & van Norren, 1996).

Lens

The lens of an eye is a lenticular-shaped and nearly transparent tissue located behind the pupil. The elastic structure of the lens allows for its shape to be adjusted by zonule fibers during accommodation. The lens efficiently absorbs short-wavelength radiation. According to G. F. Cooper and Robson (1969), the lens, in human and primates, represents a maximum absorption between 365-368 nm and no sign of absorption in the wavelength range of 450-650 nm. Because the lens is a biconvex structure, according to the law of absorption discussed in section 2.4, the transmittance of a lens depends on the effective path length. Thus, the spectral absorbance of the lens becomes a function of the pupil size, so that the transmittance of the lens decreases for smaller sizes of pupil (Weale, 1961; van de Kraats et al., 1996). A multiplicative factor of 1.16 is suggested in the literature (van Norren & Vos, 1974) to convert the spectral absorbance of the lens under completely open pupil to that of under a small pupil size (van Norren & Vos, 1974). For an average observer, Stockman and Sharpe (2000b) suggested an absorbance value of 1.765, at 400 nm, for a small 2° field of view. Figure 2.7(a) shows the two measurements of lens absorbance (OD) in the human eye (Wyszecki & Stiles, 1982; Stockman et al., 1993) under an open pupil condition [data from `http://www.cvrl.org`].

Macular Pigment

The macular pigment is a yellow area densely concentrated near the fovea. The density of this pigmented region gradually fades out from the center, fovea, towards the peripheral retina. Thus, light absorption in macular pigment contributes mainly to pre-retinal filtering of the foveal vision. The macular pigment highly absorb light of shorter wavelengths, with a maximum absorption at 460 nm (van Norren & Berendschot, 2004). Figure 2.7(b) shows the three measurements of the macular pigment absorbance (OD) in the human eye [data obtained from `http://www.cvrl.org`] (Vos, 1972; Stockman et al., 1999; Wyszecki & Stiles, 1982). As shown in this figure, there is a good deal of variation in the absorbance of macular pigment as reported in the literature [see (van Norren & Berendschot, 2004, p. 153), and also (Pease, Adams, & Nuccio, 1987; Bone, Landrum, & Cains, 1992)]. Wyszecki and Stiles (1982) suggested a value of 0.50 for the mean absorbance of the macular pigment at 460 nm. In other studies (Vos, 1972; Stockman & Sharpe, 2000b), however, a lower mean value of 0.35 was proposed for the peak of macular pigment absorbance at 460 nm. Although, there is a variation across observers, Sharpe, Stockman, Knau, and Jägle (1998) suggested that the measurement of the macular pigment absorbance is partly influenced by local variation in the absorbance of cone pigments.

2.5.3 Image Formation

The light entering the cornea of the eye from an environmental object forms an image on the retina. As discussed in section 2.5.2, the light energy is attenuated as it passes through the components of the eye. In this section, we derive an equation to relate the radiance of an environmental object to the irradiance at the image plane on the retina. Figure 2.8 shows the optical geometry of image formation

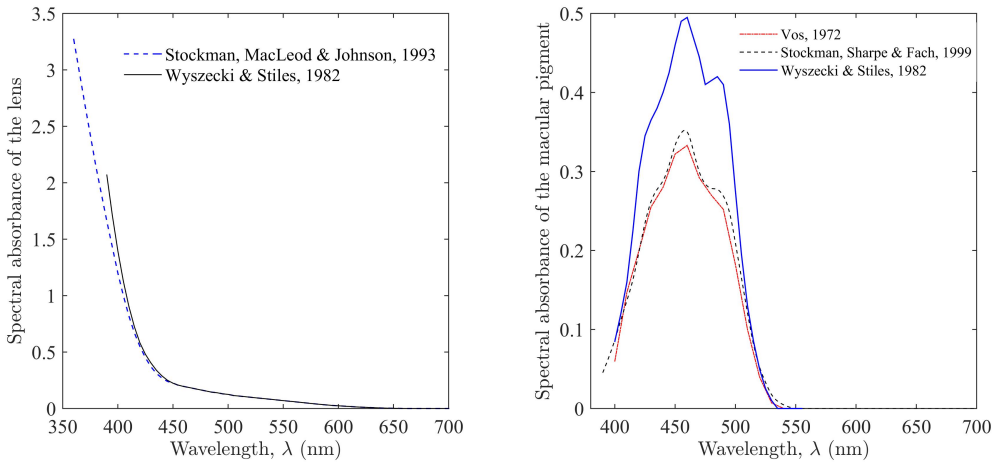

(a) (b)

Figure 2.7: Pre-receptoral filters. (a) The spectral absorbance of the lens in the human eye with completly open pupil. The solid curve is a measurement by Wyszecki and Stiles (1982) and the dashed curve is suggested by Stockman et al. (1993). (b) The spectral absorbance of the macular pigment in the human eye (Vos, 1972; Wyszecki & Stiles, 1982; Stockman et al., 1999).

on the retina. When an external surface stimulus, with spectral radiance I_ν, is viewed by an eye of focal length f and pupil area A_p, the element of radiant flux flowing through the pupil opening is,

$$\mathrm{d}\Phi = I_\nu \, \mathrm{d}\nu \, \mathrm{d}\omega \, \mathrm{d}s_0 \qquad [\mathrm{W}] \quad (2.15)$$

Considering that the pupil size of the eye, A_p, is small, we write,

$$\mathrm{d}\omega \approx \frac{A_p}{D^2} \qquad [\mathrm{sr}] \quad (2.16)$$

From Eqs. (2.15) and (2.16), we have,

$$\mathrm{d}\Phi \approx I_\nu \, \mathrm{d}\nu \, \frac{A_p}{D^2} \, \mathrm{d}s_0 \qquad [\mathrm{W}] \quad (2.17)$$

From the geometry shown in Figure 2.8,

$$\frac{\mathrm{d}s_0}{D^2} = \frac{\mathrm{d}s_r}{f^2}. \quad (2.18)$$

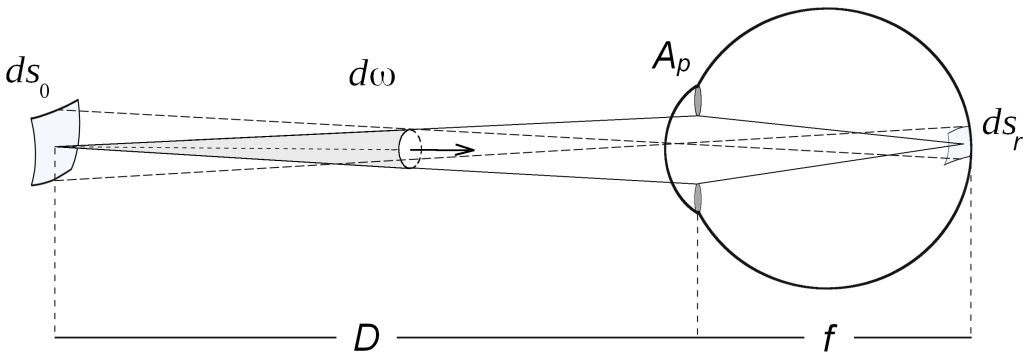

Figure 2.8: The figure shows the optical geometry of the eye, when an external source with the area of $\mathrm{d}S_0$ is viewed by an eye, with the pupil area of A_p and the focal length of f, at the distance of D from the eye. The image on the retina has the surface area of $\mathrm{d}S_r$. In this figure, $\mathrm{d}\omega$ is the solid angle subtended at a point on the external source by the pupil of the eye.

Using Eq. 2.18, we can re-write Eq. (2.17) as,

$$\mathrm{d}\Phi \approx I_\nu \, \mathrm{d}\nu \, \frac{A_p}{f^2} \, \mathrm{d}s_r \qquad [\mathrm{W}] \quad (2.19)$$

By definition presented in Eq. (2.3), we derive,

$$E_\nu = \frac{\mathrm{d}\Phi}{\mathrm{d}s_r \, \mathrm{d}\nu} \approx I_\nu \frac{A_p}{f^2} \qquad [\mathrm{W\,m^{-2}\,Hz^{-1}}] \quad (2.20)$$

from Eq. (2.19), as the spectral irradiance at the image plane in the eye (Wyszecki & Stiles, 1982; Warrant & Nilsson, 1998). Detailed calculations of retinal irradiance from a point source are given by Delori, Webb, and Sliney (2007). Campbell (1994) also suggested a method for retinal irradiance from an extended source. To account for the attenuation of light energy by pre-retinal filters, we incorporate in Eq. (2.20) the pre-retinal transmittance of the lens and macula, τ_ν. We write,

$$E_\nu \, \mathrm{d}\nu \approx \tau_\nu \, I_\nu \, \mathrm{d}\nu \, \frac{A_p}{f^2}. \qquad [\mathrm{W\,m^{-2}}] \quad (2.21)$$

2.5.4 Photoreceptors

In the human retina, there are 150,000-180,000 cone cells per mm^2 in the foveal center of the retina (Jonas, Schneider, & Naumann, 1992). As illustrated in

Figure 2.9(a), the retina of a normal observer has three classes of cone photoreceptor cells. These are L-, M-, and S-cones, referring to long, medium and short-wavelength-sensitive cone cells, respectively. The electrical activity in a receptor cell is initiated when photons are absorbed by photosensitive molecules densely packed within the outersegment disk membranes of the cell (Baylor, 1987). The large number of photopigment molecules within the outer segment of a receptor enables a single cell to absorb photons of different wavelengths (Bowmaker, 1981; Dartnall, Bowmaker, & Mollon, 1983).

The self-screening hypothesis (Alpern, Fulton, & Baker, 1987), relates the physiological activity of a cell to the amount of absorbed light energy by the cell. The amount of light energy in a cell depends on to the specific absorbance of photopigment molecules of the cell and the length of its outersegment (Stockman et al., 1993). As discussed in section 2.4 and shown by Eq. (2.12), with the assumption of axial penetration of photons through a column of pigment in a cell, the fraction of light with frequency, ν, absorbed in a photoreceptor with the outer segment length ℓ and specific absorbance D_ν, is given by,

$$J_\nu = 1 - 10^{-\ell D_\nu}. \tag{2.22}$$

where, ℓD_ν is the spectral absorbance of a cell (Knowles & Dartnall, 1977; Burns & Elsner, 1985; Stockman, Sharpe, Merbs, & Nathans, 2000).

The spectral absorption, J_ν, of a photoreceptor in Eq. (2.22), is a function of the outersegment length, ℓ, and the specific absorbance, D_ν. The specific absorbance coefficient of a cell, D_ν, of human cone and rod cells has been investigated and measured in several reports (Rushton, 1972; Bowmaker & Dartnall, 1980; Bowmaker, 1981; Schnapf, Kraft, & Baylor, 1987). Dartnall et al. (1983) reported the wavelength of maximum absorption for S-cones at 419.0 nm, for M-cones at 530.8 nm, and for L-cones at 558.0 nm. The absorption spectrum, J_ν,

is subject to a substantial variation due to a good deal of change in the values reported for the peak of absorption, the specific absorbance coefficient, and the outersegment length of cones (Stockman et al., 1993). A measured range of $\sim$ 28-36 µm was reported for the length of a cone outer segment in human and monkey (R. W. Young, 1971; Hoang et al., 2002). At the peak of absorption, Bowmaker, Dartnall, Lythgoe, and Mollon (1978) proposed the specific absorbance of $\sim 0.015\,\mu m^{-1}$ for the M cones, and $\sim 0.013\,\mu m^{-1}$ for the L cones in rhesus monkey. With a length of 35 µm for the outersegment, Bowmaker (1981) summarized the peak of observed end-on absorption for the three types of cone cells from 0.002-0.28. The normalized absorbance spectra of human cones and rod photoreceptors measured by Bowmaker and Dartnall (1980) are presented in Figure 2.9(b). Pridmore (2013) discussed significant impacts of variation in cone specific absorbance, lens and macular pigment transmittance on the variability of unique hue perception.

Cone Fundamentals

Cone fundamentals is a common term in color vision for the human cone spectral sensitivity functions measured, across the visible wavelengths, relative to the light entering the eye (Stockman, 2016). This term is suggested based on the König hypothesis (1894) of independent fundamental receptoral mechanisms that underlie human color vision. The three cone fundamentals are the axial spectral absorbance functions of the three classes of cone cells, corrected for pre-retinal filtering of short-wavelengths by the macular pigment at the fovea and the lens pigment. Thus, the cone fundamental of a receptoral mechanism is:

$$\tau_\nu\, J_\nu = \tau_\nu\,(1 - 10^{-\ell\, D_\nu}), \tag{2.23}$$

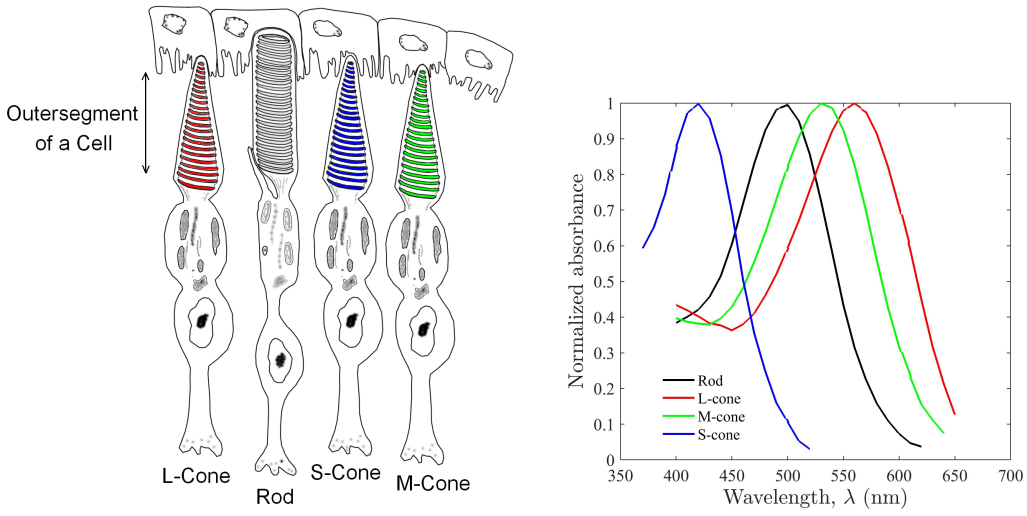

(a) (b)

Figure 2.9: Retinal receptors. (a) Schematic illustration of photoreceptor cells of two types, rods and cones, in the retina. L-, M-, and S-cone cells are sensitive to long, medium and short-wavelength region of the visible spectrum, respectively. (b) The micro-spectrophotometric measurement of absorbance spectra of three types of cone cells and rod cell extracted from the retina of the human eye by Bowmaker and Dartnall (1980).

in which τ_ν is the spectral transmittance of the lens and macular pigment. $\tau_\nu J_\nu$ in Eq. (2.23) can be calculated by a photoreceptor template of J_ν (Mansfield, 1985; Lamb, 1995; Govardovskii, Fyhrquist, Kuzmin, & Donner, 2000), combined with the transmittance spectra of the lens and macular pigment. Figure 2.10 shows classic proposals for spectra of the fundamentals of the three cone mechanisms (Smith & Pokorny, 1975; Vos & Walraven, 1971). In 2000, Stockman and Sharpe proposed the cone fundamentals for a small, 2°, and a wide, 10°, field of view for an average of normal human observer.

2.6 Trichromacy

The *trichromacy* theory of color vision (T. Young, 1802) states that color vision of a normal observer is *trichromatic*, which depends on responses from the three

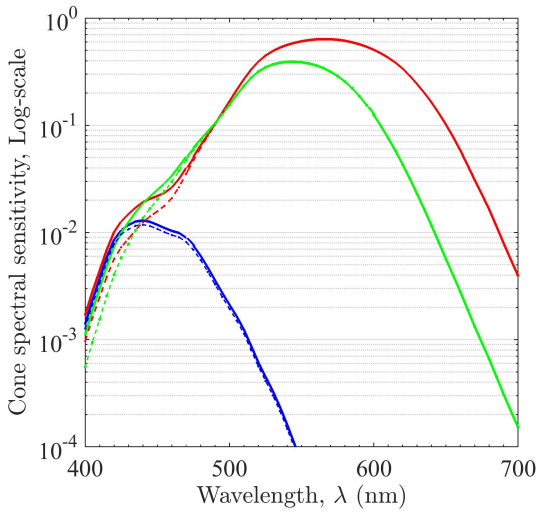

Figure 2.10: The spectral sensitivity of the L-, M-, and S-cone cells of the human retina, in logarithmic scale. The solid curves are the cone fundamentals proposed by Smith and Pokorny (1975), and the dashed curves suggested by Vos and Walraven (1971).

different receptoral mechanisms. A cone photoreceptor, independent from the other mechanisms, responds univarianly to absorbed photons. According to the principle of univariance (Rushton, 1972), a photoreceptor cell can be equally excited by different combinations of photons of different frequencies. An additive combination of three primary lights can produce a match for a monochromatic test light of varying frequency (for some specific wavelengths, however, one of the primary lights should be added to the test light). Based on the methodology of color matching in a optical setup invented by Maxwell (1860), Wright (1928-1929) and Guild (1932) performed experiments to match a monochromatic test light, in one side of a bipartite field, by a mixture of red, green and blue primaries, in the other side of the field. As shown in Figure 2.11(a), this matching experiment resulted in a set of three values for the relative amount of primaries required to match a monochromatic test light at each wavelength. The spectral color matching functions, obtained from the mixture of actual primaries of **RGB** of

645, 526, and 444 nm, can be linearly transformed into any of the virtual primary colors, such as the **XYZ** imaginary primaries suggested by the CIE (2004). This transformation resulted in several sets of color matching functions (CMFs) for an average normal observers under both a small field of view of 2° and a large field of 10°. Figure 2.11(b) shows the Judd-Vos modified 1931 CMFs for a small field of 2° (Vos, 1978).

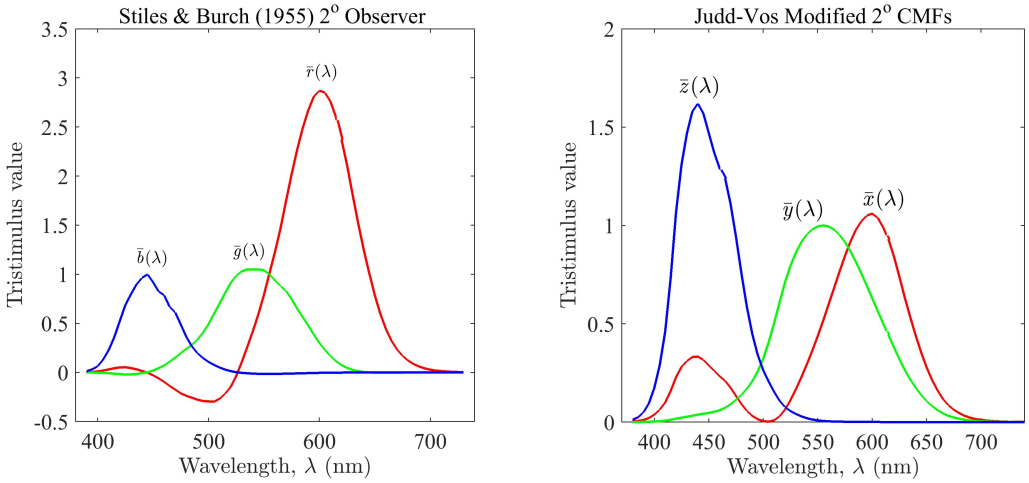

(a) (b)

Figure 2.11: Color matching functions. (a) The relative amount of primary colors required for matching a monochromatic test light of variable wavelength. A primary with negative value is mixed with the test monochromatic light to complete the match in the two sides of a bipartite field.(b) The Judd-Vos modified CIE 1931 color matching functions (CMFs).

2.6.1 Color Space

A color stimulus, with the spectral energy E_λ, can be represented by a vector within the three dimensional CIE color space by the XYZ tristimulus values, calculated as follows (Brainard & Stockman, 2010),

$$X = \int_{360}^{780} E_\lambda \, \bar{x}(\lambda) \, \mathrm{d}\lambda \, , Y = \int_{360}^{780} E_\lambda \, \bar{y}(\lambda) \, \mathrm{d}\lambda \, , Z = \int_{360}^{780} E_\lambda \, \bar{z}(\lambda) \, \mathrm{d}\lambda \, , \qquad (2.24)$$

from which the chromaticity coordinate, (x, y), is obtained by,

$$x = \frac{X}{X+Y+Z}, y = \frac{Y}{X+Y+Z}. \tag{2.25}$$

Figure 2.12(a) shows the CIE 1931 2° chromaticity xy-coordinate space.

Likewise, the L-, M-, and S-cone excitation coordinates for the spectral stimulation, E_λ, is obtained by:

$$\mathrm{L} = \int_{360}^{780} E_\lambda \, \bar{l}(\lambda) \, \mathrm{d}\lambda \, , \mathrm{M} = \int_{360}^{780} E_\lambda \, \bar{m}(\lambda) \, \mathrm{d}\lambda \, , \mathrm{S} = \int_{360}^{780} E_\lambda \, \bar{s}(\lambda) \, \mathrm{d}\lambda \, , \tag{2.26}$$

in which, $\bar{l}(\lambda)$, $\bar{m}(\lambda)$, and $\bar{s}(\lambda)$ are the cone spectral sensitivities. MacLeod and Boynton (1979) proposed a chromaticity diagram to represent a color stimulus within the cone excitation space. The MacLeod-Boynton (1979) chromaticity

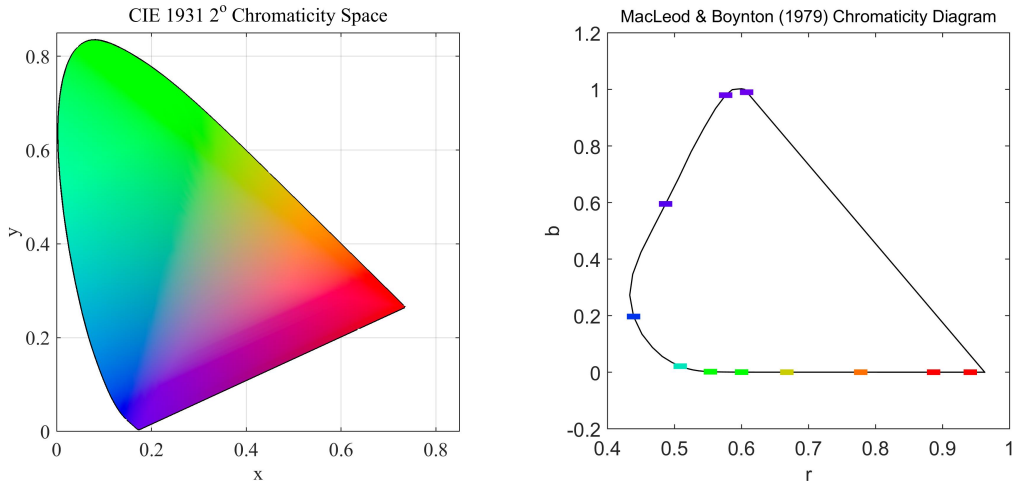

(a) (b)

Figure 2.12: Color space derived from the human sensitivity functions. (a) The CIE 1931 2° chromaticity space. (b) The MacLeod-Boynton (1979) chromaticity diagram.

coordinates, (r, b), are defined as,

$$(\mathrm{r}, \mathrm{b}) = \left(\frac{\mathrm{L}}{\mathrm{L}+\mathrm{M}}, \frac{\mathrm{S}}{\mathrm{L}+\mathrm{M}}\right). \tag{2.27}$$

in which, L+M is the MacLeod-Boynton luminance value of the stimulus. Figure 2.12(b) represent the MacLeod-Boynton diagram of the locus for spectral colors, obtained by the cone fundamentals proposed by Smith and Pokorny (1975). In this plot, the $\bar{s}(\lambda)$ function is scaled so that $\bar{s}(400) \,/\, [\bar{l}(400) + \bar{m}(400)] = 1$.

The principle of univariance (Rushton, 1972; Baylor, Nunn, & Schnapf, 1987) suggests that a photoreceptor response is the result of photon absorption, regardless of the wavelength of photons absorbed. In a color matching experiment, the mixture of the three independent red, green and blue primaries provides a match for a given test monochromatic light because both produce the same set of receptoral responses in the three fundamental cone mechanisms. Therefore, the match for a test light is determined at the level of cone mechanism (Stockman & Sharpe, 2000b; Stockman et al., 2000; Brainard & Stockman, 2010; Stockman, 2016). Accordingly, there must be a linear function of transform between the cone fundamentals and the CMFs. Assuming that the cone fundamentals are linearly related to the color-matching functions, the linear transform,

$$\begin{pmatrix} X \\ Y \\ Z \end{pmatrix} = \begin{pmatrix} 0.15514 & 0.54312 & -0.03286 \\ -0.15514 & 0.45684 & 0.03286 \\ 0 & 0 & 0.00801 \end{pmatrix}^{-1} \begin{pmatrix} \mathrm{L} \\ \mathrm{M} \\ \mathrm{S} \end{pmatrix}, \tag{2.28}$$

is applied to obtain the Judd-Vos modified CIE 1931 XYZ values (Vos, 1978) from the LMS cone excitation obtained by Eq. (2.26) with Smith and Pokorny (1975) cone fundamentals (Wyszecki & Stiles, 1982, p. 615).

2.7 Color Opponency

The results of matching a monochromatic light by a combination of three primary lights can be predicted by the trichromatic theory of color vision. This theory,

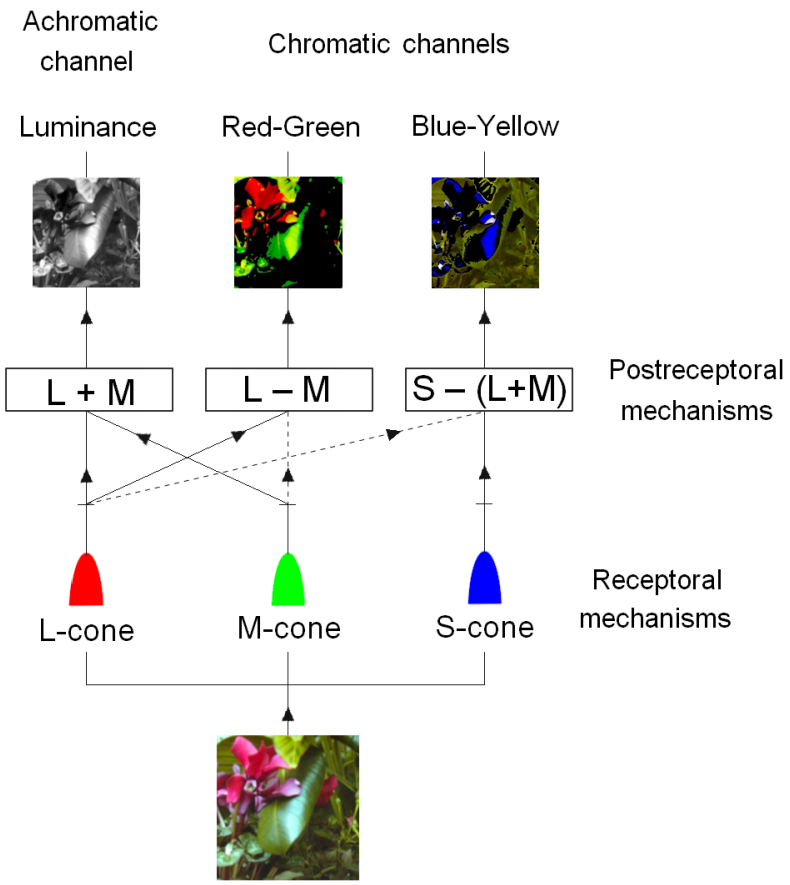

Figure 2.13: Theory of color opponency is postulated by Hering (1920). The figure is modified from the schematic illustration by Wyszecki and Stiles (1982, p. 647).

however, cannot explain the appearance of a color in terms of hue and chromatic content of the stimulus. An attempt was made by Hering (1920) to explain the appearance of a color stimulus based on the notion that a color stimulus is not perceived as either yellow-blue or red-green at the time. Following from this notion (Hering, 1920, 1964), known as color opponency, a second stage of processing was suggested that operates at postreceptoral level (Hurvich & Jameson, 1957). The notion of postreceptoral mechanism of opponent color processing is illustrated in Figure 2.13.

According to the notion of opponent color mechanism, Hurvich and Jameson

(1955) proposed a model to describe quantitatively the chromatic visual responses of a color stimulus using its CIE 1931 XYZ tristimulus values, as,

$$\begin{aligned} \text{b:y} &= 0.4Y - 0.4Z, \\ \text{r:g} &= 0.4X - 0.4Y. \end{aligned} \tag{2.29}$$

in which, b:y, and r:g are the postreceptoral responses in blue-yellow and red-green opponent channels, respectively. The spectral functions of the relative chromatic responses are plotted in Figure 2.14.

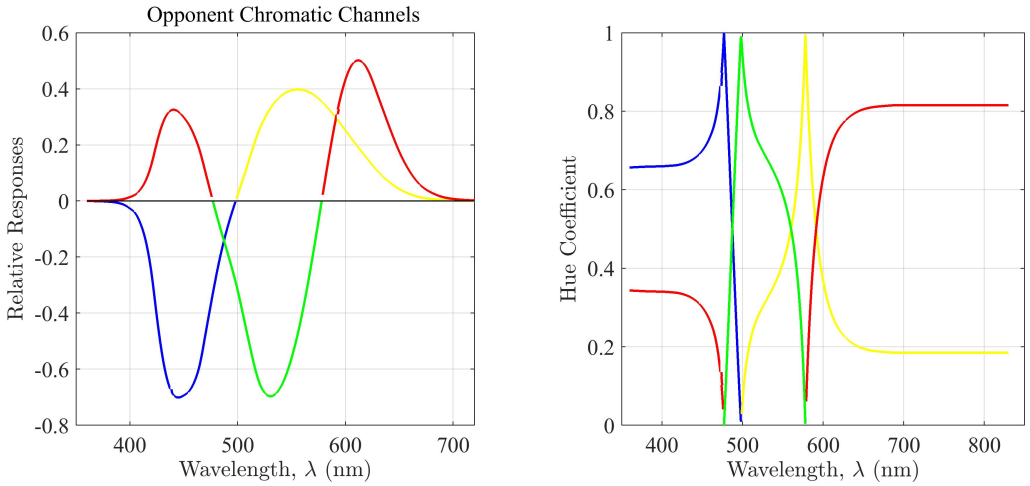

Figure 2.14: The spectral functions of visual responses in postreceptoral opponent mechanism, obtained from Eq. (2.29) applied on the CIE 1931 2° color matching functions. (a) The relative chromatic responses of opponent channels to monochromatic lights (Jameson & Hurvich, 1955; Hurvich & Jameson, 1955). (b) The spectral functions of *hue coefficients* postulated by Hurvich and Jameson (1955).

Hurvich and Jameson (1955) defined a set of coefficients to describe *hue sensations* of a color stimulus as,

$$red = \frac{r}{r+b+g+b}, \quad green = \frac{g}{r+b+g+b}, \tag{2.30}$$

$$blue = \frac{b}{r+b+g+b}, \quad yellow = \frac{y}{r+b+g+b}, \tag{2.31}$$

in which, r and g, are the magnitude of relative responses from the red-green opponent channel, and b and y are those from the blue-yellow channel. The expression in Eq. (2.31) quantifies the magnitude of *unitary hue coefficients* for a color stimulus. Figure 2.14(b) represents the spectral functions of the hue coefficients obtained across the spectrum of monochromatic lights.

The mechanism of opponent color coding in the visual system is derived originally from behavioral measurements of the appearance of colored light stimuli. This notion of opponent color coding by two separate functional pathways has been also supported by physiological measurement of retinal circuits (Demb & Brainard, 2010).

Chapter 3

The Nature of Photon Absorption by Photoreceptor Cells

In this chapter, we aim to understand the pattern of photon absorption by a population of photosensitive elements, such as photoreceptor cells in the human retina. This chapter is organized as follows. To illustrate the idea, first, we review the fundamental principles of light absorption in a photoreceptor. To clarify our fundamental assumptions, then, we discuss the distribution of cells across quantal levels of single-frequency for an array of identical cells exposed to monochromatic light. We also discuss the applicability of our model to different forms of interaction of light with cells. For exposure to light of multiple wavelengths, we then introduce the histogram distribution of individual cells of like-type across energy levels. Also, we quantify temporal variation with repeated exposure in the number of identical cells at each energy level. Finally, we clarify the elements of the model and validate the assumptions made to derive the distribution in an experiment using a digital CMOS imaging sensor.

3.1 Introduction

Understanding of color processes in the human visual system requires detailed investigation of multiple hierarchical stages through which the information from an environmental stimulus is processed and passed on to the higher visual pathways.

In the hierarchy of sequential mechanisms for the ideal observer introduced by Geisler (1989), neuronal signals from stimulated retinal cells are the very early information utilized by an observer for color detection and discrimination. An initial stage of visual processing is receptoral stimulation by light from the environment. This begins when light energy is transduced into neural signals as photons are absorbed by the photopigment molecules of the retinal cells (Baylor, 1987). The design of an array of interleaved photosensitive elements in a digital sensor for color imaging is inspired by the physiology of human retina (Bayer, July 20, 1976), both in terms of mosaic arrangement of the cells and selective absorption of light of different frequencies. The transduction process in a retinal cell and the charge release in a sensor pixel, when exposed to light, are both the consequences of photon absorption, thus influenced by the nature of light as it interacts with a photosensitive element, e.g. a retinal photoreceptor or a sensor pixel. In this chapter, we take a mathematical approach to model the consequences of such interaction, namely absorption of photon energy by a population of interleaved photosensitive elements. As a general expression, the term *cell* refers herein to a photo-sensitive element.

3.2 Problem Statement

When a cell is exposed to a photon flux, the actual number of photons absorbed in the cell varies with Poisson fluctuation, and the stochastic nature of absorption is described by the probability that a particular number of quanta is absorbed (Hecht, Shlaer, & Pirenne, 1942). This concept is shown schematically in Figure 3.1.

Now, let us consider a general case when a population of identical cells is exposed repeatedly to light of multiple frequencies. In this case, photon fluctuation

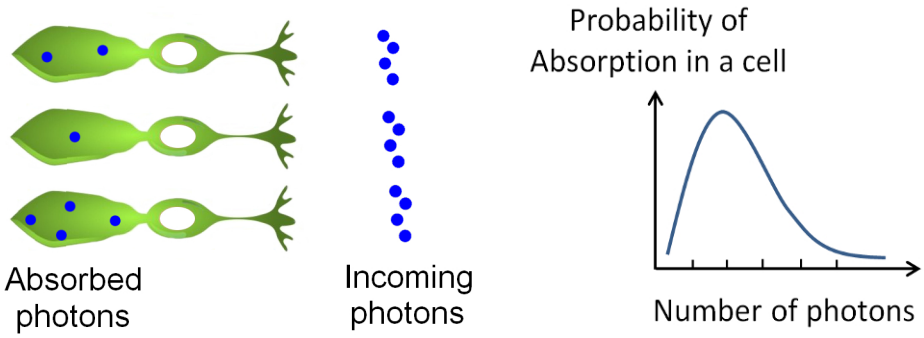

Figure 3.1: The stochastic nature of photon absorption in a cell. (a) Photon absorption in a cell is subject to fluctuation. Two identical receptors exposed to the same light of a particular wavelength may absorb different numbers of photons. (b) The actual number of photons absorbed in the cell varies with Poisson fluctuation. The plot schematically shows the probability that a particular number of quanta is absorbed in a cell.

introduces a spatial and a temporal variation. Spatial variation in absorption by individual cells is due the mosaic structure in which a cell, as an autonomous light-sensitive embodiment, interacts with incoming individual photons independent from the other neighboring cells, thus not all cells absorb the same amount of energy. Temporal variation arises when those cells are exposed repeatedly to the same light, and the actual number of cells at a given energy level varies. The main goal is to characterize such spatiotemporal variations. The photon fluctuation in retinal receptors of the human eye (Rieke & Baylor, 1998) as well as in digital camera sensors (Costantini & Susstrunk, 2004; Kuniba & Berns, 2009; Farrell, Catrysse, & Wandell, 2012) has been investigated in several studies. For a population of identical cells exposed repeatedly to multi-wavelength light, however, a model to account for spatiotemporal variations in absorption by individual cells has resisted investigation.

Our approach to characterize the spatiotemporal variations of absorbed energy

by individual photoreceptors is different from previous studies in the following regards. Previous research on retinal photoreceptors mainly concerns the Poisson distribution of photons in a cell, whereas our approach considers repeated exposure of many cells to arbitrary light of a broad spectrum. In particular, when a population of identical cells is exposed to multi-wavelength light, we characterize spatial variation in absorbed light energy by like-type individual cells because due to the principle of univariance (Rushton, 1972) the energy, rather than the number of absorbed photons, is the variable of interest. This characterization is important for understanding the retinal factors that limit color detection and discrimination in the human visual system (Barlow, 1957; Bouman, Vos, & Walraven, 1963; Geisler, 1989). Furthermore, we characterize the temporal fluctuation with repeated exposure in the number of identical cells at a given energy level. We also determine the relationship between the spatial and temporal variations. To our knowledge, the temporal variation in the histogram and its relationship to spatial variation has not been addressed in the literature. The latter may have technical significance in the analysis of microscopic imaging of the human retina (Roorda et al., 2002; Jonnal et al., 2016) in cases when the light intensity is substantially reduced before reaching the retinal cells (van de Kraats et al., 1996).

3.3 Distribution of Cells across Quantal Levels

In section 2.5.4, we noted that the presence of large number of photopigment molecules densely packed within the outer segment disk membrane of a cell enables the cell to absorb photons of different wavelengths. The probability of absorption at a particular wavelength depends on the corresponding absorbance of the cell at that wavelength (Bowmaker, 1981; Dartnall et al., 1983). Note that the photopigments have also internal energies of multiple terms explained by

an extension of the Maxwell-Boltzmann distribution (Hinshelwood, 1940). The internal energies of molecules contribute to light detection at threshold (Barlow, 1957) and the bleaching process at low energy wavelengths (Lewis, 1955; Koskelainen, Ala-Laurila, Fyhrquist, & Donner, 2000). Here, we are interested in the distribution of external light energy among cells with known absorbance capacity.

Let us consider a case in which identical photoreceptors are exposed to a uniform monochromatic light. If photon absorptions in each cell fluctuate with Poisson statistics, then two identical receptors may absorb different numbers of photons. We ask what fraction of like-type stimulated cells has absorbed no photons, what fraction has absorbed 1 photon, what fraction has absorbed 2 photons, and so forth. Suppose that a uniform single-frequency radiant flux, with m photons, is stimulating a specific retinal area containing N identical cells of a particular type. Consider an observation in which m trials of hitting quanta result in a total of k successful absorptions in N distinguishable cells all together, and $m-k$ failures. Then, the number of ways, W, in which there are N_0 cells with no photons absorbed, N_1 cells with 1 photon, N_2 cells with 2 photons, and so on is given by

$$W = \frac{N!}{N_0!\, N_1!\, N_2!\, \cdots} \, \frac{m!}{1!^{N1}\, 2!^{N2}\, \cdots\, (m-k)!}, \tag{3.1}$$

where,

$$N = \sum_q N_q \, , \; k = \sum_q q\, N_q. \tag{3.2}$$

If the probability that a given photon is absorbed successfully in a particular cell is p, then the probability that it is not absorbed by any of the N cells is $1 - Np$. Then the probability, P, of this observation is

$$P(N_0, N_1, N_2, \cdots) = W p^k \, (1 - Np)^{m-k}. \tag{3.3}$$

See Stevens (1937); Tukey (1949); Feller (1957); David (1950); Watterson (1974) for details of the distribution in Eq. (3.3). We now maximize the probability P with respect to N_q. By Stirling's approximation, $\log x! \approx x \log x - x$, we have,

$$\begin{aligned} \log P \approx N \log N - \sum_q N_q \log N_q \; + m \log m \; + \\ \sum_q q\, N_q \log\left(\frac{p}{q}\right) + (m-k) \log\left(\frac{1-Np}{m-k}\right) \end{aligned} \tag{3.4}$$

The Lagrange method is applied to maximize (3.4) subject to the constraints in Eq. (3.2), with multipliers β and γ for the first and second conditions, respectively. This gives,

$$\log N_q = -(1+\beta) - \log q! - q\,\gamma, \tag{3.5}$$

where,

$$\gamma = \log[(1-Np)/(mp-kp)]. \tag{3.6}$$

In Eq. (3.5), N_q is the number of cells that have absorbed exactly q photons of a particular frequency, and p is the chance of absorption of a photon in a single cell. Then, $Np \leq 1$, with equality when all m quanta are absorbed by all N cells. In cases where, $Np < 1$, the average number of quanta absorbed in N cells all together is mNp. Here we seek the average number of cells, $\bar{N}_q$, having absorbed exactly q photons. By taking $mNp = k$ in Eq. (3.6), and finding β to satisfy the first condition of Eq. (3.2), therefore, we have,

$$\bar{N}_q = N \exp(-mp) \left[\frac{(mp)^q}{q!}\right], \tag{3.7}$$

where, $\bar{N}_q/N$, represents the average fraction of cells with q quanta within the stimulated retinal area.

The problem addressed here is similar to random placing of Poisson balls into equal boxes according to Planck's quantum principle. Tukey (1949) found a distribution for the expected number of boxes with q balls, when m Poisson balls

are being dropped into N equal boxes. A similar problem was addressed earlier by Stevens (1937). The above arguments go along with Tukey's (1949) premise of Poisson balls placement into equal boxes. The importance of our proof is that the parameter k may equally refer to the number of photons transmitted through or reflected from all the N cells. This generalizes Eq. (3.7) to the case in which N_q refers to the number of cells that have absorbed, reflected or transmitted exactly q photons of a particular frequency, and p to the corresponding probability that a photon is absorbed in, transmitted through or reflected from a single cell. Thus, there is no argument to prevent the model from being applied to the interaction of light with cells in the form of absorption, reflection or transmission. Let J_ν be the fraction of light with frequency ν that is absorbed in, transmitted through or reflected from a photoreceptor cell. If N cells of a particular type are identical, then, a photon is equally likely to be absorbed in, transmitted through or reflected from any cell with the probability J_ν/N. Note that the number of cells is large in practice, and thus the probability of absorption of a photon in a specific cell becomes very small. This view is consistent with Poisson distribution in which the chance of an event in an observation is small (Cramér, 1946, p. 206).

3.3.1 Distribution Parameter for an External Stimulus

As discussed in section 2.5.3 and shown by Eq. (2.21), when an external surface stimulus, with spectral radiance I_ν, is viewed by an eye of focal length f and pupil area A, the retinal irradiance is given by,

$$E_\nu \, \mathrm{d}\nu = \tau_\nu \, (I_\nu \, \mathrm{d}\nu) \left(\frac{A}{f^2} \right), \tag{3.8}$$

where τ_ν is the pre-retinal transmittance of the lens and macula (Wyszecki & Stiles, 1982; Stockman & Sharpe, 2000a). Considering that m is the number of

photons available for a total of N receptors all together, we have,

$$m = \varrho N \Delta t \left(\frac{E_\nu \, \mathrm{d}\nu}{h\nu} \right), \tag{3.9}$$

in which ϱ is the collecting area of a cell and Δt is the duration of exposure. Thus, for a stimulus radiant flux of frequency ν,

$$mp = \varrho \, \Delta t \left(\frac{E_\nu \, \mathrm{d}\nu}{h\nu} \right) J_\nu = \frac{\varrho \, \Delta t}{h\nu} \left(I_\nu \, \mathrm{d}\nu \right) \left(\frac{A}{f^2} \right) \tau_\nu J_\nu, \tag{3.10}$$

where h is the Planck constant and mp refers to the average and variance of the number of photons with frequency ν absorbed in, transmitted through or reflected from the N cells all together. For the case of interaction of light in form of absorption, J_ν is given by Eq. (2.22). In the following, we discuss the interaction of light with cells in the form of absorption without losing the generality of the proposed approach to other forms of interaction.

3.4 Distribution of Cells across Photon Energy Levels

Now, consider a more complex case where the stimulating light has a broad spectrum extending over different wavelengths. The principle of univariance states that photoreceptor response is determined by photon absorption, and not by which photons are absorbed (Rushton, 1972). Due to the dependency of photon energy on wavelength and the principle of univariance, we are interested in the number of cells at an energy level rather than the number of quanta absorbed by a cell. In particular, when N identical cells are uniformly exposed to light of broad spectrum, with the assumption that cells independently absorb photons of different frequencies, we aim to determine, in statistical terms, the fraction of each type of cell that has absorbed Q units of photon energy.

From Eq. (3.7), the fraction of cells with q_1 photons of the first frequency, q_2

photons of the second frequency and so on is,

$$\exp(-m_1 p_1)\left[\frac{(m_1 p_1)^{q_1}}{q_1!}\right] \times \exp(-m_2 p_2)\left[\frac{(m_2 p_2)^{q_2}}{q_2!}\right] \times \cdots \tag{3.11}$$

Suppose $Q = h\nu_1 q_1 + h\nu_2 q_2 + \cdots + h\nu_n q_n$ is the total energy of the fraction of cells with q_1, q_2, ..., q_n absorbed photons. Now we are interested in the distribution of Q with respect to Eq. (3.11). A closed-form expression for the linear combination of Poisson variable is not readily available, but it can be very well approximated for the purpose of this research in nice terms. From Eq. (3.7), the expected value, μ_{q_i}, and the variance, $\sigma^2_{q_i}$, of the variable q_i are $m_i p_i$. Then, the expected value, μ_Q, and the variance, σ^2_Q, of the variable Q are,

$$\begin{aligned} \mu_Q &= h \sum_i \nu_i \mu_{q_i} = h \sum_i \nu_i \, m_i p_i, \\ \sigma^2_Q &= h^2 \sum_i \nu_i^2 \sigma^2_{q_i} = h^2 \sum_i \nu_i^2 \, m_i p_i. \end{aligned} \tag{3.12}$$

Using Eq. (3.10), μ_Q, and σ^2_Q can be written in integral forms as,

$$\mu_Q = \varrho \, \Delta t \int_\nu E_\nu J_\nu \, \mathrm{d}\nu \,, \;\; \sigma^2_Q = h \, \varrho \, \Delta t \int_\nu \nu E_\nu J_\nu \, \mathrm{d}\nu \,, \tag{3.13}$$

which can be approximated by sums when the spectra, E_ν and J_ν, are well resolved. In the continuum of frequencies, the energy steps in Q becomes smaller as n in q_n increases. Thus, the distribution of Q with respect to Eq. (3.11) can be estimated by a continuous probability function. According to the central limit theorem (Feller, 1945), the distribution function of the variable Q can be approximated by the normal distribution function, when the average of absorbed energy by all the cell is not too small. This is because a Poisson distribution can be approximated by a normal distribution for a large parameter value (Haight, 1967, p. 69), and Q, as a linear combination of Poisson variables, becomes a continuous variable for small energy steps. This approximation of normal distribution was

also suggested by Pelli (1985) for absorption in the human photoreceptor cells. With the assumption of normal distribution for the variable Q, therefore, the average number of cells with absorbed energy greater than ε, is given by,

$$\bar{N}_{Q\geq\varepsilon} = N\left[1 - \Phi\Big(\frac{\varepsilon - \mu_Q}{\sigma_Q}\Big)\right]. \tag{3.14}$$

where, $\Phi(\cdot)$ is the standard normal distribution function. Likewise,

$$\mathrm{d}\bar{N}_Q = \frac{N}{\sigma_Q\sqrt{2\pi}}\exp\left[-\frac{1}{2}\Big(\frac{Q-\mu_Q}{\sigma_Q}\Big)^2\right]\mathrm{d}Q \;;\; Q \geq 0, \tag{3.15}$$

represents the average number of cells, $d\bar{N}_Q$, that have absorbed photon energy between Q and $Q + \mathrm{d}Q$.

3.4.1 Temporal Variation

The actual amount of absorbed energy in a cell varies with repeated exposure, causing a temporal fluctuation in the histogram itself. In our model for identical cells, N_Q is the number of cells with energies between Q and $Q \pm \Delta Q/2$, for an instance of exposure. The average of N_Q across exposures is,

$$\bar{N}_Q = \int_{Q-\Delta Q/2}^{Q+\Delta Q/2} \mathrm{d}\bar{N}_Q\,, \tag{3.16}$$

in which $\mathrm{d}\bar{N}_Q$ is given by Eq. (3.15) with the variance σ_Q^2 representing the spatial fluctuation in absorbed light energy by cells. With repeated exposure, however, we are interested in finding $var(N_Q)$ to account for the temporal variation, with repeated exposure, in the number of cells with Q units of energy. According to Tukey (1949), the variance of the number of identical cells with q photons of a single frequency, $var(N_q)$, is $\bar{N}_q(1 - \bar{N}_q/N)$ and the covariance of the number of identical cells with q and n photons, $cov(N_q, N_n)$, is $-\bar{N}_q\bar{N}_n/N$. For an exposure to multi-wavelength light energy, $var(N_Q)$ is obtained by summing the elements

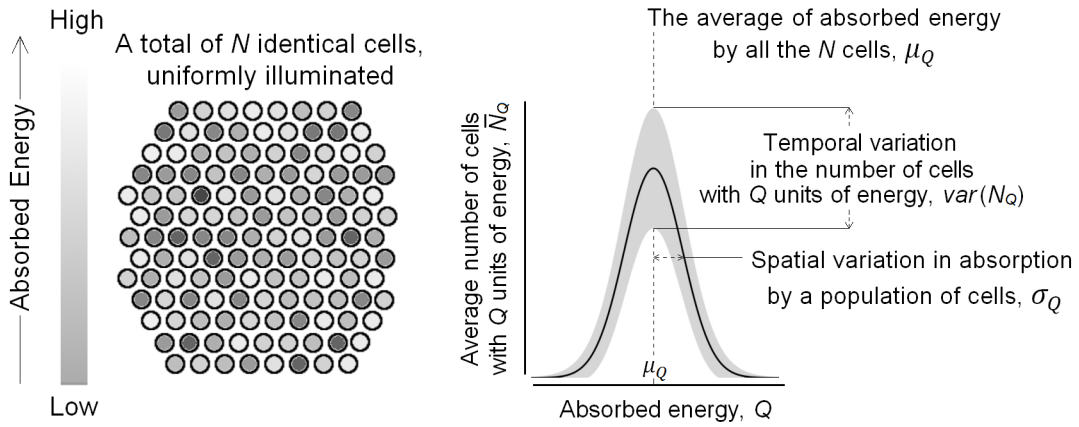

(a) (b)

Figure 3.2: Illustration of the model. (a) Identical cells exposed to uniform light absorb different amounts of energy. (b) When a population of N cells of like-type is exposed repeatedly to a uniform photon flux, the histogram of the average number of cells with Q units of absorbed energy, $\bar{N}_Q$, is approximated by a Gaussian distribution. The proportion of like-type cells is shown by $\bar{N}_Q/N$. The gray region around the black distribution curve shows the temporal variation in the number of cells at an energy level.

of variance and covariance within the range of ΔQ. This gives,

$$var(N_Q) = \bar{N}_Q(1 - \bar{N}_Q/N). \tag{3.17}$$

The proposed model is schematically illustrated in Figure 3.2.

3.5 Implementation on Digital Sensors

In an imaging sensor, photo-generated charge (Q_e) is accumulated over an integration time (Δt) when photosensitive area of a pixel (ϱ obtained from pixel pitch) is exposed to light. In an imaging device, J_ν in Eq. (2.22) is equivalent to the spectral quantum efficiency function. To implement the model in a sensor, q in Eq. (3.7) refers to the number of collected electrons, and $J_\nu/h\,\nu$ in Eq. (3.10) is the sensor responsivity. Thus, $Q_e = e_0 \sum_i q_i$, where e_0 is the elementary charge,

has the following statistics,

$$\mu_{Q_e} = e_0 \, \varrho \, \Delta t \int_\nu E_\nu \frac{J_\nu}{h\nu} \, \mathrm{d}\nu \, , \;\; \sigma^2_{Q_e} = e_0^2 \, \varrho \, \Delta t \int_\nu E_\nu \frac{J_\nu}{h\nu} \, \mathrm{d}\nu \, , \tag{3.18}$$

used, in Eq. (3.15) with Q_e as a variable, to approximate the histogram of charge collected by individual pixels. This normal approximation was suggested in the literature for an imaging device (Hasinoff, 2014) and Eq. (3.18) is consistent with previous models of photon noise in a sensor (Kuniba & Berns, 2009). However, in addition to the spatial variation (σ_{Q_e}), our model also quantifies the temporal variation in the histogram itself by,

$$var(N_{Q_e}) = \bar{N}_{Q_e}(1 - \bar{N}_{Q_e}/N). \tag{3.19}$$

This temporal variation has two important features in an imaging system. First, the temporal variance, $var(N_{Q_e})$, is reciprocally related to the spatial variation (σ_{Q_e}). Second, the histogram of temporal variation merely caused by photon fluctuation is unimodal, despite the variation of signals across exposures. In the following, we discuss the technical significance of these features in an empirical study on a CMOS sensor. Table 3.1 describes the parameters of the model applied to an image sensor.

3.5.1 Irradiance at the Image Plane

In an imaging device, the f-number, denoted by $f/\#$, is defined as the ratio of the focal length of the lens to the diameter of the effective aperture, D_a (Nakamura, 2006; Hopkinson, Goodman, & Prince, 2004),

$$f/\# = \frac{f}{D_a}. \tag{3.20}$$

To find the spectral irradiance, E_ν, at the image plane, from the spectral radiance, I_ν, of an external color patch, we use Eq. (2.21). For an imaging device, we write,

$$E_\nu \, \mathrm{d}\nu = \tau_\nu \, (I_\nu \, \mathrm{d}\nu) \, \big(\frac{A}{f^2}\big) \tag{3.21}$$

$$= \tau_\nu \, (I_\nu \, \mathrm{d}\nu) \, \big(\frac{\pi {D_a}^2}{4f^2}\big) \tag{3.22}$$

$$= \tau_\nu \, (I_\nu \, \mathrm{d}\nu) \, \big(\frac{\pi}{4}\big)\big(\frac{1}{f/\#^2}\big), \tag{3.23}$$

in which, τ_ν is the spectral transmittance of the lens, and $A/f^2 = \pi/[4(f/\#)^2]$ (Farrell et al., 2012; Hopkinson et al., 2004).

Table 3.1: The table summarizes a list of parameters for estimating spatiotemporal variations explained in section 3.5 for an imaging sensor.

Parameter	Description	Units
ν	Frequency	Hz
h	The Plank Constant	J s
e_0	The elementary charge	C
I_ν	Spectral radiance	$\mathrm{W\,sr^{-1}\,m^{-2}\,Hz^{-1}}$
E_ν	Spectral irradiance at the image plane	$\mathrm{W\,m^{-2}\,Hz^{-1}}$
J_ν	Spectral quantum efficiency function	–
ϱ	Effective area of a pixel (calculated from pixel pitch)	$\mathrm{m^2}$
A	Effective aperture area	$\mathrm{mm^2}$
f	Focal length of the lens	mm
τ_ν	Spectral transmittance of the lens	–
μ_{Q_e}	Average of charge collected by all pixels	C
$\sigma^2_{Q_e}$	Spatial variance of collected charge by N pixels	$\mathrm{C^2}$
Δt	Integration time	s
N_{Q_e}	The number of pixels with Q_e units of charge	–
$\bar{N}_{Q_e}$	Expected number of pixels with Q_e units of charge	–
$var(N_{Q_e})$	Temporal variance in the number of pixels at Q_e	–

3.5.2 Photoresponse Nonuniformity

A digital imaging sensor, in particular CMOS sensors, under illumination suffers from photoresponse nonuniformity (PRNU), which is caused by variation in the responsivity across pixels and nonuniformity in gain characteristics (Nakamura, 2006, p. 66-68). Lets consider a conversion of charge (Q_e) to digital count (DN) in a sensor pixel. We write,

$$DN = K\,Q_e + D_0, \tag{3.24}$$

where K (in ADU/C unit) is the conversion factor, and D_0 is an offset for the dark signal. With the assumption of uniform responsivity across pixels (identical pixels at the moment of absorption), we can write:

$$\left(\frac{\sigma_{DN}}{\mu_{DN}}\right)^2 = \left(\frac{\sigma_K}{\mu_K}\,\frac{\sigma_{Q_e}}{\mu_{Q_e}}\right)^2 + \left(\frac{\sigma_K}{\mu_K}\right)^2 + \left(\frac{\sigma_{Q_e}}{\mu_{Q_e}}\right)^2 + \left(\frac{\sigma_{D_0}}{\mu_{Q_e}\,\mu_K}\right)^2 \tag{3.25}$$

where, μ_{DN}/σ_{DN} is the measured SNR, μ_{Q_e}/σ_{Q_e} is the predicted SNR by (3.18), μ_K and σ_K are the spatial average and standard deviation of conversion factors across pixels (Healey & Kondepudy, 1994). The dark signals variation across pixels, σ_{D_0}, in a CMOS sensor under illumination, is significantly lower than the signal, μ_{Q_e}. Thus, $(\sigma_{DN}/\mu_{DN})^2$ in Eq. (3.25) can be approximated by,

$$\left(\frac{\sigma_{DN}}{\mu_{DN}}\right)^2 \approx \left(\frac{\sigma_K}{\mu_K}\,\frac{\sigma_{Q_e}}{\mu_{Q_e}}\right)^2 + \left(\frac{\sigma_K}{\mu_K}\right)^2 + \left(\frac{\sigma_{Q_e}}{\mu_{Q_e}}\right)^2 \tag{3.26}$$

with the assumption of insignificant contribution of dark signals variation across pixels, when $\sigma_{D_0} \ll \mu_{Q_e}\,\mu_K$. In the following experiment, we use Eq. (3.26) to estimate the contribution of PRNU to the spatial variation of digital count at higher durations of exposure.

3.6 General Methods

Our model presents a unified framework for the distribution of light energy among a population of interleaved photosensitive elements, applicable to both biological and non-living arrays of photosensitive elements. To validate the model, we repeatedly exposed a CMOS sensor, with known optical specifications, to a color checker uniformly illuminated by a 1000 W quartz-halogen lamp at a distance of about 3 m. Figure 3.3 shows the experimental setup. In the experiment, we used

Figure 3.3: In the experiment, a CMOS digital sensor with 10-bit digital output was exposed repeatedly to a uniformly illuminated color checker. The figure shows the experimental setup.

1/3.2-Inch 8 Mp CMOS digital image Sensor manufactured by ON Semiconductor (Aptina) under the name AR0835HS. The specifications of the CMOS sensor was obtained from the manufacturer's public page (`http://www.onsemi.com/pub\_link/Collateral/AR0835HS-D.PDF`, retrieved 16 Jan 2017). The spectral radiance of a color patch was measured by the PR650 spectroradiometer. Our setting provided a luminance of about 46 $\mathrm{cd\,m^{-2}}$ for the white patch. The camera device was placed at a distance of 26 inches from the color checker. We analyzed unprocessed raw image data without denoising to eliminate any biases in performance appraisal of the model. However, a dark pedestal value of 42 bits, introduced by the manufacturers imaging software, was taken off to account for

the dark voltage. Specifications of the imaging device are given in Table 3.2. As

Table 3.2: The table shows specifications of the imaging device with an 8-megapixel CMOS sensor used in the experiment. In our imaging setup, $\varrho = 1.96\,\mu m^2$ and the effective f-number is about 2.75.

Output	Array size	Pixel pitch	Image format	A/f^2
10-bit	3264×2448	1.4 µm	RGGB Raw	~ 0.104

shown in Figure 3.4(a), The sensor has a Bayer color filter array with RGGB mosaic arrangement. The spectral quantum efficiency functions (QE) of the sensor for separate RGGB channels are plotted in Figure 3.4(b). In this plot, the second green channel is shown in black for clarity. The QE of color channel was digitized from the plot on the manufacturer datasheet. The sensor has a Sunex DSL945D-650 lens with the spectral transmittance shown in Figure 3.4(c). The spectral QE modified by the lens' transmittance spectrum is presented in Figure 3.4(d).

3.6.1 Prediction

To predict the histogram for a given sensor channel, first, we found the parameters of the histogram using Eq. (3.18) in which E_ν is calculated based on Eq. (3.8) and the information given in Table 3.2. The transformation-invariant quantity of a channel-wise signal-to-noise ratio (SNR) was then predicted by μ_{Q_e}/σ_{Q_e}. As discussed in section 3.5, Eq. (3.19) holds true to predict the temporal variance both in unit of digital number (ADU) and charge unit. For details of unit conversion in an imaging sensor, see Hopkinson et al. (2004, p. 32).

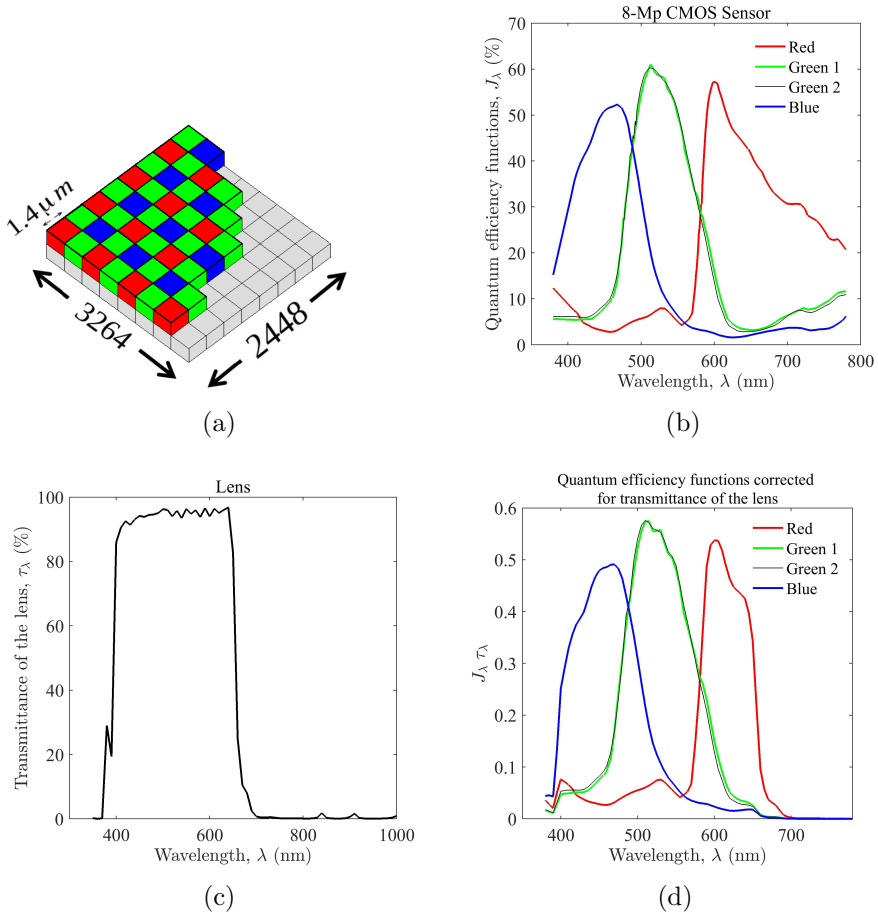

Figure 3.4: Specifications of 1/3.2-Inch 8 Mp CMOS digital image sensor. (a) The color filter array of the sensor (RGGB) (b) The quantum efficiency functions of the sensor for separate channels. (c) The spectral transmittance of the lens. (d) The quantum efficiency functions of the sensor is modified by the transmittance of the lens.

3.6.2 Measurement

As shown in Eq. (3.15), the model predicts, with repeated exposure, the expected value of the number of pixels at a given value. Thus, we obtained all the histograms, with repeated exposure, for a given color patch. We then calculated the average of all histograms, the variance of which quantifies the spatial variation. The temporal variance is measured by calculating the variance of histogram frequency at each specific pixel value (digital number, *DN*, in our 10-bit device

ranges from 0 to 1023). We measured SNR (mean divided by the standard deviation) from the statistics of the average histograms of the patch.

3.7 Experiments

In this section, we discuss the experiments performed to validate the performance of our model in a CMOS sensor. We have made the acquired RAW image data available under an open-source MIT license at `https://github.com/peyvandi/raw-image-files`. The spectral data, and MATLAB codes are also available online at `https://github.com/peyvandi/CMOS-Sensor-Noise` (Code File 2).

Experiment 3.1. In this experiment, acquisition of a raw RGGB image was performed with an exposure duration Δt of 50 ms. We obtained with repeated exposure a total of 180 images of a 24-patch X-rite mini ColorChecker Classic with a patch size of 12×12 mm. The small size of each color patch helped to reduce spatial non-uniformity of radiation across the patch which covered ~ 5000 pixels of the sensor. The luminance values measured for the three spots of a patch showed a maximum difference of $0.2\,\mathrm{cd\,m^{-2}}$, indicating a reasonable light uniformity, hence the average was taken.

Results and Discussion. To evaluate quantitatively the performance of the model in predicting the spatial variation, the average of the channel-wise histograms for each of the 24 patches was normalized by the number of pixels (1089). The Kullback-Leibler divergence, D_{KL}, (Kullback & Leibler, 1951) between the predicted distribution and the normalized average histogram was then calculated. The result is presented in Table 3.3 separately for each RGGB channel. An average D_{KL} of 0.007 across channels shows that the model accurately predicts the spatial variation of digital counts from a CMOS sensor. Thus, the assumption

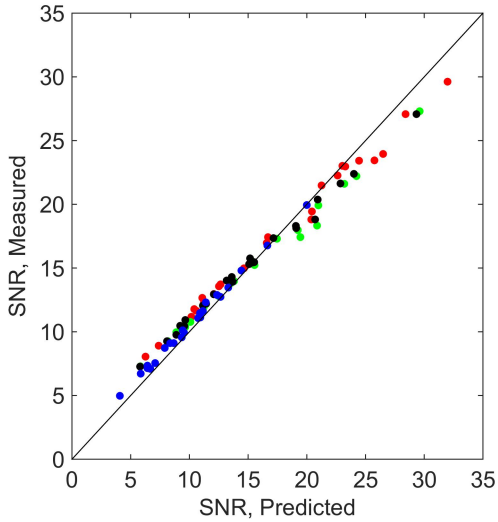

Figure 3.5: The measured SNR is plotted as a function the predicted SNR (μ_Q/σ_Q). The second green channel is shown in black for clarity.

of independent absorption of photons among cells is justified by the empirical results. Figure 3.5 shows a scatter plot of the measured SNR (μ_Q/σ_Q) versus the

Table 3.3: For each of the RGGB channels separately, the table shows statistics obtained from 24 patches of a standard color checker by calculating the Kullback-Leibler divergence, D_{KL}, of the predicted distribution for a color patch and the average of normalized histogram distributions of the patch across 180 images of the color checker.

Sensor Channel	$D_{\mathrm{KL}} \times 10^3$			
	Mean	SD	Range	Median
Red	10.1	13.9	0.5−58.6	6.7
Green 1	9.3	12.2	0.3−47.2	3.4
Green 2	7.7	8.6	0.4−33.3	3.9
Blue	4.5	6.5	0.3−28.3	1.1

predicted SNR, for each of the RGGB channels. Visual inspection of the plots in Figure 3.6(a) illustrates the performance of the model so long as spatial variation is caused by photon noise in a sensor.

Figure 3.6(a) shows a total of 180 histograms (black curves) obtained with

repeated exposure for a green and a yellow color patch, separately for each of the RGGB channels [see Code File 2 in Peyvandi, Ekroll, and Gilchrist (2017b)]. In this plot, a solid colored curve shows the predicted distribution (expected frequency). The temporal variance in the frequencies of pixel values is evident along the vertical axis. This figure illustrates that for lower temporal variation, the expected frequency predicted by the model for a color patch provides a closer fit to an actual histogram obtained from an instance of exposure to the patch. Figure 3.6(b) shows the predicted temporal variance by a unimodal solid curve at levels of digital number. The experimental results shown by dashed-curves confirm this unimodal prediction. As discussed in section 3.5, the model predicts this unimodality only if temporal noise is caused by photon fluctuation. In an imaging sensor, several sources of temporal noise, other than photon noise, contribute to the sensor output (Nakamura, 2006, p. 72-77). For instance, digital outputs from a sensor are also subject to signal-independent noise (Peyvandi, Amirshahi, Hernández-Andrés, Romero, & Nieves, 2013) which causes shifts in the histogram itself with repeated exposure. The unimodal distribution of the temporal variance in Figure 3.6(b) shows that spatiotemporal variations of the sensor signals in our setup is not appreciably influenced by such sensor-based noises. We performed an analysis to test whether the spatiotemporal variation in Experiment 3.1 and Figure 3.6 is caused by photon fluctuation.

As a consequence of photon noise, Eq. (3.19) predicts a reciprocal relationship between the spatial variation, σ_{Q_e}, and the temporal variation, $var(N_{Q_e})$. This prediction seems reasonable at higher levels of light intensity at which SNR is higher as well. But, under a given illumination, the spatial variance in Eq. (3.18) also depends on the spectral composition of the stimulating light. If spatiotemporal variation observed in the results of Experiment 3.1 is due to photon noise,

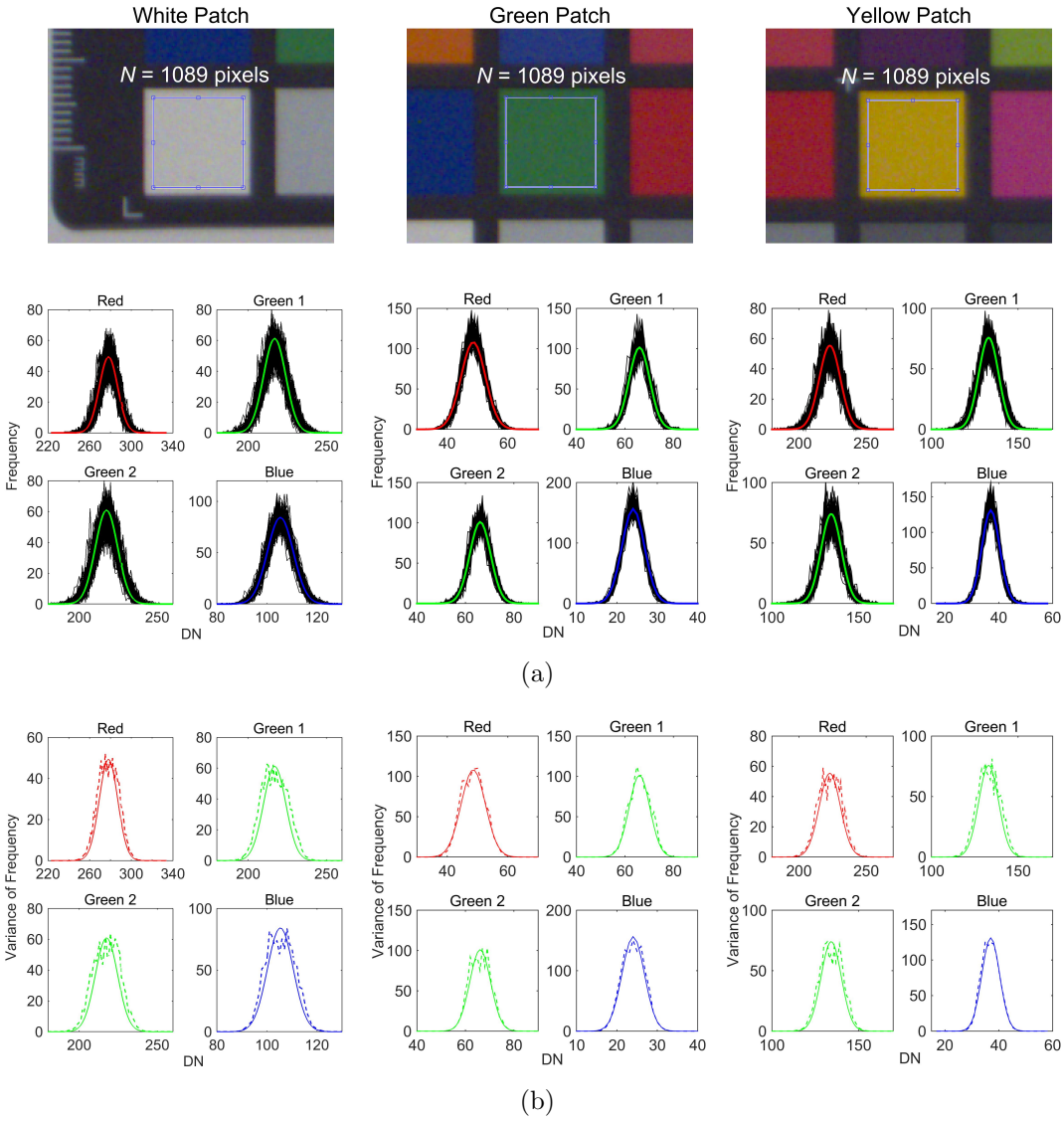

Figure 3.6: The results shown for the white (left column), a green (middle column) and a yellow (right column) patch. (a) The channel-wise histograms (frequencies at levels of digital number, DN, shown by intermixed black curves) obtained from a total of 180 trials of exposure. The predicted histogram (expected frequency) is shown by a solid colored curve. The temporal variation with repeated exposure is evident along the vertical axis. (b) The measured variance of frequencies is plotted with a dashed-curve. The solid curve shows the predicted temporal variance.

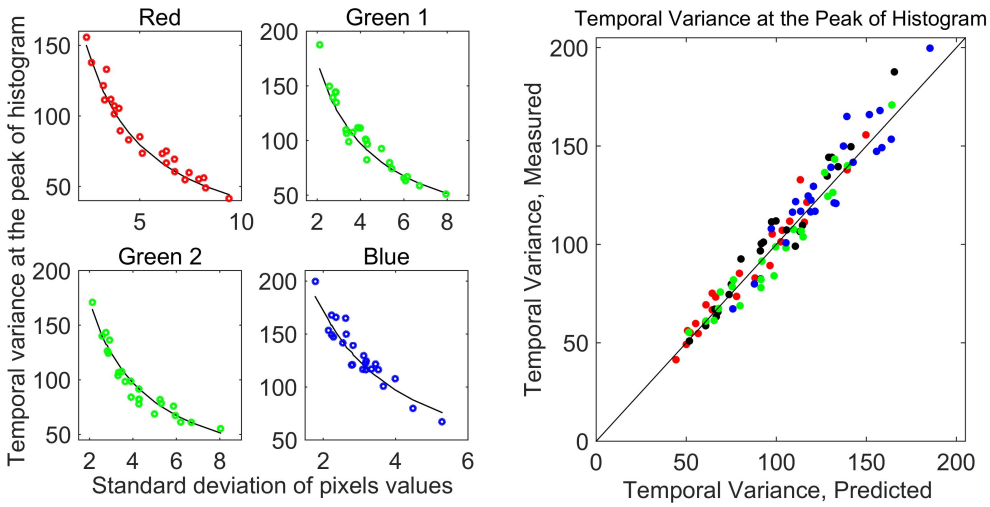

(a) (b)

Figure 3.7: The temporal variation due to photon noise is reciprocally related to the spatial variation. (a) For each of the 24 color patches, we measured the temporal variance at the peak of histogram obtained across trials of exposure. For each of the four sensor channels, the figure shows the scatterplot of this temporal variance for a color patch against the measured standard deviation of pixel values within the same patch. The total number of pixels per channel, N, is 1089. The prediction is shown by a black curve. (b) The measured temporal variance at the peak of histogram for the 24 color patches is plotted against the prediction.

we therefore expect to observe, for the 24 color patches, a reciprocal relationship between the temporal variance of a given color patch and the standard deviation of pixel values of the same patch. For each of the sensor channels, this relationship is shown at the peak of average by open circles in Figure 3.7(a). We select the histogram at the peak because the model predicts that the highest temporal variation occurs for the number of pixels with the average value of μ_{Q_e}. In this plot, the black curve represents the temporal variance predicted from the spatial variance according to (3.19). The scatterplot of the measured temporal variance against the prediction is shown in Figure 3.7(b). The results presented in Figure 3.7 confirm the predicted relation between the temporal and spatial fluctuations.

Experiment 3.2. In Experiment 3.1, a small region of the sensor was exposed to a color patch with an integration time of 50 ms. If the spatial variation shown in Figures 3.5 and 3.6 is merely caused by photon noise, we expect to observe a higher value of SNR at higher durations of exposure. Furthermore, as discussed in section 3.5.2, exposure of the sensor to a large, nearly uniform color patch illuminated with an almost uniform light source helps to detect also the contribution of sensor-based nonuniformities to the measured SNR.

Method. In Experiment 3.2, the sensor was exposed repeatedly to a 24-patch X-rite ColorChecker Classic, with a patch size of 40×40 mm, under nearly uniform illumination. A color patch covered $\sim 55,000$ pixels of the sensor. The luminance values measured for the five spots of a patch showed a maximum difference of $0.4\,\mathrm{cd\,m^{-2}}$. Image acquisition was performed over six levels of integration time, Δt of 50, 80, 110, 140, 160, 170 ms, each with a total of 310 trials of exposure.

Results and Discussion. Figure 3.8 shows the measured SNR as a function of the predicted SNR, μ_{Q_e}/σ_{Q_e} [see Eq. (3.18)]. The ratio of μ_K/σ_K was found by fitting a curve to the data based on the model specified in Eq. (3.25). We used the *fit* function by MATLAB to minimize the rmse. This gave an estimate of 76.34 for μ_K/σ_K, with a 95% confidence interval (74.05, 78.68), $r^2 = 0.972$, df = 575, rmse = 1.4144. This result shows that in our CMOS sensor, intrinsic variation of gain characteristics across pixels imposes an upper limit to the measured SNR. The result of Figure 3.8 further validates the performance of the model in predicting the spatial variation of absorbed energy by an array of pixels, because the curve is approximated by Eq. (3.26) in which μ_{Q_e}/σ_{Q_e} is the model-predicted SNR due to photon fluctuation.

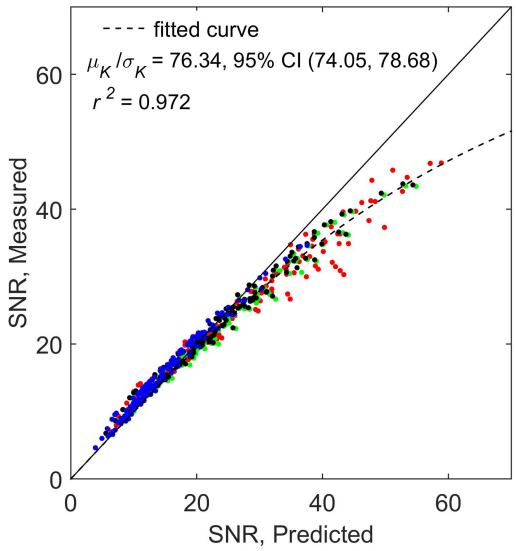

Figure 3.8: The measured SNR is plotted for each of the four RGGB channels as a function of the predicted SNR, μ_{Q_e}/σ_{Q_e}. The second green channel is shown by black for clarity. The dashed curve shows a fit to the data by the model specified in Eq. (3.25).

3.8 Conclusion

In this chapter, we proposed a model to determine the spatial variation in absorption by individual photosensitive cells and the temporal variation in the number of cells at a given energy level when a population of identical cells is exposed repeatedly to uniform multi-wavelength light. The model applies equally to the amounts of light energy transmitted through or reflected from cells. With this model, we derived a histogram for the expected number of cells absorbing each specific level of light energy, the variance of which quantifies the spatial variation in absorption by individual cells. Both the average, μ_Q, and the variance, σ_Q^2, of energy absorbed in a total of N cells all together are independent of N, but proportional to the collecting area of a cell, ϱ. The spatial variation of σ_Q implies that individual cells of the exact same type absorb different amounts of light energy.

Besides, the actual histogram varies when those cells are exposed repeatedly to the same light. We quantified this temporal variation by the variance of the number of cells at a given energy level. We showed that the temporal variation is reciprocally related to the spatial variation. Furthermore, the temporal variation becomes less appreciable when the number of cells is large. We discussed the results of a performance appraisal by a CMOS sensor, since the proposed model equally applies to an array of non-living photosensitive elements. Our results showed that the model predicts well the spatial variation of digital counts from individual pixels of the sensor and the temporal variation of the histogram itself with repeated exposure.

Chapter 4
Color Detection

Visual processing begins with photo-transduction at the cone level in the retina. The cone signals then pass through the postreceptoral stage of opponent color channels. In order to allow a better assessment of subsequent perceptual computation, the goal is to clarify what aspects of behavioral color detection can be attributed to such early low-vision processing. In this chapter, we introduce the fundamentals of a quantitative approach to color detection and discrimination. To understand the noise-limited color detection behavior and the site of noise dominant channel in retinal coding, we then describe the results of three experiments on color detection.

4.1 Introduction

A quantitative approach to color measurement, according to the Young-Helmholtz trichromatic theory of color vision (von Helmholtz, 1909/1962; T. Young, 1802), attempts to represent colors by elements of three fundamental color mechanisms within a color space. In this space, a color stimulus is represented by a vector, the elements of which correspond to univariant responses from the three color mechanisms.

A pair of color stimuli become discriminable when the difference between the two stimuli exceeds some threshold. Such stimuli can be presented by their

corresponding vectors within the geometrical space of color mechanism. The difference between their corresponding vectors shows the magnitude of the difference between the two stimuli at the detection threshold level. Accordingly, this magnitude is assumed to be determined by the properties of the fundamental color responses. The line element model for color detection is proposed according this notion, presented in Figure 4.1, by which the contributions of the three fundamental mechanisms are quantified by their corresponding elements within the Euclidian response space. The line-element model of color detection (von Helmholtz, 1909/1962; Schrödinger, 1920/1970), based on receptoral stimulation, defines a threshold, ΔC, by the difference in the level of absorbed light energy in the three classes of cone photoreceptors,

$$\Delta C^2 = \alpha\,\Delta L^2 + \beta\,\Delta M^2 + \gamma\,\Delta S^2 \tag{4.1}$$

where, α, β, and γ are the weighting coefficients for each classes of cone mechanism.

The basic idea of the line-element model for color detection, presented in Eq.(4.1), was later generalized to porstreceptoral opponent channels (Le Grand, 1949; Koenderink, van de Grind, & Bouman, 1972), as

$$\Delta O^2 = {\Delta O_{lum}}^2 + {\Delta O_{rg}}^2 + {\Delta O_{by}}^2 \tag{4.2}$$

in which, ΔO is the difference in opponent space, and O_{lum}, O_{rg}, and O_{by} are responses from opponent channels, as shown in Figure 2.13. This two-stage model, in Eq.(4.2), involves responses from both the first level of receptoral mechanisms and the second stage of interaction between the activities of the three cone classes (Boynton & Kambe, 1980; Nagy, Eskew, & Boynton, 1987).

The notion of line-element for color detection and discrimination was later criticized by Stromeyer, Cole, and Kronauer (1985). The main criticism is that

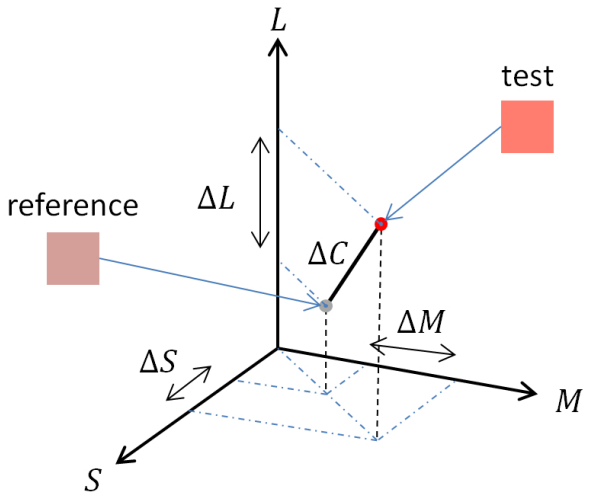

Figure 4.1: Two color stimuli become discriminable when the difference between the two stimuli, ΔC, is perceptually detectable. In the LMS cone excitation space, these two color stimuli are shown by their corresponding vectors, the difference of which quantifies the magnitude of perceived difference between them at the threshold level. In this plot, ΔL, ΔM, and ΔS are the differential elements of responses from each of the three cone mechanisms, stimulated by the reference and test patch colors.

the line-element model predicts a symmetrical, ellipsoidal contour for the positions of colors discriminated at threshold from a centered reference patch. If this prediction is true, this also must be the case when discrimination judgment is obtained towards any direction in a cone excitation space. This prediction failed in an experimental condition where both luminance and chromatic channels interact to determine the threshold (Stromeyer, Lee, & Eskew, 1992). Chaparro et al. (1993) showed that detection at threshold is elongated, in a parallel manner, more towards the incremental-decremental luminance channel than the chromatic one (Cole, Stromeyer, & Kronauer, 1990; Chaparro, Stromeyer, Chen, & Kronauer, 1995). According to the shape of the discrimination contour, being parallel along the red-green detection mechanism, Stromeyer et al. (1985) reported evidence for postreceptoral adaptation in the opponent pathways. The results of a chromatic discrimination experiment by Eskew, Newton, and Giulianini (2001) also

showed a deviation from an ellipsoidal discrimination contour. Giulianini and Eskew (1998) argued that the shape of discrimination contours can be specified by some detection mechanisms which may linearly or non-linearly respond to the cone contrast at threshold. Later, Eskew (2009) suggested that discriminability judgments are mediated by the contributions of a limited number of higher-order detection mechanisms at threshold level. In favor of contribution from higher levels of the visual pathway to color discrimination judgment, some studies also reported a asymmetrical detection contour (Vingrys & Mahon, 1998; Shepard, Swanson, McCarthy, & Eskew, 2016).

The visual mechanism underlying color detection and discrimination, inferred from the shape of the detection contour, became an issue of controversy. Wandell (1985a) found a discrimination contour with a mixture of 540 and 650 nm test lights, along the increment-decrement luminance axis. His data presented a symmetrical discrimination contour. Poirson and Wandell (1990) stated that color discrimination can be best explained by an ellipsoidal contour. Knoblauch and Maloney (1996) directly investigated possible deviations from an ellipse in discrimination contours, yet found ellipsoidal-shaped contours. A symmetrical, elliptical-shaped contour was not unexpected in Knoblauch and Maloney (1996) experiment because colors being discriminated mainly belong to the same *categorical region of color space* for an iso-luminance adapting condition (Wandell, 1985b).

4.1.1 Detection Theory

Another school of thought holds a fundamental view of the mechanisms of signal coding in early stages of visual processing that could potentially mediate color detection at threshold. Geisler (1987) developed the concept of the ideal observer as a tool for modeling the behavior of visual phenomena, in particular detection

and discrimination tasks (Geisler, 1989). The ideal observer theory is introduced based on sequential mechanisms, through which the information from an environmental stimulus is processed from an early visual mechanism to later stages of the visual system (Geisler, 1989). The model observer was further developed into a Bayesian model for quantitative evaluation of the performance in a visual task that maximizes the utility across available options (Geisler, 2011). Brainard et al. (2006) applied a Bayesian extension of an ideal observer model to optimally estimate chromatic properties of a color stimulus presented on a cone mosaic array.

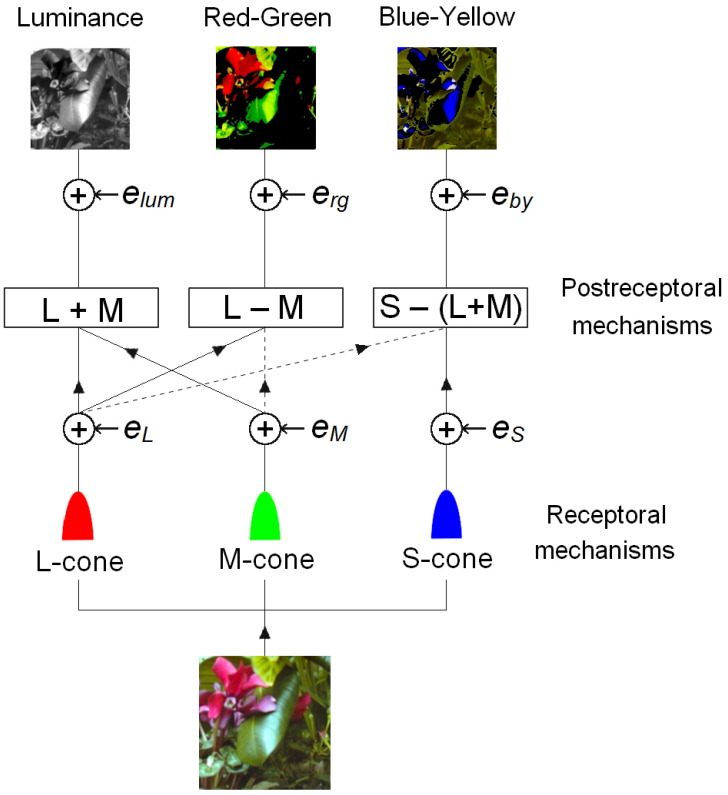

Figure 4.2: The signal detection theory for color threshold is proposed based on an uncertainty involved in visual signals due to the presence of noise. In this figure, a noise is added to signals from a receptoral mechanism. The noisy receptoral output is transformed into the postreceptoral stage of opponent mechanisms. The output of a postreceptoral channel is further contaminated with an additive noise before passing through higher visual stages (Stockman & Brainard, 2010).

The ideal observer theory incorporates the processing of a visual signal through stages of possibly noisy mechanisms. Before a discrimination judgment is made perceptually, the neural signals from a population of stimulated retinal cells are passed through several post-processing stages of connected networks. A noisy response from a receptoral or postreceptoral mechanism is assumed to impose a limit on a color detection mechanism. This is due to an uncertainty in signals from the visual mechanism (Pelli, 1985). This form of noisy transformation of signals from the receptoral zone to postreceptoral stage is shown schematically in Figure 4.2. This figure is plotted based on the assumption that output signals from both receptoral and postreceptoral channels are contaminated by some sources of additive noise.

4.2 Problem Statement

In 1942, Hecht et al. measured the light intensity at threshold when activity in photoreceptor cells is triggered by only a small number of photons. As discussed in section 3.1, the probability of photon absorption in a cell follows Poisson statistics. As a consequence of this Poisson fluctuation in absorption, there is a variability involved in the receptoral response to a dim-light stimulus. The probability of seeing light is modeled by random absorption of photons by a cell, in a discrete manner due to the quantum nature of light (Hecht et al., 1942; de Vries, 1943; van de Velden, 1946). Random absorption of photons in cells is the basis of fluctuation theory for detection, stating that the performance of color detection is influenced by noise at the retinal level. Fluctuation theory for detection of light at threshold was originally developed to predict the detection threshold when rod cells respond to dim flashes of light (Barlow, 1956, 1957). This theory

was later generalized from rod to cone cells to predict the behavioral sensitivity of chromatic vision (Bouman et al., 1963; P. L. Walraven, 1966). Likewise, the theory is built upon the assumption that discriminability judgment is limited by the presence of noise in a receptoral or postreceptoral channel (Trabka, 1968; Buchsbaum & Goldstein, 1979a, 1979b). To predict the behavior of color discrimination, fluctuation theory has been framed into models that incorporate Poisson noise characteristic in retinal coding (Bouman et al., 1963; Zhaoping, Geisler, & May, 2011; Bouman & Walraven, 1972). The source of this noise is either photon fluctuation or internal physiological mechanisms. Nevertheless, several sources of noise in early stages of visual coding may potentially contribute to limiting the performance of chromatic discriminability (Field, Sampath, & Rieke, 2005). In fact, some studies have shown that intrinsic sources of noise inherent in the physiological activities of retinal cells also play a role in light detection at threshold (Teich, R., Vannucci, & Breton M. E., 1982a, 1982b).

Although physiological investigations of retinal coding as well as behavioral analysis of color detection have advanced our understanding of the visual mechanisms that underlie discriminability judgments, it is still not well understood which characteristic mechanism is responsible for the noise-limited behavior of color discrimination, and how the physical properties of a color stimulus impact such behavior. Moreover, it is still not obvious which site of retinal coding gets involved in a noise-limited behavior at higher levels of light intensity when Poisson variation in absorption is thought to be insignificant relative to the signal level.

4.3 Distribution of Cone Excitations in Color Space

In Chapter 3, we introduced a model to determine the spatial variation in absorption by individual cells and the temporal variation in the number of cells at a given energy level when a population of identical photoreceptors is exposed repeatedly to uniform multi-wavelength light. Table 4.1 describes the parameters of the model, discussed in section 3.4, applied to a population of retinal photoreceptor cells.

Figure 4.3(a) represents the spatial variation of absorption in each class of cone cells, quantified as the variation of the corresponding histogram distribution. The temporal variation in the histogram itself is shown, in this plot, by a colored region around the expected histogram. Given that identical cells exposed to uniform light absorb different levels of energy, the excitation produced by one L-, M-, and S-cone triplet set might have different coordinates from the excitation in another LMS triplet. This notion is schematically illustrated in Figure 4.3(b). Due to the spatial variation in absorption by individual cells, our model predicts that a visual stimulation by light produces a distribution of responses within cone excitation space. Note that an additive noise model (see Figure 4.2) assigns a variation to pooled responses from a cone mechanism, whereas in our model the spatial and temporal sources of variation are characterized separately. Nevertheless, the spatial variation and additive noise model both predict that color detection and discriminability judgment is a noise-limited behavior. We will further discuss in Experiments 4.2 and 4.3, that our model determines the site of a noise-dominant channel based on the time parameter, Δt. As shown in Figure 4.4, we can directly plot the distribution of cone excitations in the MacLeod-Boynton (1979) chromaticity diagram.

Table 4.1: The table summarizes a list of parameters for estimating the histogram of absorption by individual cells. In Eq. (3.13), the collecting area, ϱ, is the effective area of a cell for capturing photons by photopigments packed within the outersegment disk membrane. In primates, the diameter of the disk sacks are about 1-3 µm depending on the retinal location and varies along the cell from the base to the tip (R. W. Young, 1971; Hoang et al., 2002). The spectral absorptance, J_ν, is a function of outer segment length, ℓ, and the absorptivity, D_ν. In Eq. (3.13), $\tau_\nu J_\nu$ is the cone fundamental (see section 2.5.4). The pupil area, A, can be calculated from the pupil diameter in Eq. (2.14), as a function of the stimulus luminance (Pokorny & Smith, 1997). The model is equally applicable to interaction of light with cells in forms of transmission or reflection. To obtain the histogram of the number of cells at levels of light energy transmitted through or reflected from cells, J_ν refers to the spectral transmittance or reflectance of a single photoreceptor.

Parameter	Description	Units
ν	Frequency	Hz
h	The Plank Constant	J s
E_ν	Spectral irradiance at the image plane	$\mathrm{W\,m^{-2}\,Hz^{-1}}$
$\ell\, D_\nu$	The spectral absorbance of a cell	–
ϱ	Collecting area of a cell	$\mu\mathrm{m}^2$
A_p	Pupil area	mm^2
f	Focal length of the eye (=16.6832)	mm
τ_ν	Pre-retinal spectral transmittance	–
J_ν	Spectral absorptance of a cell	–
$\tau_\nu J_\nu$	Cone fundamental	–
μ_Q	Average of absorbed energy by all the cells	J
σ_Q^2	Spatial variance of absorbed energy	J^2
Δt	Duration of exposure	s
N	The total number of like-type stimulated cells	–
N_Q	The number of cells with Q units of energy	–
$\bar{N}_Q$	Expected number of cells with Q units of energy	–
$var(N_Q)$	Temporal variance in N_Q	–

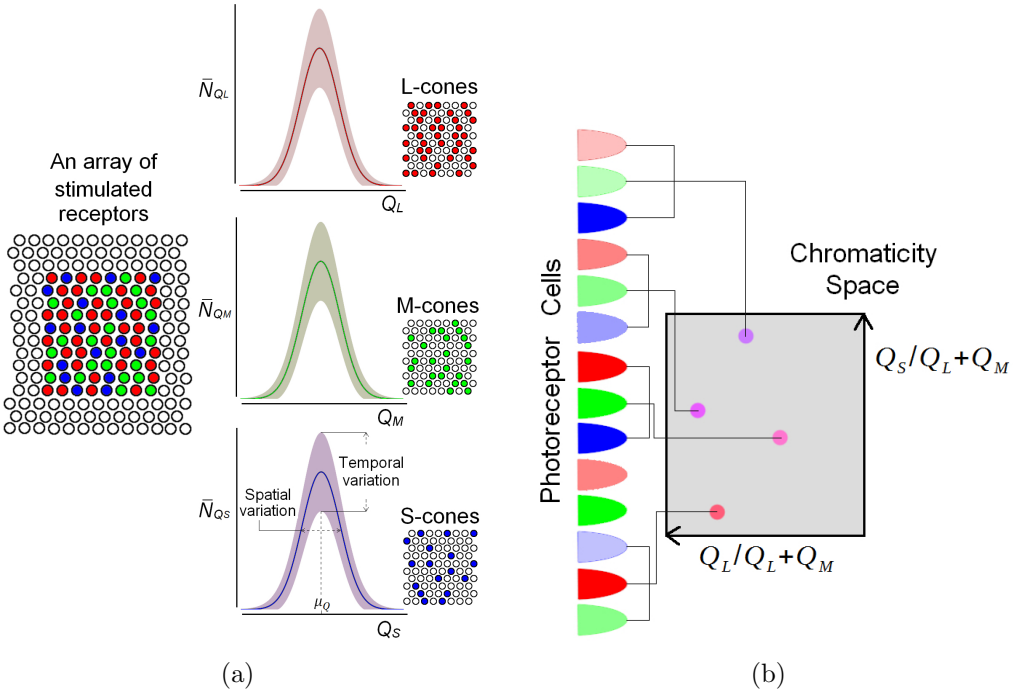

Figure 4.3: The spatiotemporal variation due to photon fluctuation. (a) When a population of N cells of like-type (L-, M-, or S-cone) is exposed repeatedly to a uniform photon flux, the histogram of the expected number of cells with Q units of absorbed energy, $\bar{N}_Q$, forms a Gaussian distribution, the variance of which quantifies the spatial variation of absorption in like-type cells. The region around the expected distribution shows the temporal variation in the number of cells at an energy level. (b) Two identical cells of the same class exposed to the same light absorb different levels of light energy. The excitation produced in one L-, M-, and S-cone triplet set might have a different coordinate from the excitation in another LMS triplet. Thus, spatially homogeneous color stimulation does not produce a single response point within the physiological cone excitation space.

To illustrate the distribution of excitation scatterings due to photon fluctuation, we selected 25 color centers of MacAdam's (1942) ellipses. The spectral radiance of a color at the luminance of $50\,\mathrm{cd\,m^{-2}}$ is produced by a mixture of three Gaussian-shaped virtual primaries with the center wavelengths of 455, 520, 650 nm and a FWHM (full width at half maximum) of 30 nm. We used the Monte Carlo method to randomly generate excitations in the three types of cone cells using Eq. (3.15). The model parameters for the human cone cells are listed in

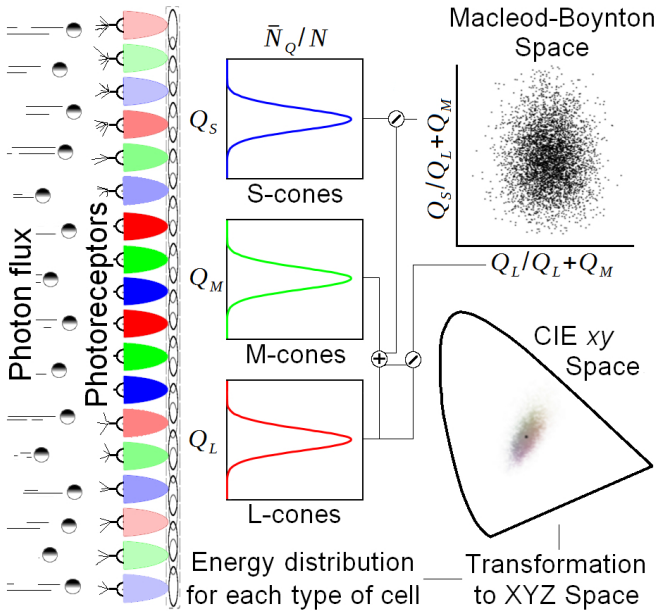

Figure 4.4: Photoreceptors of like-type exposed to uniform stimulating light absorb different levels of energy. Due to spatial variation in absorption by individual cells, a visual stimulation produces a distribution of responses within the cone excitation space. Such excitations in cone cells can be presented within the MacLeod-Boynton chromaticity diagram, where $(\mathrm{r}, \mathrm{b}) = (Q_L/Q_L+Q_M\,,\, Q_S/Q_L+Q_M)$ and Q_L, Q_M, and Q_S are energies absorbed by individual L-, M-, and S-cone cells, respectively. As shown in Eq. (2.28), the triplet, (Q_L, Q_M, Q_S), can be linearly transformed to the CIE XYZ space (Wyszecki & Stiles, 1982, p. 615).

Table 4.1. For the purpose of illustration, we take $\Delta t = 1\,\mathrm{s}$ and $\varrho = 2\,\mu\mathrm{m}^2$, and use the Smith and Pokorny (1975) cone fundamentals. Figure 4.5(a) shows the distribution of cone excitations for each of the 25 MacAdam color stimuli in the MacLeod-Boynton (1979) chromaticity diagram. Note that the MacLeod-Boynton (1979) r and b coordinates, $(\mathrm{r}, \mathrm{b}) = (Q_L/Q_L + Q_M\,,\, Q_S/Q_L + Q_M)$, in this plot are not independent variables and their joint probability follows a form of ratio distribution (Pham-Gia, Turkkan, & Marchand, 2006). The distribution of cone excitations represented within the Judd-Vos modified CIE 1931 chromaticity space in Figure 4.5(b) closely resemble those of the magnified chromaticity scatterings obtained by MacAdam (1942) for the variability of color matches.

The MATLAB codes for generating the plots in Figure 4.5 is available, under an open-source MIT license, at `https://github.com/peyvandi/light-energy-distribution-among-photoreceptors` [see Code File 1 in Peyvandi, Ekroll, and Gilchrist (2016)].

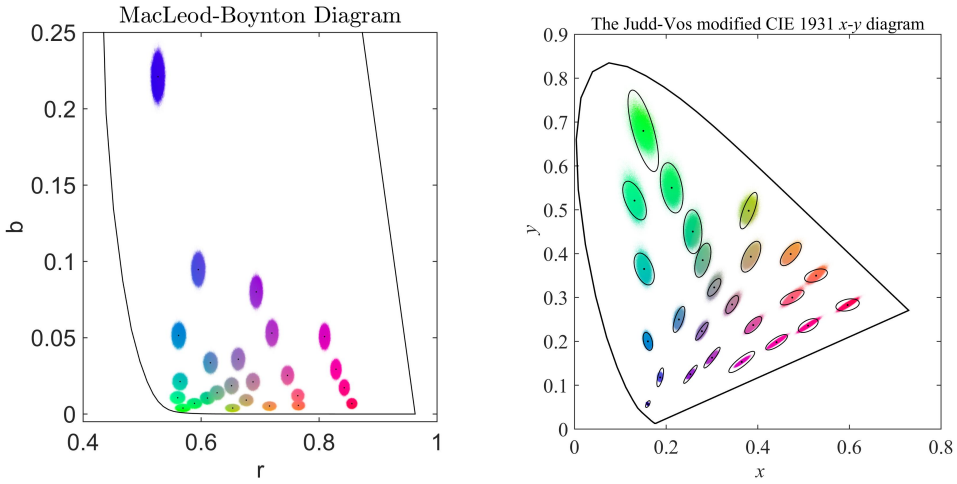

(a) (b)

Figure 4.5: A Monte-Carlo simulation of the distribution of receptoral excitation responses from a population of L-, M-, and S-cone cells, stimulated by uniform light. (a) A Monte Carlo simulation of excitations in cone cells exposed to the 25 MacAdam color stimuli shown within the MacLeod-Boynton chromaticity diagram. (b) Assuming that the cone responses are linearly related to the color-matching functions (Stockman, 2016), the triplet, (Q_L, Q_M, Q_S), is linearly transformed to the Judd-Vos modified CIE 1931 XYZ space from which distributions for the same 25 stimuli are plotted within the xy chromaticity space (see Eq. (2.28)). The black contours are ellipses observed by MacAdam (1942), re-plotted from the data given by Wyszecki and Stiles (1982, p. 309).

The simulation result presented in Figure 4.5 is not trivial because the distribution of chromaticities for a color stimulus is directly obtained from the corresponding cone excitations and it also supports the notion of a probabilistic representation of color within a color space rather than a deterministic one (Wandell, 1982). The simulated distribution shown in Figure 4.5(b) closely resemble MacAdams classic measurements of the variability of color matches in

terms of shape, orientation and relative size. Note that we did not obtain such scattering for a color stimulus by defining an uncertainty criterion for perceptual color detection mechanism. However, Pelli's (1985) theory of uncertainty for color discrimination requires detection to occur when a channel response exceeds a specific criterion value. The shape of scattering obtained in a color matching sensitivity experiment (MacAdam, 1942) was found to be different from a contour obtained by discrimination judgment experiments (Wright, 1941, 1947). Wyszecki and Stiles (1982, p. 574-575) suggested that this disagreement, although difficult to explain, may not be large enough to be significant. It might be the case that MacAdam's (1942) variability of color matches is attributable to the variation in receptoral signals, as shown in Figure 4.5, which may not require a criterion-based judgment for detection. This is because the difference between a pair of stimuli may not be large enough to trigger such a detection mechanism. This assumption implies that the identical perception of physically different colors is inescapable, right at the receptoral level, because the cells triggered by the two stimuli statistically provide the same responses.

Although the abovementioned assumption attributes the variability of color matches to the spatial variation of excitations in the three cone channels when photons are captured by photopigments, the behavioral color sensitivity predicted by this model is the same as an uncertainty model which incorporates noise in the outputs of receptoral channels (Vorobyev & Osorio, 1998). This is because both interpretations fit within the framework of fluctuation model that incorporates a limiting role of receptoral noise on color detection performance. However, if receptoral noise, caused by photon fluctuation in each cone channel, limits the performance of color detection, our model should predict color detection behavior by a criterion-based contour obtained from a fixed set of parameters.

4.4 Color Detection

We carried out an experiment to empirically evaluate color detection behavior at threshold.

Experiment 4.1. We hypothesized that two color stimuli are not perceived as being different until the energy distribution of the two stimuli for cone mechanisms are separated at a specific statistical distance.

Participants. 15 undergraduate students (ages 18-24) at Rutgers-Newark volunteered to serve as subjects to satisfy a course requirement. All subjects were tested for normal color vision using the Ishihara color plates (Ishihara, 1974). The study was approved by the Institutional Review Board (IRB) at Rutgers University and all subjects received the consent form before participation.

Stimuli. Stimuli were presented on a LaCie (electron-19-blue) monitor with a vertical refresh rate of 60 Hz. Based on the procedure suggested by Brainard (1989), the monitor was calibrated to obtain a linear relation between 8-bit digital output and luminance values, ranging from $\sim 0.5\,\mathrm{cd\,m^{-2}}$ up to $\sim 75\,\mathrm{cd\,m^{-2}}$. A stimulus is a $2 \times 2\,\mathrm{cm}^2$ square-shaped target located at the center of an equiluminant neutral surround of luminance $5\,\mathrm{cd\,m^{-2}}$. The monitor screen was placed at the distance of 60 cm from an observer ($\sim 2^\circ$ target view angle). The observers head was stabilized by a chin rest in front of the display.

Method. The experiment started after one minute of dark adaptation, followed by 30 s of adaptation to the neutral gray surround with a CIE-xy coordinate of (0.333, 0.333). The colorimetric purity of the target was changed at random towards a given point on the spectral locus. The formula of colorimetric purity, p_c, is given by Wyszecki and Stiles (1982, p. 175). At each wavelength, a total of 200 target stimuli, with different purities, was presented to an observer, each

for 1 s. The task for the subject was to judge whether the small disk is chromatic or neutral patch, as suggested by the original uncertainty model (Pelli, 1985). The purity at threshold with 50% probability of occurrence was found by fitting a Weibull psychometric function to the data. We tested color detection towards a total of 10 different dominant wavelengths.

As predicted by our model, a color stimulus can be characterized by a distribution of energy absorbed by like-type cells for a cone mechanism. This distribution is shifted by gradual departure from the reference surround gray towards a given test point on the spectral locus. We measured the Bhattacharyya (1943) distance (BD) between the energy distributions of the surround gray and the test stimulus as a magnitude of overlap between the two distributions. For the three independent mechanisms, the BD between trivariate energy distributions of the two stimuli is the product of the BDs measured for each type of cone mechanism.

Results. The results of this experiment define an equiluminant detection contour shown in Figure 4.6. The average detection threshold at $5\,\mathrm{cd\,m^{-2}}$ is located approximately on a contour which satisfies $BD = 0.995$ between the trivariate energy distributions of the reference white and a deviated stimulus towards a spectral color. The purity at threshold is presented in Figure 4.6(b) as a function of wavelength.

Discussion. The detection behavior at threshold shown in Figure 4.6(a) well represents an elliptical contour. This result is consistent with the finding reported by Knoblauch and Maloney (1996). This consistency is not unexpected. Stockman and Brainard (2010) suggested that deviation from an ellipse is more likely to be observed under the condition that color detection is determined by different mechanisms simultaneously. This condition is satisfied in some previous experiments (Stromeyer et al., 1985, 1992; Chaparro et al., 1993; Giulianini &

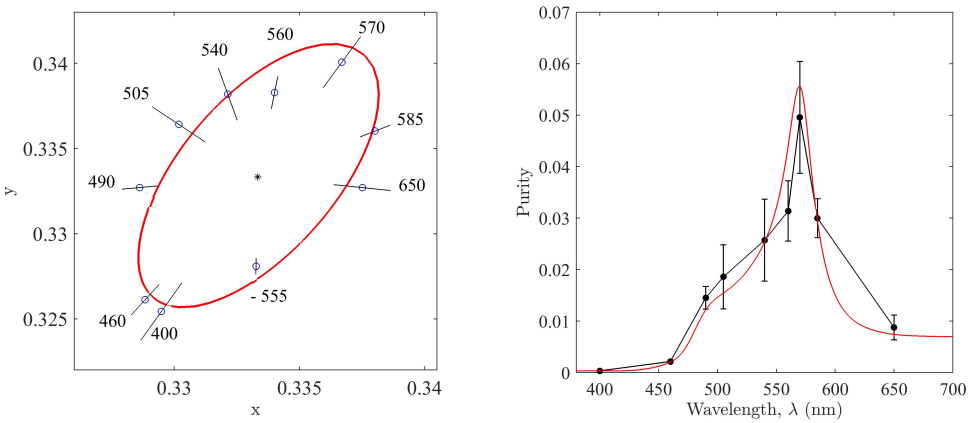

(a) (b)

Figure 4.6: The color detection behavior at threshold for target colors on an equiluminant gray surround with the CIE-xy coordinate of (0.333, 0.333) at $5\,\mathrm{cd\,m^{-2}}$. (a) The average of empirical results at each dominant wavelength is shown by a blue open circle with one standard deviation around the mean shown by a black line. The red contour is predicted by the model. All the points located on the red contour satisfy $BD = 0.995$ between the trivariate energy distributions of the reference surround and deviated stimuli across the spectrum. (b) Purity at threshold is plotted as a function of wavelength. Data points are means ± SD. The solid curve shows the prediction.

Eskew, 1998), in which different regions of a detection contour are determined by chromatic and luminance mechanisms. In our experimental condition, we do not expect to observe a significant deviation from an elliptical contour because the color stimuli, in our experimental condition, triggers the same L+M luminance mechanism, and thus falls within the same categorical region in color space.

As shown in Figure 4.6(b), the level of purity at threshold peaks at 570 nm dominant wavelength. This result, as predicted by the model, is consistent with the previous observation by Wright (1947, p. 161-166). The result, shown in Figure 4.6, can be also predicted by the line-element model. This model, in Eqs. (4.1) and (4.2), also predicts an elliptical contour for the behavior of chromatic detection at threshold. The difference is that our model predicts detection as a Poisson

noise-limited behavior. Vorobyev and Osorio (1998) suggested that noise is generated in the receptoral mechanism, but propagates into the postreceptoral stage and that threshold is determined by the mechanism in which noise is dominant. Several studies (Stromeyer et al., 1985; Cole, Hine, & McIlhagga, 1993; Stromeyer et al., 1992) reject the notion that receptoral mechanism plays a role in detection threshold and instead support contribution from the postreceptoral mechanism. We address this problem in details in section 4.7.

4.5 Intensity Dependency of Chromatic Discrimination

The result of Experiment 4.1 merely shows that the shape of the color detection contour is approximated by incorporating receptoral noise. However, this experiment does not show the performance of the model in predicting the dependence of chromatic detectability on the absolute luminance of the stimulus. Such dependency is the key to find out whether the chromatic discrimination judgment is a noise-limited behavior or not. If so, it helps to understand the nature of noise source and further determine the site of retinal coding where such noise is so dominant that limits the performance of color discrimination.

The noise-limited behavior of chromatic discrimination as predicted by fluctuation theory (Bouman & Walraven, 1972) predicts poorer discrimination at lower luminance level. Nevertheless, in the classic experiment by Wright and Pitt (1934), the intensity was not kept the same across the spectrum, with the assumption that the magnitude of discrimination is roughly independent of intensity within a wide range. Wright and Pitt (1934), however, reported that discrimination deteriorated appreciably at very low level of light intensity. The assumption of intensity-independent discrimination behavior was later confirmed in an experiment by Bedford and Wyszecki (1958) within a relatively wide range

of intensity levels. The authors even reported a non-significant converse result, that discrimination was slightly better at the lowest light intensity. To seek a resolution of the discrepant findings reported in the literature (Wright & Pitt, 1934; Bedford & Wyszecki, 1958; Bouman & Walraven, 1972), we performed a numerical analysis of the spectral discrimination at different light intensities, as predicted by our model. To perform this analysis, we kept all the parameters of our model, including the duration of exposure, $\Delta t = 1\,\mathrm{s}$, constant. To predict the behavior of color detection and discrimination, we changed only the luminance at three different levels of the stimulating light.

4.5.1 Color Detection and Wavelength Discrimination

Let's take an equal energy white of a specific luminance as a reference patch. A gradual departure from the reference white toward the test wavelength, λ, is given by a weighted mixture (m) of white light, I_W, with a narrowband monochromatic light, I_λ, of the same luminance, using, $m = (1-\omega)I_W + \omega I_\lambda$, in which the weight ω increases from 0 to 1, and so the colorimetric purity. To perform a numerical analysis, we take a narrowband monochromatic light simulated by a Gaussian-shaped radiance function with FWHM $= 5\,\mathrm{nm}$. As a criterion for the discriminability judgment, we take the chance level of discrimination at $BD = 0.5$. For each wavelength, we increased the weight ω until this criterion is satisfied. The numerical experiment was done by having MacLeod-Boynton luminance, V, constant at 0.147, 1.031, and 4.418 levels. For the three luminance levels, Figure 4.7(a) shows the value of $-log(\Delta p_c)$ necessary to reach the defined chance level of $BD = 0.5$. The spectral curve of purity discrimination is consistent with behavioral observations by Wright and Pitt (1937). This behavior is also confirmed by our experimental result in Figure 4.6(b). As shown in Figure 4.7(a),

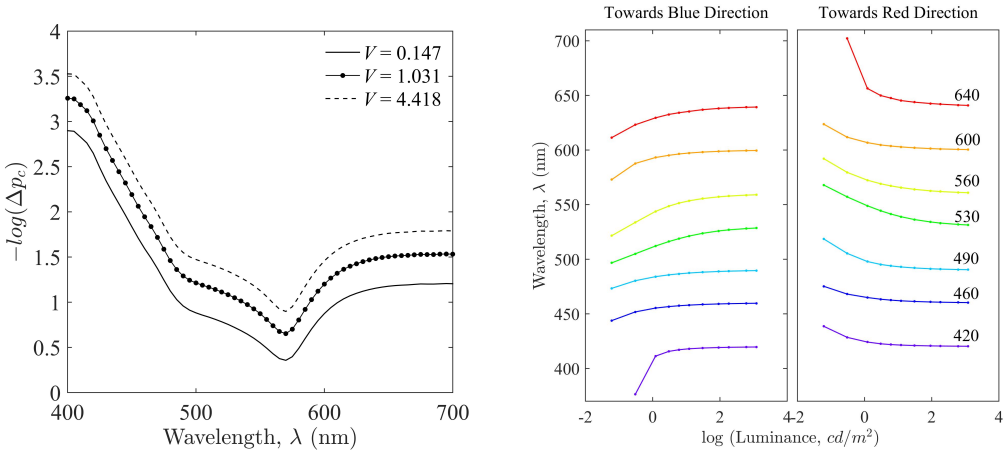

(a) (b)

Figure 4.7: The performance of color detection and discrimination, predicted by our model with a fixed set of parameters. (a) The spectral curve of purity discrimination at different levels of stimulus intensity. The performance of color detection behavior at threshold is enhanced at higher levels of light intensity. This prediction, within such a small range of the stimulus luminance, is apparently not consistent with the previous observation by Bedford and Wyszecki (1958). (b) Wavelength discrimination deteriorates with decreasing the light intensity up to a magnitude of 3-4 log-cd m^{-2}. This prediction is consistent with a fluctuation model that incorporates the photon-generated receptoral noise into a color detection model (Bouman & Walraven, 1972). This prediction is also consistent with previous observations (Weale, 1951; Thomson & Trezona, 1951).

with a fixed set of parameters, the model predicts better sensitivity at higher levels of stimulus intensity. Although consistent with the Bouman and Walraven (1972) fluctuation hypothesis, there is reason to be skeptical about this prediction because the enhancement of sensitivity is significantly greater than what one might expect for such a small range of intensity variation, from ~ 5 up to $160\,\mathrm{cd\,m^{-2}}$. Bedford and Wyszecki (1958) performed experiments within a much wider intensity range, yet no significant increase in discriminability was observed.

Several studies (Weale, 1951; Brown, 1951; Thomson & Trezona, 1951) showed that discrimination deteriorates with decreasing luminance levels and that the effect of luminance on color discrimination is also a function of wavelength. We

performed a numerical experiment by taking a narrowband monochromatic light, I_λ, of a specific luminance as a reference stimulus. Departures from the reference monochromatic stimulus of wavelength λ toward longer and shorter wavelengths, specified by $+\Delta\lambda$ and $-\Delta\lambda$, results in decreasing the BD between the trivariate energy distributions of the reference and shifted stimuli. With MacLeod-Boynton luminance constant at a specific level, we measured the deviation from a reference stimulus toward longer and shorter wavelengths until the criterion, BD = 0.5, was satisfied in each direction. In Figure 4.7(b), wavelength discrimination as a function of luminance levels is presented toward red and blue directions, separately. In each plot, each dot indicates the wavelength at which BD = 0.5 is satisfied for the corresponding luminance level. In agreement with previous observations (Weale, 1951; Thomson & Trezona, 1951), the performance of wavelength discrimination deteriorated with decreasing luminance. The prediction of better discrimination at higher levels of stimulus intensity holds true only if we assume that receptoral noise becomes smaller relative to the signal when the stimulus luminance increases. If a stimulus of varying intensity does not significantly influence an equilibrium condition at the cone level, then there should not be a significant change in discrimination performance. The result shown in Figure 4.7 was predicted when all the parameters of our model, including the time Δt, was held constant at different levels of stimulus intensity. We discuss, in the following sections, conditions under which the parameter of time becomes a function of light intensity.

4.5.2 The State of Equilibrium

To reconcile this contradictory finding, we should pay attention to the parameter of time, Δt, which has been mainly overlooked in the literature on fluctuation

hypothesis. Ignoring this parameter, however, might be justified by the fact that a stimulating light energy is expressed by the rate of photons incident upon the retinal cells, thus absorption and subsequent excitation is assumed to be proportional to the rate of incoming photons. We argue that this is not a valid assumption so far as fluctuation in absorption is concerned. In order for Eq. 3.7 to be physically valid, the argument mp in Eq. (3.10) must be dimensionless because it is an exponent in Eq. (3.7). Thus, the factor of time must take a quantity to satisfy this requirement. As explained in section 3.3.1, Δt refers to the duration of exposure. The model presented in section 3.4 originally applied to dark adapted-photoreceptors exposed to flashes of light. This condition requires the presentation of light to be so fast that the receptoral adaptation state is not distorted by the light stimulus. In an experimental condition where the stimulus is left on for a long period of time, it might be the case that the factor of time in our model takes a value to reflect energy at an equilibrium condition. This is because, due to the bleaching process, absorptance by a cell becomes a time dependent parameter up until the point when photochemical activation at equilibrium is reached (Rushton & Henry, 1968; Sabesan, Hofer, & Roorda, 2015).

The assumption of a receptoral state of equilibrium might reconcile the apparent contradictory findings reported in the literature on the effect of luminance on color discrimination performance (Weale, 1951; Thomson & Trezona, 1951; Bedford & Wyszecki, 1958). This assumption implies insignificant change in the performance of color detection and discrimination within some ranges of stimulus intensity where receptoral equilibrium is reached and is approximately constant for a long enough period of exposure. If this assumption is true, then the performance of color detection should be a function of both exposure time and stimulus intensity, with a significant interaction.

4.6 Time-Luminance Interaction in Color Detection

We designed an experiment to evaluate the performance of color detection as a function of luminance, at two levels of stimulus exposure.

Experiment 4.2. The general hypothesis is that the performance of color detection at threshold becomes independent of the field luminance if the state of equilibrium in the noise-dominant channel is not altered by changing the stimulus luminance. We measure the behavior of color detection at two levels of exposure time and different levels of stimulus intensity. If light intensity does not facilitate color detection across all possible exposure durations whatsoever, then the fluctuation hypothesis based on the assumption of Poisson-noise-limited behavior is clearly wrong.

Participants. A total of 10 naïve observers, undergraduate students at Rutgers University, participated in this experiment in exchange for course credit. All subjects were tested for normal color vision using the Ishihara color plates (Ishihara, 1974). Each observer participated in all experimental conditions.

Stimuli. Stimuli were presented on a calibrated LaCie (electron-19-blue) monitor with a refresh rate of 60 Hz. The observer-stimulus geometry was the same as the geometry used in Experiment 4.1, with $\sim 2^{\circ}$ field of view for the target. An equiluminant target stimulus was presented on a gray surround at two luminance levels of 5.0 and 20.0 $\mathrm{cd\,m^{-2}}$, with the CIE-xy coordinate of (0.333, 0.333). For accurate timing in the brief presentation, we presented the target stimulus within a time frame imposed by the refresh rate of the display. That is, the number of *ticks* multiplied by the timing interval of 1000/60 ms, where 60 is the display refresh rate (Garaizar, Vadillo, López-de-Ipiña, & Matute, 2014). At each luminance level, we tested two levels of exposure duration, $\sim$ 70 and 200 ms, i.e. 4

and 12 ticks, respectively. We used Python code with PsychoPy software package (Peirce, 2007) to design the experiment. We tested detection of colors with the dominant wavelengths of 460 and 520 nm.

Method. The experiment was conducted in a dark room after one minute of dark adaptation. We measured detection thresholds with a two-alternative forced choice staircase (2AFC) method using a procedure similar to that suggested by Eskew et al. (2001). The observer initiated the experiment after 30 seconds of adaptation to the steady gray surround. An experimental condition consisted of 120 pairs of alternatives. The observer selected one of the two alternatives that included a detectable color patch. The two alternatives were separated temporally with a time interval equal to $2 \times \Delta t$, in which Δt is the duration of exposure. We decreased the target-surround color contrast after each incorrect response. The contrast was increased after three correct responses. The color detection thresholds, with 90% probability of occurrence, was found by fitting a Weibull psychometric function to the data.

Results. Figure 4.8 shows the threshold purity for detecting colors with dominant wavelengths of 460 and 520 nm. In each plot, the mean threshold of purity is plotted for $\sim$ 70 and 200 ms presentation of an equiluminant target on a gray surround of 5.0 and 20.0 cd m^{-2} luminance levels. The effect of the field luminance on color detection threshold is significant for a brief presentation of $\sim$ 70 ms (460 nm: $t(9) = 3.53, p < 0.05$, and 520 nm: $t(9) = 5.20, p < 0.01$). Besides, there was no significant effect of the luminance on color detection for a presentation of $\sim$ 200 ms (460 nm: $t(9) = 1.13, p = 0.289$, and 520 nm: $t(9) = 0.88, p = 0.402$).

A 2×2 repeated measures ANOVA was conducted on exposure time, Δt, with luminance as factors. The main effect of exposure time was significant for both of the target colors (460 nm: $\mathrm{F}(1, 9) = 46.74, p < 0.01$, and 520 nm:

$F(1,9) = 55.49, p < 0.01$). The main effect of luminance was also significant for both of the target colors (460 nm: $F(1,9) = 26.32, p < 0.01$, and 520 nm: $F(1,9) = 35.45, p < 0.01$). The interaction was not significant for the case of 460 nm ($F(1,9) = 4.60, p = 0.061$), but significant for detecting a color of 520 nm ($F(1,9) = 10.59, p < 0.01$).

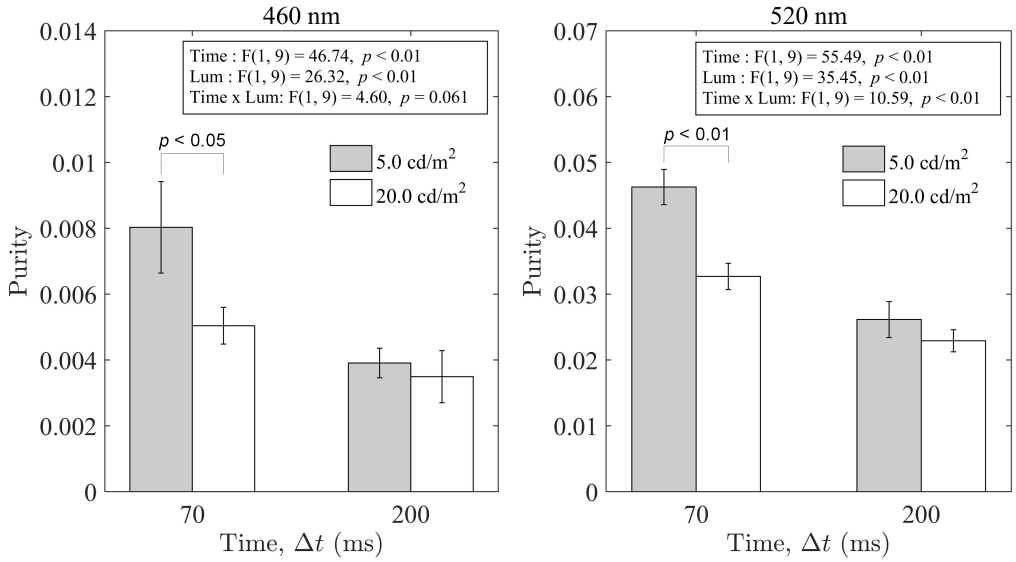

Figure 4.8: The purity at threshold for detecting colors with dominant wavelengths of 460 and 520 nm. The stimuli were briefly presented, for $\sim$ 70 and 200 ms, on an equiluminant gray surround, with the CIE-xy coordinate of (0.333, 0.333), at 5.0 and 20.0 cd m^{-2} luminance levels. Each plot shows the result of a 2×2 repeated measures ANOVA. Error bars are standard errors of the mean ($n = 10$). (a) The mean purity at threshold for detecting a color of 460 nm. (b) The mean purity at threshold for detecting a color of 520 nm.

Discussion. In this experiment, we evaluated color detection at threshold for a brief stimulus presentation. The state of adaptation is assumed to be constant when a target stimulus is presented briefly on an equiluminant surround (Wandell, 1985b, 1985a, 1982). In this case, momentary-produced signals by a brief change in the adapting field were not influenced by a slow adaptation mechanism, but were affected by an instantaneous neuronal adaptation mechanism of

the transducer process (Rinner & Gegenfurtner, 2000).

It is very unlikely that receptoral adaptation is altered significantly within such a small range of adapting luminance. This is because, first, the presentation of the stimulus is fast enough to hold the state of adaptation constant. Second, if receptoral adaptation influenced our detection threshold, then we would expect to observe a significant effect of field luminance across all conditions. The exposure duration of 200 ms is much smaller than the time course of cone adaptation over which the photochemical activation reaches a steady state. Yet, there was no significant effect of luminance on detection threshold. If we assume that Poisson source of noise, due to photon fluctuation, is present in the receptoral stage, this result indicates that the signal to noise ratio is not altered by brief stimulation of varying luminance in our experimental conditions. The elevation of the field luminance improved detection for a brief presentation of 70 ms. This observation is in agreement with our prediction that signal to noise ratio is elevated in a postreceptoral channel by increasing the field luminance. Nevertheless, given that the range of adapting luminance in this experiment is small (5.0 and 20.0 $\mathrm{cd\,m^{-2}}$), the result does not reject the possibility that detection can also be affected by cone adaptation (Shapley, Kaplan, & Purpura, 1993).

4.7 Temporal Dynamics of Detection Threshold

In Experiment 4.2, we studied the performance of color detection as a function of stimulus luminance, at two levels of stimulus exposure time. The result of this experiment shows that the detection threshold is influenced by light intensity for a brief stimulus presentation. Now we ask "is this behavior caused by a source of noise in the retina?" If so, then "where is the site of the noise-dominant channel in this case"? Another important question is why isoluminant color

detection at higher exposure duration is not altered significantly by changes in the stimulus intensity from 5.0 to 20.0 cd m^{-2}. If the detection threshold is limited by light-driven fluctuations of a Poisson nature in a noise-dominant channel in the retina, then there must be a condition of brief exposure under which the detection threshold is improved by light intensity. This is because, in general, an increase in light intensity is expected to provide a higher signal to noise ratio (see Experiment 3.1). However, the original model of Poisson fluctuation hypothesis (Bouman & Walraven, 1972) predicts deterioration of detection at lower stimulus intensity, whereas our model predicts that the signal to noise ratio in a response channel remains the same, regardless of the field luminance, so long as the state of equilibrium is being held constant in this channel. We addressed the above-mentioned questions in an experiment where the isoluminant detection threshold is evaluated behaviorally as a function of both exposure duration of a stimulus and its intensity.

Experiment 4.3. This experiment is a version of Experiment 4.2 extended to four levels of exposure duration. This allowed for investigating the time course of color detection threshold at two levels of luminance.

Participants. In a within-subjects design, a total of 10 naïve observers with normal color vision volunteered to serve as subjects to satisfy a course requirement.

Stimuli. The color stimuli, device and viewing geometry were all similar to those of Experiment 4.2. In this experiment, an equiluminant target was presented briefly on a neutral gray surround at two levels of the field luminance levels of 6.0 and 24.0 cd m^{-2}. Experimental conditions included a brief exposure of a target at 33.3, 83.3, 150.0 and 250.0 ms (i.e. 2, 5, 9 and 15 ticks, respectively). We tested detection of a blue, a green, a yellow and a red color with the dominant wavelengths of 460, 490, 570 and 600 nm, respectively.

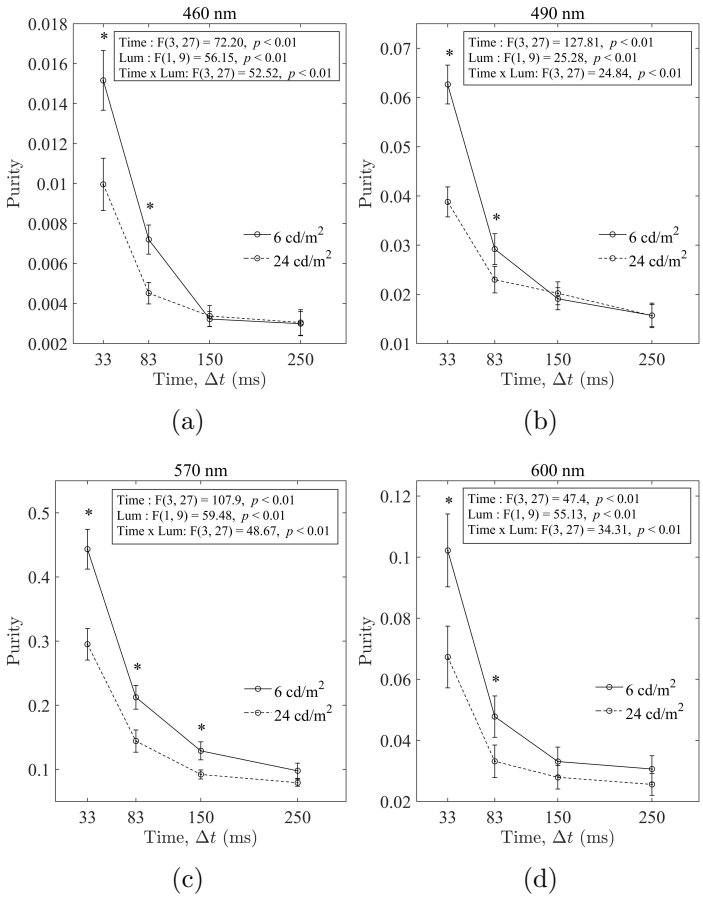

Figure 4.9: The temporal dynamics of purity at threshold for detecting (a) a blue (460 nm), (b) a green (490 nm), (c) a yellow (570 nm), and (d) a red (490 nm) color on an equiluminant neutral gray surround at two luminance levels of 6.0 and 24.0 cd m^{-2}. Each plot shows the result of a 4×2 repeated measures ANOVA. Data are means $\pm$ SE ($n = 10$). Significant difference for an instance of stimulus exposure time, Δt, is denoted by an asterisk ($p < 0.05$).

Method. The procedure was the same as that of Experiment 4.2. In this experiment, observers took a 2-3 minute break in a dark room between conditions.

Results. Each plot in Figure 4.9 shows the temporal dynamics of color detection threshold, for a selected dominant wavelength, as a function of luminance. Each plot also shows the result of a 4×2 repeated measures ANOVA, performed on the exposure duration, Δt, and the stimulus luminance as factors. For the four selected wavelengths, both the exposure duration and the stimulus luminance had

significant impacts on the threshold. The interaction was also significant for all of the four target colors. The behavioral data of color detection and the temporal dynamics at two levels of the field luminance, obtained from an observer, are shown in Figure 4.10.

The stimulus luminance did have a significant impact on the detection threshold for the exposure duration of 33.3 ms (460 nm: $t(9) = 8.66, p < 0.01$; 490 nm: $t(9) = 6.71, p < 0.01$; 570 nm: $t(9) = 8.82, p < 0.01$; 600 nm: $t(9) = 24.67, p < 0.01$). However, as shown in Figure 4.9, the stimulus intensity is less likely to have a significant impact on the detection threshold at higher durations of stimulus presentation.

Discussion. Three distinct characteristics are evident from the results shown in Figures 4.9 and 4.10. First, a temporal dynamic of isoluminant detection threshold represents a rapid non-linear decay. Investigations on the effect of retinal illuminance on the state of a photochemical equilibrium of cone absorption shows a sluggish temporal dynamic (Rushton & Henry, 1968; Smith, Pokorny, & van Norren, 1983). The time course of visual threshold represents the order of magnitude in minutes when cone photopigments regenerate over time (Rushton, 1965, 1963). If this behavior were due to adaptation at the cone level, we should have observed a much slower time course of color detection. The rapid non-linear decay of a dynamic curve within 200-300 milliseconds supports the notion that momentary-produced signals by a brief change in the adapting field are not influenced by slow adaptation in cone mechanism, but are affected by an instantaneous neuronal adaptation mechanism (Kaplan & Benardete, 2001). Second, the dynamic curves show that the elevation of the field luminance improved color detection only for a short duration of stimulus presentation. One possible explanation is that the detection threshold is limited by fluctuations of a Poisson nature and that such

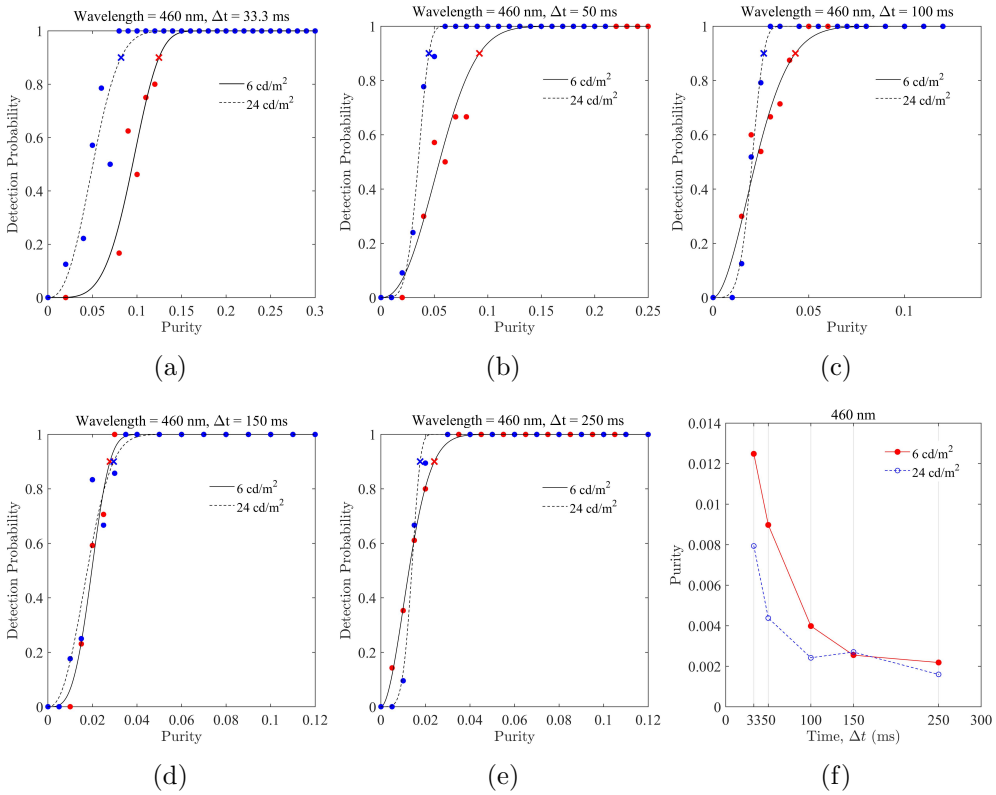

Figure 4.10: The results of color detection behavior obtained from one observer. An equiluminant target, with the dominant wavelength of 460 nm, was presented on a neutral gray surround. The behavioral data obtained at the two luminance levels of 6.0 and 24.0 cd m^{-2} are shown by red and blue dots, respectively. The Weibull psychometric function was fitted to behavioral data. A cross sign in each plot shows the threshold at 90% probability of occurrence. The results for the five durations of exposure, Δt, are presented in (a) at $\sim$ 33 ms, (b) at 50 ms, (c) at 100 ms, (d) at 150 ms, and (e) at 250 ms. (f) The temporal dynamics of purity at threshold are plotted at two levels of luminance.

elevation is caused by a higher signal to noise ratio. It is very unlikely that such elevation is caused by higher signal to photon noise ratio at the cone level. This is because a brief stimulus exposure of about 30 ms within a small range of the field luminance from 6.0 to 24.0 cd m^{-2} cannot significantly alter the photochemical equilibrium, but it does influence neuronal signals in the postreceptoral stage. Therefore, the behavior of detection threshold in our experimental condition is possibly determined by postreceptoral processing. If the detection threshold is

limited by fluctuations of a Poisson nature in the postreceptoral mechanism, then our fluctuation model should approximately predict detection deterioration when the field luminance is decreased from 24 to 6.0 $\mathrm{cd\,m^{-2}}$. Figures 4.11(a) and 4.11(b) shows detection contours for a brief presentation of color stimuli on an equiluminant gray surround at 30 ms, for the two levels of the stimulus luminance. To evaluate the performance of the model in predicting the difference between detection contours, we plotted in Figure 4.11(c), the difference between the threshold purity under 6.0 and 24.0 $\mathrm{cd\,m^{-2}}$ as a function of wavelength. This plot supports the assumption that detection contour is limited by a fluctuation of Poisson type.

The third characteristic of the data shown in Figure 4.9 is that dynamics of isoluminant color detection at two levels of field intensity converge non-linearly to an asymptote of threshold. The original model of the Poisson fluctuation hypothesis predicts deterioration of detection at lower stimulus intensity, whereas our notion of an equilibrium condition predicts that the signal to noise ratio in the postreceptoral response channel remains the same, regardless of the field luminance, so long as the state of equilibrium in this channel is being held constant.

4.8 Conclusion

In this chapter, we showed that some levels of uncertainty in color vision, are due to low-level vision and the quantum nature of light itself as it interacts with an array of interleaved photoreceptors. Our model of the spatial variation in absorption by individual cells implies that visual stimulation of a cone cell produces a distribution of responses in the cone excitation space. We showed that the resulting excitations reproduce MacAdams classic measurements of the variability of color matches. To understand which characteristic mechanism is responsible

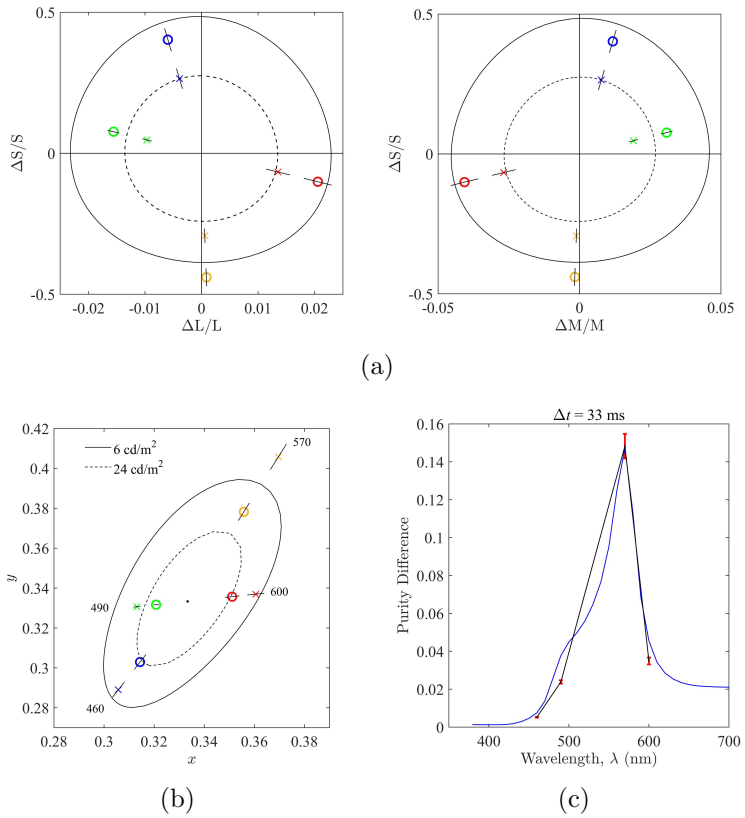

Figure 4.11: For a brief presentation of 30 ms, the detection threshold was improved by an increase in the stimulus luminance from 6.0 (predicted solid contour) to 24.0 cd m^{-2} (predicted dashed contour). (a) The two plots represent the detection data in (ΔS/S, ΔL/L) and (ΔS/S, ΔM/M) cone contrast space. The detection data for 6.0 and 24.0 cd m^{-2} are shown by open circles and cross signs, respectively. (b) The detection data shown in the CIE 1931 xy chromaticity space. (c) The difference between the threshold purity under 6.0 and 24.0 cd m^{-2} is plotted as a function of wavelength. The solid curve shows the predicted difference.

for the noise-limited behavior of color detection, we measured behaviorally the temporal dynamics of human color detection when a target is briefly presented on an equiluminant surround of two luminance levels. We found evidence to support the assumption that fluctuations of a Poisson nature in the postreceptoral stage limit the performance of color detection behavior. The result of this experiment, however, does not reject the possibility that color detection is also influenced by receptoral fluctuation.

The original fluctuation theory of color detection supports "the general deterioration of discrimination with decreasing luminance" (Bouman & Walraven, 1972, p. 501). This prediction is consistent with the behavioral data obtained in some reports (Brown, 1951; Weale, 1951; Thomson & Trezona, 1951), but not consistent with some observations showing an insignificant change of threshold within a wide range of intensity (Bedford & Wyszecki, 1958; Wright & Pitt, 1934). Our model predicts that if the signal to noise ratio in a receptoral channel is approximately constant within a range of light intensity, receptoral noise does not determine a change in threshold by varying stimulus intensity.

Vorobyev and Osorio (1998) argued that source of noise originates in the cone level, and that postreceptoral noise is not independent of receptoral noise because of their neuronal connections. The behavior of color detection shown in Figure 4.9 clearly support the opposite, that noise of Poisson nature cannot be originated at the receptoral level in our experimental condition because stimulation in our experiment does not distort receptoral adaptation. Note that this is not to say that receptoral noise cannot be a source of noise-limiting detection behavior, but the fact that postreceptoral channels receive inputs from receptors does not merely imply that that postreceptoral mechanism is a noise-free encoding system of receptoral signals. Thus, we suggest that an insignificant change in the performance of color detection within a range of stimulus intensity is plausible so long as the receptoral equilibrium is approximately constant. In the case where the receptoral equilibrium is not altered significantly, we suggest that the performance of color detection of brief stimulation is determined by a noise-dominant channel in the postreceptoral stage.

Chapter 5
Chromatic Induction

In this chapter, we aim to investigate, in general, the nature of the chromatic induction, and in particular, the role of retinal adaptation in this visual phenomenon. First, we introduce the fundamental concept, previously proposed mechanisms and rules for the behavior of chromatic induction. Then, we discuss the results of our experiments in the ganzfeld where a small, physically neutral disk aperture is viewed on a large homogenous chromatic spherical surround.

5.1 Introduction

Chromatic induction is a visual phenomenon in which the color appearance of an object is influenced by the presence of neighboring colors (von Helmholtz, 1909/1962; Kirschmann, 1891). This phenomenon is also called simultaneous color contrast to emphasize that the induced color on an infield target is simultaneously present with the surrounding color (Rinner & Gegenfurtner, 2000; Ekroll, Faul, & Niederée, 2004). This phenomenon is illustrated in Figure 5.1. In this figure, the small squares located in a hue circle are identical across quadrants of the plot, but exhibit a hue shift on different colored surround.

Though studied extensively, the mechanisms behind this phenomenon are still not well understood. Early studies suggested that chromatic adaptation

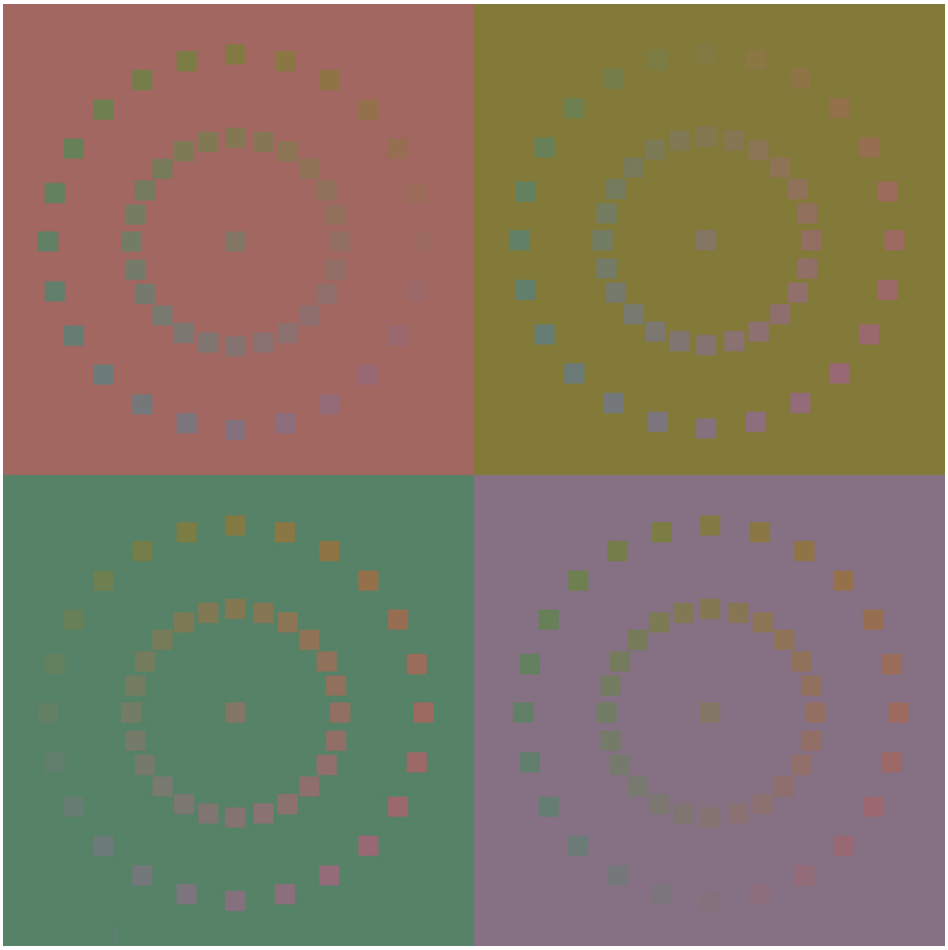

Figure 5.1: In each quadrant of this plot, the small squares in a ring are located in a hue circle of the same saturation. The squares are all physically identical across the four quadrants of the plot. These squares appear differently in color on different surrounds. The change of color appearance is evident when the hue of an individual square changes across the four quadrants of the plot.

(MacAdam, 1956), the root mechanism of color constancy, may underlie the mechanism of color contrast (MacAdam, 1950). According to the von Kries (1904) gain control model, adaptation changes the overall sensitivity of each of the three types of cone cells, i.e. the spectral sensitivity function of each cone is multiplied with a scalar factor ρ_i specific to each cone type $i = L, M, S$. The von Kries (1904) model is taken as a plausible physiological account for color constancy (von Helmholtz, 1909/1962). The notion of von Kries adaptation as an underlying mechanism

of chromatic induction was first rejected by Hurvich and Jameson (1972). The von Kries model predicts that the shift in perceived color for a given surround can be described as a linear transform in color space. Accordingly, the shift in perceived colour, measured in terms of chromaticity coordinates, should be independent of the brightness of the target. According to Hurvich and Jameson (1972), however, the hue shift becomes a function of target luminance, and therefore, the gain model fails to explain color contrast phenomenon. Jameson and Hurvich (1959) suggested a dual-process interpretation, stating that in addition to gain factors, an incremental or a decremental process is required to identify the induced color. As opposed to Jameson and Hurvich (1959), J. Walraven (1976) supported a single-process model based on early-retinal-stage adaptation mechanism. J. Walraven (1976) postulated that the gain model is valid if applied to the difference between test stimulus and background rather than the absolute receptoral response. Walraven's (1976) notion of "discounting the background" was later articulated by Whittle (2003) in terms of Weber cone contrast.

The issue of single-process or dual-process mechanism became a source of controversy (J. Walraven, 1979; Shevell, 1980; Werner & Walraven, 1982). Shevell (1978) rejected Walraven's (1976) notion in favor of Hurvich and Jameson's (1972) dual-process model. An attempt was made by Adelson (1981) to test Walraven's (1976) hypothesis, by locating a red penlight under the lower lid of the eye and letting light of a reddish cast to cover the entire retina. Adelson (1981) tried to satisfy Walraven's condition in an experiment where a complete disappearance of the red cast occurred after one minute of adaptation. In agreement with the dual-process model, surface colors of various intensities shifted differently in Adelson's experiment. Later, Chichilnisky and Wandell (1995) examined different adaptation mechanisms in a dichoptic matching paradigm and suggested that

the receptoral gain mechanism, as a single process model can best explain the induction effect. They also reported an appearance change for incremental and decremental stimuli as evidence for a differential adaptation effect (Chichilnisky & Wandell, 1997) rather than an increment-decrement asymmetry (Niederée & Mausfeld, 1997).

5.2 Problem Statement

The most extant theories of the chromatic induction phenomenon appeal to either early-retinal-stage photoreceptor sensitivity adjustment (J. Walraven, 1976; Chichilnisky & Wandell, 1995), later-stage postreceptoral mechanisms (Krauskopf, Zaidi, & Mandler, 1986) or a combination of both (Shevell, 1978). Ekroll and Faul (2012a) suggested that chromatic induction is determined by local contrast with only a marginal contribution from temporal adaptation. Moreover, some behavioral research on chromatic induction suggested rules on the nature of this phenomenon (Kirschmann, 1891). These rules tend to characterize this visual phenomenon with respect to the physical attributes of a stimulus. These suggested rules themselves, however, became subjects of caveat in other studies (Ekroll & Faul, 2012b; Bosten & Mollon, 2012). Although, behavioral research on color induction has advanced our understanding of the visual mechanism behind this phenomenon, the contribution of receptoral and postreceptoral processes in chromatic induction effect is still not well understood.

In this chapter, we aim to investigate the influence of temporal adaptation on chromatic induction. For our study we sought to create an adapting field that, unlike a computer monitor, could be highly saturated, bright enough, and large enough to fill the entire visual field with no spatial transient information. A

brightly illuminated surround probably facilitates the accomplishment of temporal adaptation (Fairchild & Reniff, 1995). We achieved these conditions by placing the observers head inside a large, opaque hemisphere that could be diffusely illuminated with highly saturated light close to the chromaticity of a spectral color. Our experiment specifically requires a high level of surround saturation. This is because a dual role of surround color became unequivocally pronounced in Shevell's (1978) experiment under the condition of an intense surround. We further discuss this effect in Experiment 5.1. Prolonged exposure to this visual field eliminates any potential influence of pre-adaptation states. Besides, the effect of temporal adaptation through eye movements is further satisfied in the ganzfeld. Thus, we expect that our experimental condition must be dominated by temporal adaptation.

5.3 General Methods

We carried out experiments in a colored ganzfeld of varying saturation at the same luminance. At each saturation level of an inducing surround, we evaluated induced color on a physically neutral, but adjustable, disk of a specific luminance.

5.3.1 Apparatus

We designed an apparatus with a large, opaque hemisphere, the interior of which contained a 3° disk surrounded by a chromatic ganzfeld that filled the remainder of the visual field. This apparatus, as opposed to a monitor display, not only allowed us to fill the observer's entire visual field, but also to obtain a highly saturated surround of high luminance. Figure 5.2(a) shows the structure of the dome apparatus. The surround color is produced by passing light of up to four

500-1000 W Quartz Halogen bulbs through a Roscolux red filter (R19). The red filter and an adjacent neutral filter of approximately the same transmittance were mounted on a large slide that could be moved horizontally past a large rectangular aperture through which light entered the integrating chamber surrounding the dome. Light scattering within the white chamber provides an essentially uniform color on the surround region.

The target consisted of a white patch seen through a disk-shaped aperture, 2 cm diameter, located at the center of the hemispherical background and from a distance of $\sim$ 40 cm (see Figure 5.2(b)). It was seen through a circular aperture that opened into a separate chamber sealed on the backside of the dome. We mechanically controlled the color and luminance of the target disk by two actuators attached to two separate panels that slid perpendicularly to each other in front of a 250 W Quartz Halogen bulb within the tube. The luminance of the target disk could be adjusted by a panel that slid vertically. The color of the target disk was controlled by a horizontal panel with two filters, a red filter of the same surround color and an adjacent dichroic neutral density filter of the same transmittance. This arrangement allowed a constant luminance on the target disk while changing its saturation. A transparent super heat shield was placed between light bulbs and colored filters to protect them at high temperatures.

5.3.2 Procedure

The experiments were conducted in a dark room. After one minute of dark adaptation, observers' heads were placed inside the large opaque hemisphere of the apparatus. They were instructed to have their eyes closed before the lights are turned on. To obtain a substantial completion of temporal adaptation to a chromatic surround (Fairchild & Reniff, 1995), an observer then adapted for 45-60

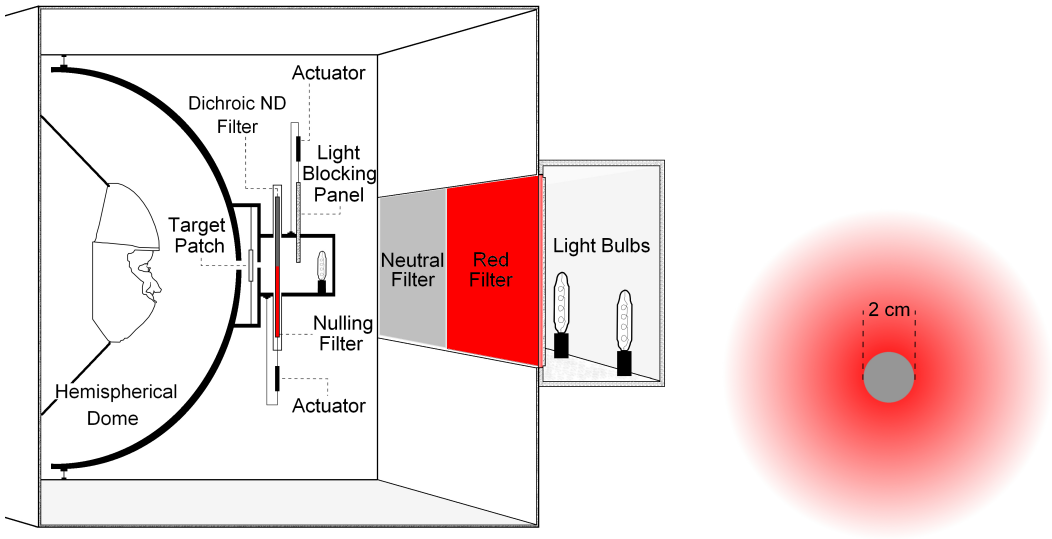

(a) (b)

Figure 5.2: The experiment was performed in a dome apparatus where a small disk aperture is located on a homogenous colored surround of a fixed luminance. (a) The figure shows a side-view diagram of the dome. (b) A 3° small disk surrounded by a uniformly colored ganzfeld with no spatial transition is viewed by an observer.

seconds to a colored surround. After chromatic adaptation, an observer judged and named the color of the surround and the target patch. When the hemisphere was illuminated with red light, it made the physically neutral target appear green, due to chromatic induction. In a nulling task, we measured how much red light needed to be added to the target to make it appear neutral again. The quality of a color stimulus measured by this method is called *color valence*. The observer then changed the disk color to make it appear neutral (neither reddish nor greenish) by operating an actuator that controlled the horizontal movement of the chromatic-neutral filter panel. After the nulling task, observers were asked to describe the color quality and appearance of the neutralized target. Observers' descriptions of the color quality of a neutralized target indicated whether they were satisfied with the gray produced by a nulling task.

We measured the spectral radiance functions of the target and surround with a Photoresearch PR-650 spectroradiometer. The L, M, and S cone quantum absorptions for a color was calculated by multiplying its radiance spectrum by the Smith and Pokorny (1975) cone fundamentals. The MacLeod-Boynton (1979) (r,b) chromaticity coordinates were calculated as r = L/(L+M) and b = k S/(L+M), where the scaling factor k was chosen such that the b-coordinate of equal energy white equals unity.

5.4 Chromatic Induction in the Ganzfeld

We aimed to investigate the influence of temporal adaptation as well as an additive component of the inducing surround on chromatic induction in a spatially uniform center-surround Ganzfeld under the condition of prolonged exposure that highly satisfied von Kries (1904) adaptation.

Experiment 5.1. We hypothesized that an inducing surround exerts an incremental or a decremental component on an induced color, even under a dominant influence from temporal adaptation to surround color.

Participants. A total of 20 undergraduate students (ages 18-24) at Rutgers-Newark volunteered to serve as subjects in order to satisfy a course requirement. All subjects were tested for normal color vision using the Ishihara color plates (Ishihara, 1974). The study was approved by IRB and all subjects received the consent form before participation. To control for the influence of variability across observers, each observer participated in all experimental conditions.

Stimuli. Conditions, in this experiment, included six red surround saturation levels, within a range of 0.736-0.868 in r = L/(L+M) coordinates, all at a luminance of 90 ± 0.44 cd/m^2. The plots in Figure 5.3 represent the chromaticity

coordinates of the surround color. We evaluated induction on four target disk values, including two decremental targets (40, 60 cd m^{-2}), one equiluminant, and incremental target (100 cd m^{-2}). We obtained a total of 480 data points ($n = 20$). Table 5.1 shows the values of the CIE xy 1931 chromaticities and the MacLeod-Boynton (r, b) coordinates (1979) of the surround colors.

Table 5.1: The chromaticity of the physical target patch (2750 Kelvin) and the surround at six levels of saturation ($s1$-$s6$ refer to inducing surrounds with increasing saturation). The table shows the CIE x, y 1931 chromaticity coordinates and the MacLeod-Boynton (1979) (r, b) coordinates.

Chromaticity	Test Target	Surround (Inducer)					
	(2750 K)	$s1$	$s2$	$s3$	$s4$	$s5$	$s6$
x	0.4558	0.5060	0.5323	0.5472	0.5933	0.6380	0.6711
y	0.4096	0.3855	0.3793	0.3708	0.3480	0.3291	0.3148
r = L/L+M	0.7040	0.7358	0.7511	0.7625	0.7989	0.8366	0.8677
b = S/L+M	0.0048	0.0042	0.0035	0.0033	0.0025	0.0015	0.0007

5.4.1 Kirschmann's Fourth Law

Results. We plot in Figure 5.4, the target saturation, r_t value of a neutralized target of a specific luminance level against surround saturation, r_s. As presented in Figure 5.4(a), within-subject t-tests showed that the color valence of the decremental target on the surround with $r_s = 0.86$ was not significantly different from that on either the surround with $r_s = 0.83$ $[t(19) = 1.361, p = 0.189]$ or with $r_s = 0.83$ $[t(19) = 1.091, p = 0.289]$. Likewise, the fall-off observed in Figure 5.4(b) is not significant ($t(19) = 1.196, p = 0.250$; $t(19) = 0.659, p = 0.518$). A 4×6 repeated measures ANOVA was performed on the inducer saturation and target luminance as factors. Both the surround saturation, F(5,95) = 25.82, $p < 0.01$, and the target luminance, F(3,57) = 161.03, $p < 0.01$, had a significant

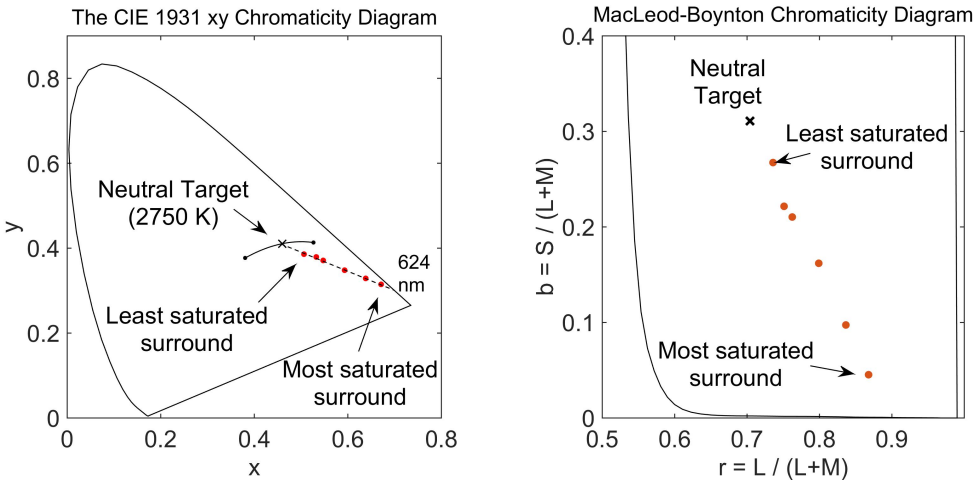

Figure 5.3: A color stimulus involved a neutral target (2750 Kelvin) viewed on a red surround. The figure shows the chromaticity coordinates of the target (2750 Kelvin) and surrounds of different saturations. The luminance of an inducer color was 90 ± 0.44 cd/m^2. (a) The CIE 1931 chromaticity coordinate of the target was approximately located on a line connecting the chromaticities of the least to the most saturated surround. (b) The figure shows the Macleod-Boynton (1979) excitation coordinates of the target and surrounds of six saturation levels.

impact on the induced color. The interaction was also significant, F(15,285) = 11.79, $p < 0.01$.

Discussion. Kirschmann's (1891) fourth law suggests a non-linear relationship between the magnitude of chromatic induction on an equiluminant infield target and the inducing surround saturation.

> "*Der simultane Contrast zwischen einem farbigen Eindrucke und einem Grau von gleicher Helligkeit wächst mit der Sättigung der inducirenden Farbe, jedoch nicht dieser letzteren proportional sondern in geringerem Maße, wahrscheinlich in einem logarithmischen Verhältnisse.*" (Kirschmann, 1891, p. 491)

> "*The level of contrast between a color and a grey of the same lightness grows with the saturation of the inducing field, not proportionally but to a lesser extent, probably in a logarithmic relationship.*" (Bosten & Mollon, 2012, p. 40)

While several authors have supported Kirschmanns fourth law (Valberg, 1974;

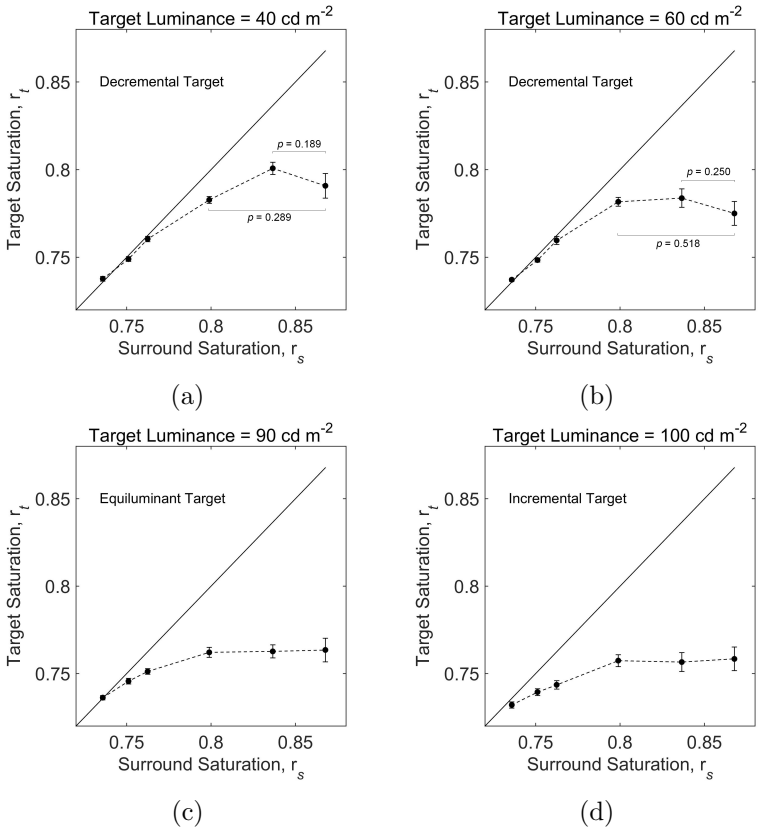

Figure 5.4: The Macleod-Boynton r coordinate of a neutralized target, r_t (t refers to target), is plotted against that of the surround, r_s (surround luminance = 90 ± 0.44 cd/m^2). Data are means $\pm$ SE ($n = 20$). (a) The color valence on a decremental target of $40\,\mathrm{cd\,m^{-2}}$ increases by surround saturation up to $r_s = 0.8366$ and then falls off. (b) The color valence on a decremental target of $60\,\mathrm{cd\,m^{-2}}$ increases by surround saturation up to $r_s = 0.8366$ and then falls off. (c) The color valence on an equiluminant target of $90\,\mathrm{cd\,m^{-2}}$ (d) The color valence in an incremental target of $100\,\mathrm{cd\,m^{-2}}$.

Krauskopf et al., 1986), some research has shown an insignificant effect of background saturation on induced color (Kinney, 1962). Furthermore, Ekroll and Faul (2012b) suggested that induction increases as the surround color approaches the vicinity of the target color. This argument is against Kirschmann's fourth law. Bosten and Mollon (2012) attributed this form of relationship to the method of measurement rather than the nature of the induction phenomenon.

In Figure 5.4, the r coordinate of a neutralized target increases non-linearly

with that of the surround. The Weber cone contrast rule (Whittle, 2003) predicts that different stimuli appear the same on different surrounds when their cone contrasts with their immediate surrounds are the same. The non-linearity in this figure, in conflict with Weber cone contrast prediction, becomes more pronounced at higher surround saturations (r_s <0.76).

Our observation based on a nulling task, shown in Figure 5.4, is in general agreement with Kirschmann's (1891) fourth law, with some limitations. For the two decremental targets (40 and 60 $cd\,m^{-2}$) in Figure 5.4, we also observe a fall-off at higher surround saturations ($r_s > 0.8$). This effect, although non-significant, supports Shevell's (1978) notion of dual role of surround in color induction. Shevell (1978) suggested that the surround color plays a dual role in chromatic induction, a gain control adaptation effect and an additive effect. The former changes the color signals by a multiplicative factor, and the latter alters the color signals by a specific amount. On a very intense red surround, Shevell (1978, p. 1654-1657) (see Figures 6, 8 and 11) observed a reverse effect of surround color on red incremental targets, when his data-points converged to approximately same amount of green added for canceling the induced color towards a unique yellow. If an inducing surround does not exert an additive effect on the target, then the color valence of induction should flatten out at higher surround saturation. The results shown in Figures 5.4(a) and 5.4(b) strongly support this additive effect from an inducing surround. One explanation for this behavior is that the additive contribution from an inducing surround overrides its adaptation-related effect. In Experiment 5.2, we analyze the behavior of induction on a surround of lower saturation when such an additive role is less significant.

Temporal Adaptation

Whittle's (2003) cone contrast rule for chromatic induction is derived from von Kries adaption. The non-linearity shown in Figure 5.4 is in conflict with the Weber cone contrast prediction. If the behavior of chromatic induction at higher surround saturation shown in Figure 5.4 were predicted by the von Kries (1904) mechanism, then the cone excitation ratio of a neutralized target on two different surrounds would be the same regardless of the target luminance. The results presented in Figure 5.5 show a clear violation of this prediction.

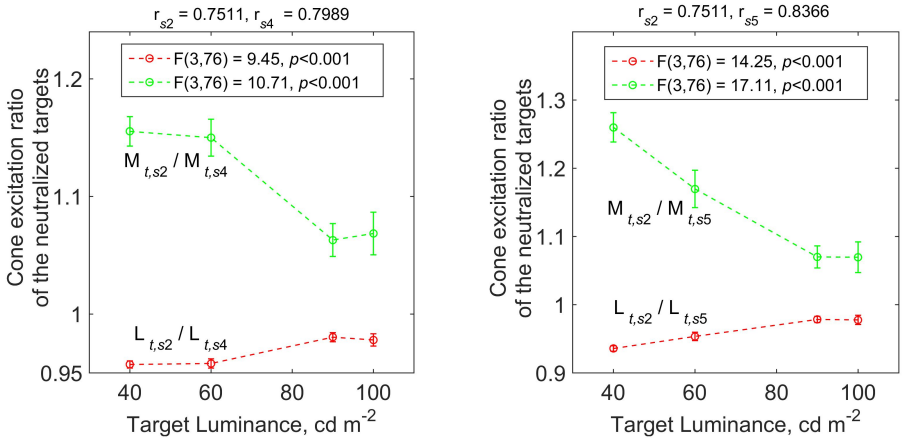

Figure 5.5: The L- and M-cone excitation ratios of a neutralized target on two selected surrounds are plotted as a function of the target luminance. (a) The dotted-lines show the ratio of L-, and M-cone excitations for neutralized targets on the second (r_s=0.7511) and fourth (r_s=0.7989) surround colors. (b) The L- and M-cone excitation ratios of neutralized target on the second (r_s=0.7511) and fifth (r_s=0.8366) surround colors. A one-way ANOVA shows a significant effect of target luminance on the L- and M-cone excitation ratio in both cases.

5.4.2 Kirschmann's Third Law

One of the reasons for rejecting the gain model, as a single mechanism for induction, follows from Kirschmann's (1891) third law, stating that largest induction

effect is at minimum luminance difference between target and background. Here, we analyze Kirschmann's third law.

Results. To investigate the effect of target luminance on color contrast, we plot in Figure 5.6, an r coordinate of a neutralized target against the target luminance value. Each plot in this figure represents the average gray setting made by observers ($\pm$ SE, $n = 20$) on a surround color of a specific saturation shown by r_s, where the subscript s refers to surround. As shown in each of the six plots of Figure 5.6, a one-way ANOVA revealed a significant effect of target luminance on gray setting.

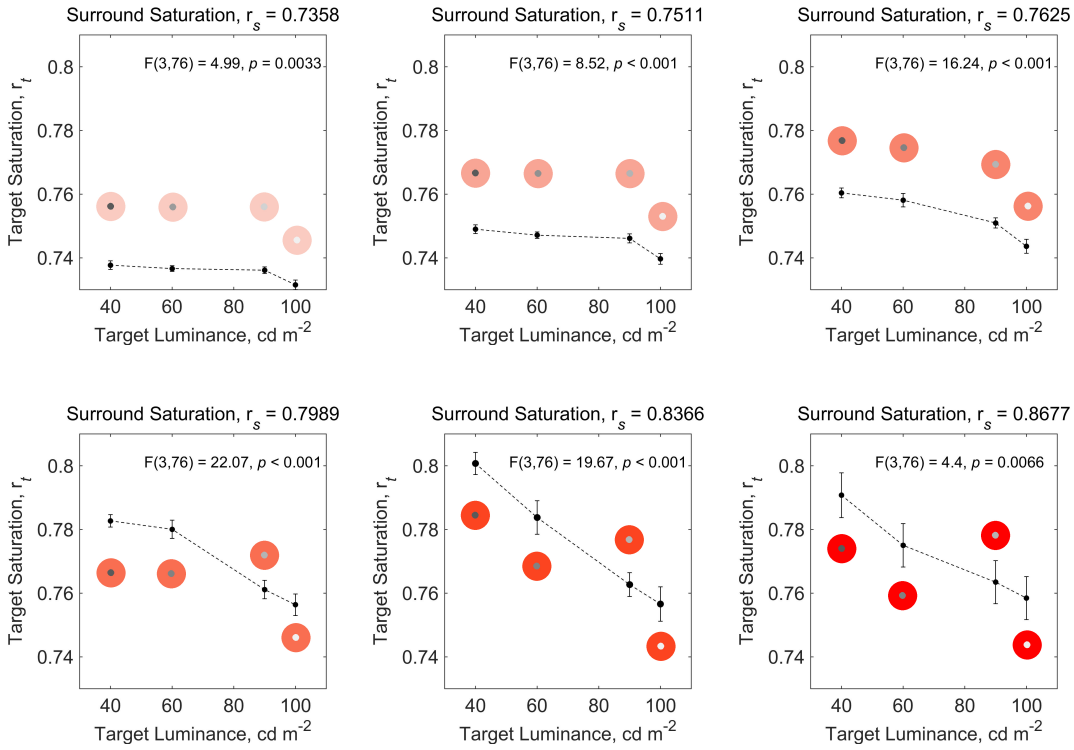

Figure 5.6: The Macleod-Boynton r coordinate of the target, r_t, is plotted as a function of the target luminance. Each plot shows the result of nulling the induced color on a target disk located on one of the six surround saturations. The surround saturation, r_s, varies at six levels at a constant luminance of 90 ± 0.44 cd/m^2. For all of the six surround saturations, the effect of target luminance on the amount of red color added to neutralize the target disk is significant.

Discussion. Consistent with Kinney's (1962) results, we observe that more surround color was needed to null the induced color on a darker target than on a brighter one. The pattern of data shown in this figure, however, does not agree with Kirschmann's (1891) third law or with the results reported by Gordon and Shapley (2006). In Figure 5.6, we observe that the magnitude of induction on a more saturated surround changes at a higher rate with increasing target luminance. Because induction is an effect produced by a colored surround, its strength is expected to be not more than the color added physically to the inducing field. Thus we expect that induction is hardly changed by reducing the luminance of a target on an inducer of low saturation.

5.5 Temporal Adaptation at Lower Levels of Surround Saturation

According to von Kries adaptation, the chromaticity of all targets which look neutral in a given surround should be the same at all luminance levels. Our data presented in Figures 5.6 and 5.4 show clear violations of this prediction, in particular at higher surround saturations.

In Experiment 5.1, however, a complete disappearance of surround color was not reported by all participants, even after several minutes of temporal adaptation to a surround color. Except for the least saturated surround with $r_s = 0.736$, where a majority of (14 out of 20) participants perceived the surround as being white, all of the observers could detect a pinkish-reddish color on an inducing surround in other conditions.

Experiment 5.2. The main goal of the following experiment is to evaluate the behavior of chromatic induction when a complete disappearance of surround is

approximately achieved by temporal adaptation to an inducing surround color. This experiment is in fact an attempt to test Walraven's (1976) notion of "discounting the background" by temporal adaptation to inducers of low saturation.

Participants. A total of 15 undergraduate students, with normal color vision, volunteered to serve as subjects in order to satisfy a course requirement. To control for the influence of variability across observers, each observer participated in all experimental conditions.

Method. The task for the subject is nulling the induced color, with the exact same procedure used in Experiment 5.1.

Stimuli. We carried out an experiment at equiluminant conditions with four surround saturations, within a range of $r_s = 0.709$ - 0.737.

Results. Figure 5.7 shows the magnitude of induction as a function of the surround saturation. The plot also shows the number of participants, from a total of $n = 15$, who detected a tinge of color on an inducing surround after adaptation.

Discussion. For the first three conditions of lowest surround saturation ($r_s < 0.72$), a majority of participants reported no tinge of surround color after adaptation. In this range, the amount of red color required to null the induction is approximately equal to that of a surround and increases linearly with surround saturation. According to von Kries receptoral gain coefficients, the induced color is due to selective changes in the amplitudes of cone sensitivities by adaptation to the stimulation of a surround color. As predicted by this mechanism, Figure 5.7 shows that the magnitude of induction is a linear function of inducer saturation with a gradient of 1 when a complete disappearance of low saturated surround color is obtained by temporal adaptation. This is because, according to von Kries adaptation, targets that appear neutral on a neutral surround should have the same chromaticity as the surround.

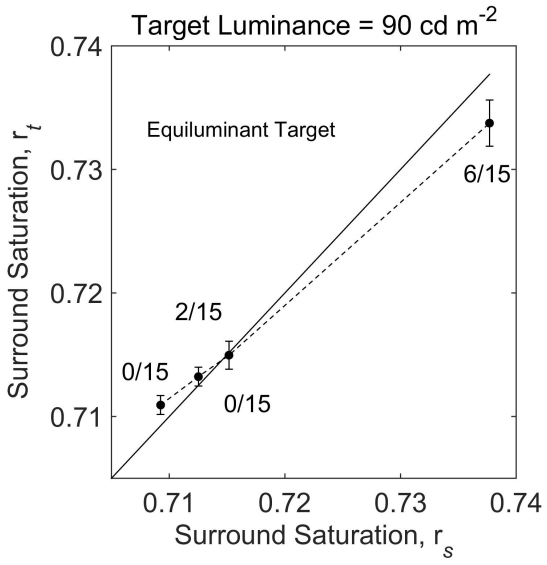

Figure 5.7: The Macleod-Boynton r coordinate of a neutralized equiluminant target, r_t, is plotted against that of a surround, r_s (surround luminance = 90 ± 0.44 cd/m^2). Data are means $\pm$ SE ($n = 15$). The values presented near the data points show the number of participants (out of a total of 15) who detected pinkish-reddish color of a surround after prolonged exposure to the adapting surround.

A slight fall-off is observed in the last condition, $r_s = 0.737$, where 6 out of 15 participants detected a tinge of color on the inducer surround shows that data starts to deviate from linearity at higher inducer saturation (see also Figure 5.4(c)). This probably occurs when the additive effect of surround color significantly exerts its influence on induction. The figure shows that temporal adaptation to surround color with a complete disappearance of surround color is more likely observed at lower inducer saturation. The result of this experiment shows that temporal adaptation does influence chromatic induction. But this observation does not reject a dual role of an inducing surround.

5.6 Dual Color Perception

In Experiment 5.2 where the magnitude of induction was evaluated by a nulling method, a majority of participants were never completely satisfied with the gray obtained on the neutralized target and reported that attempting to null the target may only minimize red and green on the target so that, at the best condition, the target appears both red and green at the same time. The phenomenon of perceiving dual colors or forbidden colors is reported in many studies (Crane & Piantanida, 1983; Brenner & Cornelissen, 1991; Billock, Gleason, & Tsou, 2001; Billock & Tsou, 2010; Livitz, Yazdanbakhsh, Eskew, & Mingolla, 2011). The perception of transparency in induction was proposed by Ekroll, Faul, Niederée, and Richter (2002) to explain this peculiar observation in which a dual color perception is evoked at low contrast, making the nulling task difficult for participants. We illustrate the difficulty involved in the task in Figure 5.8. In this figure, small squares in each column are physically identical, but perceived to be rather different in color on different surrounds. The surround purity increases from the top row to the bottom. In each column, those squares below the diagonal appear bluish while those squares above the diagonal appear yellowish. A dual perception of blue-yellow color becomes somewhat salient around the diagonal where the color of a square approaches the vicinity of the surround color. As illustrated in each row, a nulling method requires adding to a small square some amount of the surround color to make it look achromatic. The difficulty involved in a nulling task is obvious in this illustration.

In a weakly saturated surround of our ganzfeld apparatus, however, the effect of this dual color perception should be minimal in the case of a complete disappearance of surround color. This is because as shown in Figure 5.7, the chromaticity of a target that appears gray becomes equal to that of the surround.

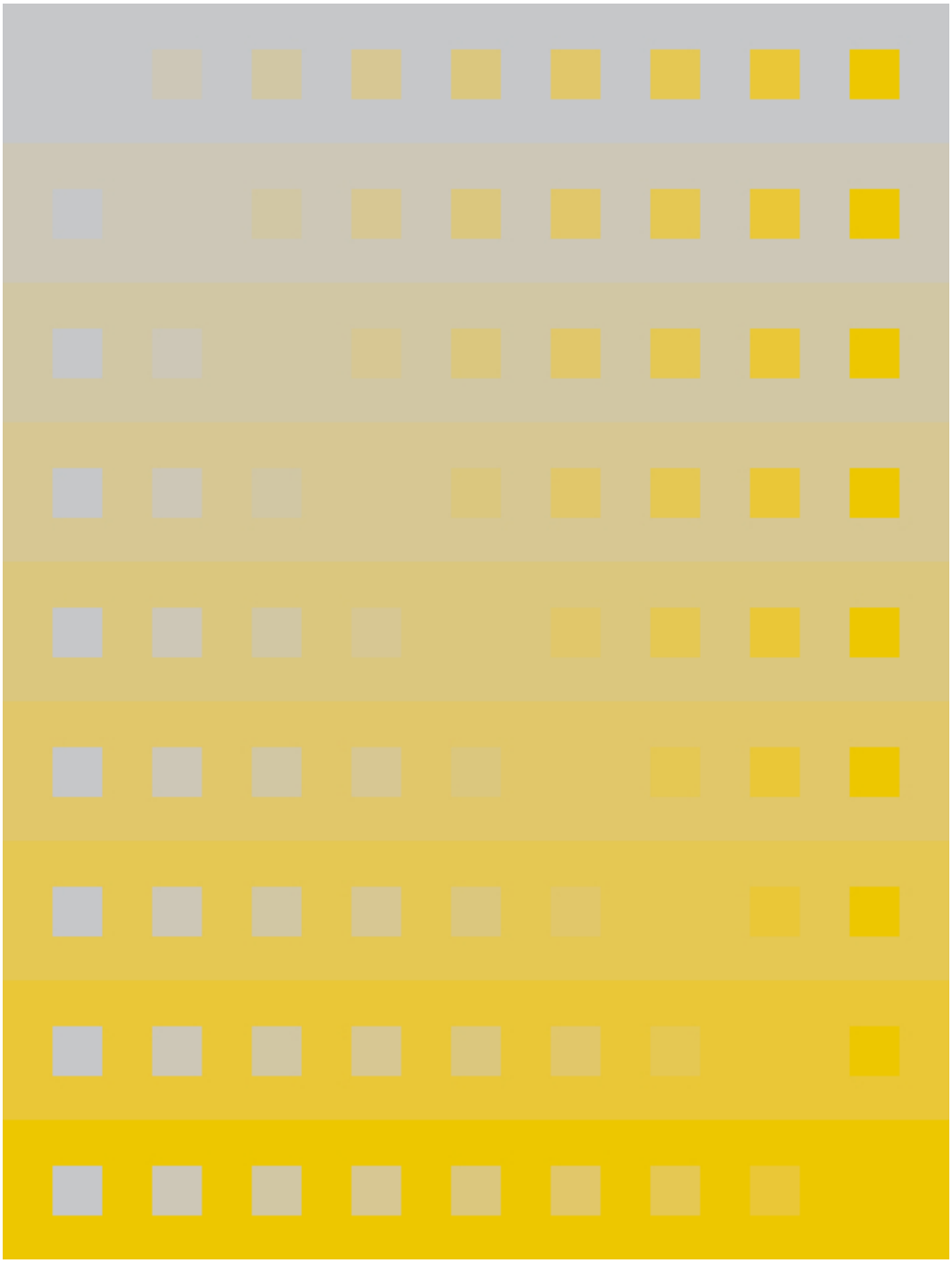

Figure 5.8: Small squares in each column are physically identical, yet rather different in appearance on different surrounds. From the top row to the bottom, the surround purity increases. Perceptual transparency becomes salient around the diagonal where the color of a square approaches the vicinity of the surround color. A nulling method or cancelling technique can be illustrated in each row where subject adds to a small square some amount of the surround color to make the square appear achromatic.

This implies that a gray setting should be less variable at a lower surround saturation. In Figure 5.9, we plot the standard error of the mean of a neutralized target r coordinate, rt, against the surround saturation, rs. We found a significant positive correlation between the standard error of the mean and surround saturation, $r = 0.941, n = 34, p < 0.01$. Consistent with the notion of extension and truncation suggested by Ekroll et al. (2004), when the color of a patch approaches the vicinity of its embedding surround, a greater area of color space encompasses "missing colors" on a more saturated surround. The fall-off behavior of induction as a function of the surround saturation shown in Figure 5.4 could be the result of an attempt made by observers to avoid falling into such extended region of missing colors.

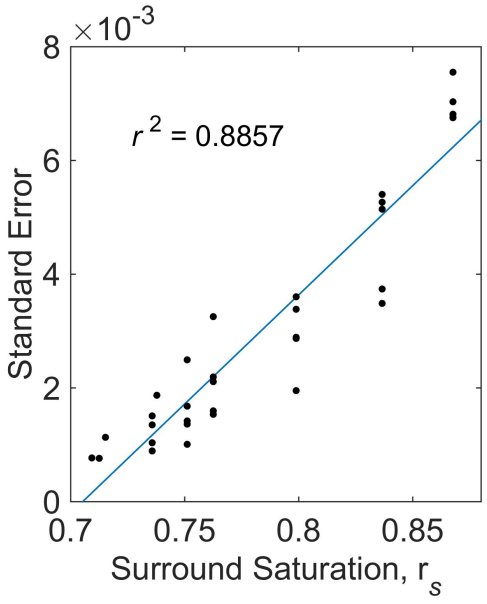

Figure 5.9: The standard error of the mean of the Macleod-Boynton r coordinate for a neutralized target is plotted as a function of the surround saturation, r$_s$. The data are collected from a total of 34 standard errors of gray settings in Experiments 1, 2, and 3. A straight line is fitted to the data ($r^2 = 0.886$).

5.7 Conclusion

We found strong evidence for an additive effect of surround color on an infield target in addition to the temporal adaptation effect. We observed that the color valence of induction non-linearly increases with inducing surround saturation. One explanation for such a non-linear effect is a partial adaptation to surround color. However, this partial discount of surround color cannot fully explain our behavioral data. This is because we observed, in Figures 5.4(a) and 5.4(b), a fall-off for the two decremental targets on a highly saturated surround. Jameson and Hurvich (1959) suggested two-process mechanism for induction, an adaptation-related gain control process and a second incremental-decremental effect of the surround. According to Shevell (1978), surround color can exert either a non-antagonistic or antagonistic effect on an infield target. The latter was supported by a reverse effect of the surround color on induction.

In sum, our behavioral data shows that chromatic induction is influenced by the von Kries (1904) adaptation mechanism. However, von Kries (1904) gain control model does not per se determine the induced color because the surround color exerts an additive effect on the target. Our results show that temporal adaptation does not solely underlie chromatic induction, but plays an essential role in it.

Chapter 6
Summary

In this thesis, we investigated the role of retinal processing in color vision, in particular, the impact of receptoral and postreceptoral noise on color detection and the essential role of temporal adaptation on chromatic induction.

6.1 Photon Absorption

The electrical activity in a retinal photoreceptor is initiated when photons are absorbed by the cell. The actual number of photons absorbed in a cell varies with Poisson fluctuation. This fluctuation introduces a spatial variation in absorption among all the cells and a temporal variation, with repeated exposure, in the number of cells absorbing each specific level of light energy. In Chapter 3, we proposed a model to quantify this spatiotemporal variation. We also quantified the relationship between the two kinds of variations, spatial and temporal, caused by photon fluctuation. The spatial variation in absorption by cone cells implies that visual stimulation by a single color stimulus produces a distribution of responses in cone excitation space. In Section 4.3, we showed that the resulting excitations directly reproduce MacAdam's (1942) variability of color matches in terms of shape, relative size and orientation (Peyvandi & Gilchrist, 2016). Since the model is applicable to both a living and a non-living array of photosensitive elements, we evaluated the performance of the model by a CMOS sensor exposed

repeatedly to a uniformly illuminated color patch (Peyvandi, Ekroll, & Gilchrist, 2017a).

Our findings suggest that spatial fluctuation in absorbed light energy by cells is invariant with respect to the total number of like-type cells from which the histogram is obtained. However, temporal variation with repeated exposure in the proportion of cells at a specific level of absorbed light energy decreases as the spatial variance increases. The model also suggests that the histogram of absorbed energy in like-type individual cells is independent of their spatial dispersion within the sub-mosaic array. Note that this is different from the case when spatial sampling by cone cells is distorted by aliasing (Williams, Sekiguchi, Haake, Brainard, & Packer, 1991), but valid when light radiates uniformly upon the stimulated region.

The temporal variance in the number of cells having absorbed Q units of energy, $var(N_Q)$, depends on the spatial variance and the number of cells from which the distribution is obtained. A possible behavioral consequence of such variation is the perceptual uncertainty in perceived color for small stimuli (Krauskopf, 1964; Hofer, Singer, & Williams, 2005) where color is reconstructed from noisy input signals (Brainard, Williams, & Hofer, 2008). In this case, an excitation falling well beyond the nominal chromaticity gamut might be classified by an observer as an *indescribable* color when neighboring cells receive a very low level of light energy (dark background) (Hofer et al., 2005). When many neighboring cells receive stimulation well above threshold level (dimly illuminated background) (Sabesan, Schmidt, Tuten, & Roorda, 2016), such out-of-gamut colors are possibly very unlikely to occur. Further investigation, however, is required to validate this assumption by direct observation from the human retina.

Variability in the absorptance of individual cones was also observed in microscopic images of the human retina (Roorda & Williams, 1999) which was found to be primarily related to the intrinsic fluctuation in reflectance of photoreceptors (Pallikaris, Williams, & Hofer, 2003; R. F. Cooper et al., 2011). In the digital domain, a CMOS sensor suffers from photo-response non-uniformities and gain variation (Nakamura, 2006). Thus the spatial variation of digital outputs in a sensor is partly attributed to such non-uniformities. We expect that the proposed characterization helps to identify and decompose sources of spatiotemporal variations in a sensor output signals.

6.2 Color Detection

The line-element model, an early attempt to quantify color detection and discrimination behavior, was suggested based on Young-Helmholtz theory of trichromacy in color vision (T. Young, 1802; von Helmholtz, 1909/1962). Over the past decades, researchers performed physiological and behavioral studies to understand the visual mechanisms behind color discrimination and detection judgments. In general, discrimination models assume that either receptoral mechanisms (Stiles, 1964; Trabka, 1968; Wandell, 1985a) or postreceptoral processing (Foster & Snelgar, 1983; Stromeyer et al., 1985, 1992) is responsible for such behavior in color vision. Fluctuation hypothesis for color detection behavior suggests that discriminability judgment is a noise-limited behavior (Bouman et al., 1963). Several studies (Trabka, 1968; Bouman & Walraven, 1972) support detection performance as being limited by receptoral noise in the retina. The fluctuation hypothesis based on receptoral characteristic was criticized in favor of contributions from the postreceptoral stage (Boynton, Ikeda, & Stiles, 1964; Sperling & Harwerth, 1971).

In Chapter 4, we suggested that color detection performance is limited by both receptoral and postreceptoral sources of noise. The original receptoral-noise-based fluctuation model (Bouman & Walraven, 1972) predicts better detection performance at higher stimulus intensities. We showed that within a range of varying stimulus intensity, signal to noise ratio remains approximately constant so long as state of equilibrium is held constant. In this case, we found evidence to support the assumption that fluctuations of a Poisson nature in the postreceptoral stage limit the performance of color detection behavior. We suggested that an insignificant change in the performance of color detection within a range of intensity is plausible when the receptoral equilibrium is not altered significantly by the variation in stimulus intensity.

Vorobyev and Osorio (1998) suggested a receptoral-based model with the assumption of noise source in receptoral level and not in opponent mechanisms. However, color detection behavior from the results of our Experiment 4.3 provided evidence for fluctuation of Poisson nature in the postreceptoral stage. Since the receptoral adaptation was not distorted in this experiment, a change in color detection threshold is not attributable to receptoral fluctuation. We observed that the temporal dynamics of the isoluminant detection threshold represent rapid non-linear decay, converging to an asymptote of threshold at two levels of light intensity. The characteristic of a detection time course supports the assumption that color detection is limited by postreceptoral sources of noise.

6.3 Chromatic Induction

Chromatic induction is a visual phenomenon in which the appearance of an infield target is influenced by neighboring colors. In Chapter 5, we studied a dual influence of an adapting surround on chromatic induction, specifically an adaptation-related role and an additive (incremental) component. We carried out experiments in a simple center-surround stimulus. The difference of our method from previous approach is that we performed experiments in a red ganzfeld, at the center of which was a neutral aperture that appeared green due to the induction effect. Prolonged exposure to this hemispherical visual field creates a condition that is highly influenced by temporal adaptation.

In general agreement with Kirschmann's (1891) fourth law, we found that the induced color increases non-linearly with surround saturation, with a non-significant fall-off at highly saturated surrounds for decremental targets. This non-linearity is in conflict with the Weber cone contrast prediction. We found evidence for a significant contribution of von Kries (1904) adaptation. However, such an early-stage receptoral mechanism per se cannot explain the behavioral data of chromatic induction in our ganzfeld condition, in particular at higher surround saturation. This is because our behavioral data provided support for a dual role of inducing surround color on an infield target. We suggested that temporal adaptation, although essential for chromatic induction, does not determine the non-linearity in induction magnitude. Consistent with a dual-process interpretation (Hurvich & Jameson, 1972; Shevell, 1978), the behavior observed in Experiment 5.1 supports that inducing surround exerts an incremental influence on chromatic induction.

6.4 Significance

Human color perception is a complex process performed through hierarchical mechanisms of the visual system. The color processes in the human brain has been the source of inspiration for developing algorithms in color imaging applications and theorizing process in industrial color management.

The present research involves a fundamental approach to color vision with an aim of understanding the physiological mechanism as well as perceptual processing of the human color vision. Our work has technical importance in imaging applications and fundamental significance in studying human color vision. First, the model suggested in Chapter 3 accounts for the interaction of light with cells, not only in the form of absorption, but also in the form of transmission or reflection. This generality of the proposed model has technical and clinical importance for overcoming limitations in the analysis of microscopic images of the human retina in the case when the light intensity is substantially reduced before reaching the cells. Second, the model involves the parameter of time reflecting the duration for a mechanism to reach the state of equilibrium. The state of equilibrium had not been taken into account in prior models of color detection threshold. Because receptoral and neuronal stages of retinal processing respond to stimulating light with different time duration, this characteristic helps to determine the noise-dominant channel in the retina, and therefore specifies the mechanism that limits the performance of color detection behavior under a given experimental condition. Third, while photon-noise-based temporal variation had not been successfully characterized previously for a population of cells being exposed to light, we succeeded by defining it as the variation in the number of cells at each given energy level. As our approach applies to any array of photosensitive elements, living or non-living, this helps to identify and decompose sources of temporal

variations in the output signals of a sensor. Thus, the model has also technical significance in color imaging applications.

References

Adelson, E. H. (1981). Looking at the world through a rose-colored ganzfeld. *Vision Res.*, *51*(5), 749-750.

Alpern, M., Fulton, A. B., & Baker, B. N. (1987). "self-screening" of rhodopsin in rod outer segments. *Vision Res.*, *27*(9), 1459-1470.

Barlow, H. B. (1956). Retinal noise and absolute threshold. *J. Opt. Soc. Am.*, *46*(8), 634-639.

Barlow, H. B. (1957). Increment thresholds at low intensities considered as signal/noise discriminations. *J. Physiol.*, *136*(3), 469-488.

Bayer, B. E. (July 20, 1976). *Color imaging array.* (US patent 3,971,065)

Baylor, D. A. (1987). Photoreceptor signals and vision. Proctor lecture. *Invest. Ophthalmol. Vis. Sci.*, *28*(1), 34-49.

Baylor, D. A., Nunn, B. J., & Schnapf, J. L. (1987). Spectral sensitivity of cones of the monkey macaca fascicularis. *J. Physiol.*, *390*, 145-160.

Bedford, R. E., & Wyszecki, G. W. (1958). Wavelength discrimination for point sources. *J. Opt. Soc. Am.*, *48*(2), 129-122.

Bhattacharyya, A. (1943). On a measure of divergence between two statistical populations defined by their probability distributions. *Calcutta Math. Soc. Bull.*, *35*, 99-109.

Billock, V. A., Gleason, G. A., & Tsou, B. H. (2001). Perception of forbidden colors in retinally stabilized equiluminant images: an indication of softwired cortical color opponency? *J. Opt. Soc. Am. A*, *18*(10), 2398-2403.

Billock, V. A., & Tsou, B. H. (2010). Seeing forbidden colors. *Sci. Am.*, *302*, 72-77.

Bone, R. A., Landrum, J. T., & Cains, A. (1992). Optical density spectra of the macular pigment in vivo and in vitro. *Vision Res.*, *32*(1), 105-110.

Bosten, K. H., & Mollon, J. D. (2012). Kirschmann's fourth law. *Vision Res.*, *53*(1), 40-46.

Bouman, M. A., Vos, J. J., & Walraven, P. L. (1963). Fluctuation theory of luminance and chromaticity discrimination. *J. Opt. Soc. Am.*, *53*(1), 121-128.

Bouman, M. A., & Walraven, P. L. (1972). Color discrimination data. In D. Jameson & L. M. Hurvich (Eds.), *Handbook of sensory physiology* (Vol. 7/4, p. 484-516). NY: Springer-Verlag.

Bowmaker, J. K. (1981). Visual pigments and colour vision in man and monkeys. *J. Roy. Soc. Med.*, *74*(5), 348-356.

Bowmaker, J. K., Dartnall, H. J., Lythgoe, J. N., & Mollon, J. D. (1978). The visual pigments of rods and cones in the rhesus monkey, macaca mulatta. *J. Physiol.*, *274*, 329-348.

Bowmaker, J. K., & Dartnall, H. J. A. (1980). Visual pigments of rods and cones in a human retina. *J. Physiol.*, *298*, 501-511.

Boynton, R. M., Ikeda, M., & Stiles, W. S. (1964). Interactions among chromatic mechanisms as inferred from positive and negative increment thresholds. *Vision Res.*, *4*(1-2), 87-117.

Boynton, R. M., & Kambe, N. (1980). Chromatic difference steps of moderate size measured along theoretically critical axes. *Color Res. Appl.*, *5*(1), 13-23.

Brainard, D. H. (1989). Calibration of a computer controlled color monitor. *Color Res. Appl.*, *14*(1), 23-34.

Brainard, D. H., Longére, P., Delahunt, P., Freeman, W. T., Kraft, J. M., & Xiao, B. (2006). Bayesian model of human color constancy. *J. Vision*, *6*(11), 1267-1281.

Brainard, D. H., & Stockman, A. (2010). Colorimetry. In M. Bass (Ed.), *OSA Handbook of Optics* (3rd ed., p. 10.1-10.56). NY: McGraw-Hill.

Brainard, D. H., Williams, R. W., & Hofer, H. (2008). Trichromatic reconstruction from the interleaved cone mosaic: Bayesian model and the color appearance of small spots. *J. Vision*, *8*(5), 15.

Brenner, E., & Cornelissen, F. W. (1991). Spatial interactions in color vision

depend on distances between boundaries. *Naturwissenschaften*, *78*(2), 70-73.

Brindley, G. S. (1955). The colour of light of very long wavelength. *J. Physiol.*, *130*(1), 35–44.

Brown, W. R. J. (1951). The influence of luminance level on visual sensitivity to color differences. *J. Opt. Soc. Am.*, *41*(10), 684-688.

Buchsbaum, G., & Goldstein, J. L. (1979a). Optimum probabilistic processing in colour perception. I. Colour discrimination. *Proc. R. Soc. Lond. B Bio.*, *205*(1159), 229-247.

Buchsbaum, G., & Goldstein, J. L. (1979b). Optimum probabilistic processing in colour perception. II. Colour vision as template. *Proc. R. Soc. Lond. B Bio.*, *205*(1159), 249-266.

Burns, S. A., & Elsner, A. E. (1985). Color matching at high illuminances: the color-match-area effect and photopigment bleaching. *J. Opt. Soc. Am. A*, *2*(5), 698-704.

Campbell, C. (1994). Calculation method for retinal irradiance from extended sources. *Ophthal. Physiol. Opt.*, *14*(5), 326-329.

Chaparro, A., Stromeyer, C. F., Chen, G., & Kronauer, R. E. (1995). Human cones appear to adapt at low light levels: Measurements on the red–green detection mechanism. *Vision Res.*, *35*(22), 3103-3118.

Chaparro, A., Stromeyer, C. F., Huang, E. P., Kronauer, R. E., Cole, G. R., & Eskew, R. T. (1993). Color is what the eye sees best. *Nature*, *361*, 348-350.

Chichilnisky, E. J., & Wandell, B. A. (1995). Photoreceptor sensitivity changes explain color appearance shifts induced by large uniform backgrounds in dichoptic matching. *Vision Res.*, *35*(2), 239-254.

Chichilnisky, E. J., & Wandell, B. A. (1997). Increment-decrement asymmetry in adaptation. *Vision Res.*, *37*(5), 616.

CIE. (2004). *Colorimetry*, 3rd edition, CIE Publication 15:2004, Bureau Central de la CIE, Vienna..

Cole, G. R., Hine, T., & McIlhagga, W. (1993). Detection mechanisms in L-, M-, and S-cone contrast space. *J. Opt. Soc. Am. A*, *10*(1), 38-51.

Cole, G. R., Stromeyer, C. F., & Kronauer, R. E. (1990). Visual interactions with luminance and chromatic stimuli. *J. Opt. Soc. Am. A*, *7*(1), 128-140.

Cooper, G. F., & Robson, J. G. (1969). The yellow color of the lens of man and other primates. *J. Physiol.*, *203*(2), 411-417.

Cooper, R. F., Dubis, A. M., Pavaskar, A., Rha, J., Dubra, A., & Carroll, J. (2011). Spatial and temporal variation of rod photoreceptor reflectance in the human retina. *Biomed. Opt. Express.*, *2*(9), 2577-2589.

Costantini, R., & Susstrunk, S. (2004). Virtual sensor design. In *Proc. SPIE* (Vol. 5301, p. 408-419). SPIE.

Cramér, W. (1946). *Mathematical methods of statistics*. Princeton, NJ: Princeton University Press.

Crane, H. D., & Piantanida, T. P. (1983). On seeing reddish green and yellowish blue. *Science*, *221*(4615), 1078-1080.

Crawford, B. H. (1949). The scotopic visibility function. *Proc. Phys. Soc. B*, *62*(5), 321-334.

Dartnall, H. J. A., Bowmaker, J. K., & Mollon, J. D. (1983). Human visual pigments: Microspectrophotometric results from the eyes of seven persons. *Proc. R. Soc. Lond. B Bio.*, *220*(1218), 115-1130.

David, F. N. (1950). Two combinatorial test of whether a sample has come from a given population. *Biometrika*, *37*(1-2), 97-110.

de Groot, S. G., & Gebhard, J. W. (1952). Pupil size as determined by adapting luminance. *J. Opt. Soc. Am.*, *42*(7), 492-495.

Delori, F. C., Webb, R. H., & Sliney, D. H. (2007). Maximum permissible exposures for ocular safety (ANSI 2000), with emphasis on ophthalmic devices. *J. Opt. Soc. Am. A*, *24*(5), 1250-1265.

Demb, J. B., & Brainard, D. H. (2010). Neurons show their true colours. *Nature*, *467*, 670-671.

de Vries, H. L. (1943). The quantum character of light and its bearing upon threshold of vision, the differential sensitivity and visual acuity of the eye. *Physica*, *10*(7), 553-564.

Einstein, A. (1907). Planck's theory of radiation and the theory of specific heat. *Annalen der Physik*, *22*, 180–190.

Ekroll, V., & Faul, F. (2012a). Basic characteristics of simultaneous color contrast revisited. *Psychol. Sci.*, *23*(10), 1246-1255.

Ekroll, V., & Faul, F. (2012b). New laws of simultaneous contrast? *Seeing Perceiving*, *25*(2), 107-141.

Ekroll, V., Faul, F., & Niederée, R. (2004). The peculiar nature of simultaneous color contrast in uniform surrounds. *Vision Res.*, *44*(15), 1765-1786.

Ekroll, V., Faul, F., Niederée, R., & Richter, E. (2002). The natural center of chromaticity space is not always achromatic: A new look at color induction. *PNAS*, *99*(20), 13352-13356.

Eskew, R. T. (2009). Higher order color mechanisms: A critical review. *Vision Res.*, *49*(22), 2686-2704.

Eskew, R. T., Newton, J. R., & Giulianini, F. (2001). Chromatic detection and discrimination analyzed by a bayesian classifier. *Vision Res.*, *41*(7), 893-909.

Fairchild, M. F., & Reniff, L. (1995). Time course of chromatic adaptation for color-appearance judgments. *J. Opt. Soc. Am. A*, *12*(5), 824-833.

Farrell, J. E., Catrysse, P. B., & Wandell, B. A. (2012). Digital camera simulation. *Appl. Opt.*, *51*(4), A80-A90.

Feller, W. (1945). The fundamental limit theorems in probability. *Bull. Amer. Math. Soc.*, *51*(11), 800-832.

Feller, W. (1957). *An introduction to probability theory and its applications* (Vol. 1). NY: John Wiley & Sons.

Field, G. D., Sampath, A. P., & Rieke, F. (2005). Retinal processing near absolute threshold: from behavior to mechanism. *Annu. Rev. Physiol.*, *67*, 491-514.

Foster, D. H., & Snelgar, R. S. (1983). Test and field spectral sensitivities of colour mechanisms obtained on small white backgrounds: Actions of unitary opponent-colour processes? *Vision Res.*, *23*(8), 787-797.

Garaizar, P., Vadillo, M. A., López-de-Ipiña, D., & Matute, H. (2014). Measuring software timing errors in the presentation of visual stimuli in cognitive neuroscience experiments. *PLOS ONE*, *9*(11), e112033.

Geisler, W. (1987). Ideal observer analysis of visual discrimination. In *Frontiers*

of Visual Science: Proceedings of the 1985 Symposium (p. 17-31). Washinton, D.C.: National Academy of Sciences.

Geisler, W. (1989). Sequential ideal-observer analysis of visual discrimination. *Psychol. Rev.*, *96*(2), 267-314.

Geisler, W. (2011). Contributions of ideal observer theory to vision research. *Vision Res.*, *51*(7), 771-781.

Giulianini, F., & Eskew, R. T. (1998). Chromatic masking in the (ΔL/L, ΔM/M) plane of cone-contrast space reveals only two detection mechanisms. *Vision Res.*, *38*(24), 3913-3926.

Goodeve, C. F. (1936). Relative luminosity in the extreme red. *Proc. R. Soc. A-Math. Phy.*, *155*(886), 664–683.

Gordon, J., & Shapley, R. (2006). Brightness contrast inhibits color induction: evidence for a new kind of color theory. *Spatial Vision*, *19*(2-4), 133-146.

Govardovskii, V. I., Fyhrquist, N., Kuzmin, D. G., & Donner, K. (2000). In search of the visual pigment template. *Visual Neurosci.*, *17*(4), 509-528.

Griffin, D. R., Hubbard, R., & Wald, G. (1947). The sensitivity of the human eye to infra-red radiation. *J. Opt. Soc. Am.*, *37*(7), 546–554.

Guild, J. (1932). The colorimetric properties of the spectrum. *Philosophical Transactions of the Royal Society of London A*, *230*(681-693), 149-187.

Haight, F. A. (1967). *Handbook of the Poisson distribution.* NY: John Wiley & Sons.

Hasinoff, S. W. (2014). Photon, Poisson noise. In I. Ikeuchi (Ed.), *Computer Vision: A Reference Guide* (p. 608-610). New York: Springer.

Healey, G. E., & Kondepudy, R. (1994). Radiometric CCD camera calibration and noise estimation. *IEEE Trans. Pattern Anal. Mach. Intell.*, *16*(3), 267-276.

Hecht, S., Shlaer, S., & Pirenne, M. H. (1942). Energy, quanta, and vision. *J. Gen. Physiol.*, *25*(6), 819-840.

Hering, E. (1920). *Grundzge der lehre vom lichtsinn.* Berlin: Springer.

Hering, E. (1964). *Outlines of a theory of the light sense.* Cambridge, MA: Harvard University Press.

Hinshelwood, C. N. (1940). *The kinetics of chemical change.* Oxford: Clarendon Press.

Hoang, Q. V., Linsenmeier, R. A., Chung, C. K., & Curcio, C. A. (2002). Photoreceptor inner segments in monkey and human retina: Mitochondrial density, optics, and regional variation. *Visual Neurosci.*, *19*(4), 395-407.

Hofer, H., Singer, B., & Williams, D. R. (2005). Different sensations from cones with the same photopigment. *J. Vision*, *5*(5), 5.

Hopkinson, G. R., Goodman, T. S., & Prince, S. R. (2004). *A guide to the use and calibration of detector array equipment.* Bellingham, WA: SPIE Press.

Hurvich, L. M., & Jameson, D. (1955). Some quantitative aspects of an opponent-colors theory. II. brightness, saturation, and hue in normal and dichromatic vision. *J. Opt. Soc. Am.*, *45*(8), 602-616.

Hurvich, L. M., & Jameson, D. (1957). An opponent-process theory of color vision. *Psychol. Rev.*, *64*(6), 384-404.

Hurvich, L. M., & Jameson, D. (1972). Color adaptation: Sensitivity, contrast, after-images. In D. Jameson & L. M. Hurvich (Eds.), *Handbook of sensory physiology* (Vol. 7/4, p. 568-581). Berlin: Springer-Verlag.

Ishihara, S. (1974). *Tests for color-blindness.* Tokyo: Kanehara Shuppan Co.

Jameson, D., & Hurvich, L. M. (1955). Some quantitative aspects of an opponent-colors theory. I. chromatic responses and spectral saturation. *J. Opt. Soc. Am.*, *45*(7), 546-552.

Jameson, D., & Hurvich, L. M. (1959). Perceived color and its dependence on focal, surrounding, and preceding stimulus variables. *J. Opt. Soc. Am.*, *49*(9), 890-898.

Jonas, J. B., Schneider, U., & Naumann, G. O. (1992). Count and density of human retinal photoreceptors. *Graef. Arch. Clin. Exp.*, *230*(6), 505-510.

Jonnal, R. S., Kocaoglu, O. P., Zawadzki, R. J., Liu, Z., Miller, D. T., & Werner, J. S. (2016). A review of adaptive optics optical coherence tomography: Technical advances, scientific applications, and the future. *Invest. Ophthalmol. Vis. Sci.*, *57*(9), OCT51-OCT68.

Judd, D. B. (1951). Report of U.S. secretariat committee on colorimetry and artificial daylight. In *CIE Proceedings* (Vol. 1, p. 11). Paris: Bureau Central de la CIE.

Kaiser, P. K., & Boynton, R. M. (1996). *Human color vision.* Washington, DC: Optical Society of America.

Kaplan, E., & Benardete, E. (2001). The dynamics of primate retinal ganglion cells. *Prog. Brain Res.*, *134*, 17-34.

Kinney, J. A. S. (1962). Factors affecting induced color. *Vision Res.*, *2*(12), 503-525.

Kirschmann, A. (1891). Ueber die quantitative verhältnisse des simultanen helligkeits-und farben-contrastes. In W. Wundt (Ed.), *Philosophische studien* (Vol. 6, p. 417-491). Leibzig: Verlag von Wilhelm Engelmann.

Knoblauch, K., & Maloney, L. T. (1996). Testing the indeterminacy of linear color mechanisms from color discrimination data. *Vision Res.*, *36*(2), 295-306.

Knowles, A., & Dartnall, H. J. A. (1977). The photobiology of vision. In H. Davson (Ed.), *The Eye* (Vol. 2B). NY: Academic Press.

Koenderink, J. J., van de Grind, W. A., & Bouman, M. A. (1972). Opponent color coding: A mechanistic model and a new metric for color space. *Kybernetik*, *10*(2), 78-98.

König, A. (1894). Über den menschlichen sehpurpur und seine bedeutung für das sehen. In *Sitzungsberichte der Königlich Preussischen Akademie der Wissenschaften zu Berlin* (p. 577-598). Berlin.

Koskelainen, A., Ala-Laurila, P., Fyhrquist, N., & Donner, K. (2000). Measurement of thermal contribution to photoreceptor sensitivity. *Nature*, *403*(13), 220-223.

Krauskopf, J. (1964). Color appearance of small stimuli and the spatial distribution of color receptors. *J. Opt. Soc. Am.*, *54*(9), 1171.

Krauskopf, J., Zaidi, Q., & Mandler, M. B. (1986). Mechanisms of simultaneous color induction. *J. Opt. Soc. Am. A*, *3*(10), 1752-1757.

Kullback, S., & Leibler, R. A. (1951). On information and sufficiency. *Ann. Math. Statist.*, *22*(1), 79-86.

Kuniba, H., & Berns, R. S. (2009). Spectral sensitivity optimization of color image sensors considering photon shot noise. *J. Electron. Imaging*, *18*(2), 023002.

Lamb, T. D. (1995). Photoreceptor spectral sensitivities: common shape in the long-wavelength region. *Vision Res.*, *35*(22), 3083-3091.

Land, M. F. (2006). Visual optics: The shapes of pupils. *Curr. Biol.*, *16*(5), R167-R168.

Lau, E., & Leo, W. (1948). Über die augenempfindlichkeit an der ultraroten grenze. *Annalen der Physik*, *437*(5-6), 242–255.

Le Grand, Y. (1949). Les seuils différentiels de couleurs dans la théorie de young [color difference thresholds in youngs theory. *Color Res. Appl., 19*, 296-309] (K. Knoblauch (1994), Trans.). *Revue d'Optique*, *28*, 261-278.

Le Grand, Y. (1968). *Light, color and vision* (2nd ed.). London: Chapman & Hall.

Lewis, P. R. (1955). A theoretical interpretation of spectral sensitivity curves at long wavelengths. *J. Physiol.*, *130*(1), 45-52.

Livitz, G., Yazdanbakhsh, A., Eskew, R. T., & Mingolla, E. (2011). Perceiving opponent hues in color induction displays. *Seeing and Perceiving*, *24*(1), 1-17.

Loewenfeld, I. E. (1999). *The pupil: Anatomy, physiology, and clinical applications* (2nd ed.). Boston: Butterworth-Heinemann.

MacAdam, D. L. (1942). Visual sensitivities to color differences in daylight. *J. Opt. Soc. Am.*, *32*(5), 247-274.

MacAdam, D. L. (1950). Loci of constant hue and brightness determined with various surrounding colors. *J. Opt. Soc. Am.*, *40*(9), 589-595.

MacAdam, D. L. (1956). Chromatic adaptation. *J. Opt. Soc. Am.*, *46*(7), 500-513.

MacLeod, D. I. A., & Boynton, R. M. (1979). Chromaticity diagram showing cone excitation by stimuli of equal luminance. *J. Opt. Soc. Am.*, *69*(8), 1183-1186.

Mansfield, R. J. W. (1985). Primate photopigments and cone mechanisms. In A. Fein & J. S. Levine (Eds.), *The Visual System* (p. 89-106). New York: Alan R. Liss.

Maxwell, J. C. (1860). On the theory of compound colours, and the relations of the colours of the spectrum. *Philosophical Transactions of the Royal Society*

of London, *150*, 57-84.

McCluney, W. R. (1994). *Introduction to radiometry and photometry.* Boston: Artech House.

Mielenz, K. D. (1976). Comments on spectrometry nomenclature. *Anal. Chem.*, *48*(7), 1093-1094.

Moon, P., & Spencer, D. E. (1944). Visual data applied to lighting design. *J. Opt. Soc. Am.*, *34*(10), 605-617.

Nagy, A. L., Eskew, R. T., & Boynton, R. M. (1987). Analysis of color-matching ellipses in a cone-excitation space. *J. Opt. Soc. Am. A*, *4*(4), 756-768.

Nakamura, J. (2006). *Image sensor and signal processing for digital still cameras.* FL, USA: CRC Press.

Nicodemus, F. E., & Kostkowski, H. J. (1976). Distribution of optical radiation with respect to position and direction – radiance. In F. E. Nicodemus (Ed.), *Self-Study Manual on Optical Radiation Measurements: Part 1 – Concepts, Chapters 1 to 3* (p. 10-44). Gaithersburg, MD: Natl. Bur. Stand. U.S. NBS Tech. Note 910-1 (National Bureau of Standards).

Niederée, R., & Mausfeld, R. (1997). Increment-decrement asymmetry in dichoptic matching with haploscopically superimposed backgrounds. *Vision Res.*, *37*(5), 613-615.

Nutting, P. G. (1912). *Outlines of applied optics.* Philadelphia: P. Blakiston's Son & Co.

Pais, A. (1979). Einstein and the quantum theory. *Rev. Mod. Phys.*, *51*(4), 863–914.

Pallikaris, A., Williams, D. R., & Hofer, H. (2003). The reflectance of single cones in the living human eye. *Invest. Ophthalmol. Vis. Sci.*, *44*(10), 4580-4592.

Pease, P. L., Adams, A. J., & Nuccio, E. (1987). Optical density of human macular pigment. *Vision Res.*, *27*(5), 705-710.

Peirce, J. W. (2007). Psychophysics software in python. *J. Neurosci. Methods.*, *162*(1–2), 8-13.

Pelli, D. G. (1985). Uncertainty explains many aspects of visual contrast detection and discrimination. *J. Opt. Soc. Am. A*, *2*(9), 1508-1532.

Peyvandi, S., Amirshahi, S. H., Hernández-Andrés, J., Romero, J., & Nieves, J. L.

(2013). Generalized inverse-approach model for spectral-signal recovery. *IEEE Trans. Image Process.*, *22*(2), 501-510.

Peyvandi, S., Ekroll, V., & Gilchrist, A. (2016). *MATLAB codes for the distribution of photon energy among a population of interleaved photoreceptors.* `https://github.com/peyvandi/light-energy-distribution-among-cells`. (retrieved 31 Oct 2016)

Peyvandi, S., Ekroll, V., & Gilchrist, A. (2017a). Characterization of spatiotemporal fluctuation in absorbed light energy by an array of interleaved photosensitive elements. In *Human Vision and Electronic Imaging 2017 Proceedings.* Burlingame, CA.

Peyvandi, S., Ekroll, V., & Gilchrist, A. (2017b). *MATLAB codes for the spatiotemporal variations in a CMOS sensor.* `https://github.com/peyvandi/CMOS-Sensor-Noise`. (retrieved 29 March 2017)

Peyvandi, S., & Gilchrist, A. (2016). Does spatially homogeneous color stimulation produce a single response point within the physiological cone excitation space? In *the 16th annual optical society fall vision meeting.* Rochester, NY.

Pham-Gia, T., Turkkan, N., & Marchand, E. (2006). Density of the ratio of two normal random variables and applications. *Commun. Stat. Theor.*, *35*(9), 1569-1591.

Planck, M. (1900). Zur theorie des gesetzes der energieverteilung in normalspectrum (German) [on the theory of the energy distribution law of the normal spectrum] (D. ter Haar, Trans.). *Deutsche Physikalische Gesellschaft, Verhandlungen*, *2*, 237-245.

Poirson, A. B., & Wandell, B. A. (1990). The ellipsoidal representation of spectral sensitivity. *Vision Res.*, *30*(4), 647-652.

Pokorny, J., & Smith, V. C. (1997). How much light reaches the retina? In C. R. Cavonius (Ed.), *Colour Vision Deficiencies XIII* (p. 491-511). Dordrecht: Kluwer.

Polyak, S. L. (1941). *The retina*. Chicago: University of Chicago Press.

Pridmore, R. W. (2013). Cone photoreceptor sensitivities and unique hue chromatic responses: Correlation and causation imply the physiological basis of unique hues. *PLOS ONE*, *8*(10), e77134.

Rieke, F., & Baylor, D. A. (1998). Single-photon detection by rod cells of the

retina. *Rev. Mod. Phys.*, *70*(3), 1027-1036.

Rinner, O., & Gegenfurtner, K. R. (2000). Time course of chromatic adaptation for color appearance and discrimination. *Vision Res.*, *40*(14), 1813-1826.

Roorda, A., Romero-Borja, F., Donnelly III, W. J., Queener, H., Hebert, T. J., & W., C. M. C. (2002). Adaptive optics scanning laser ophthalmoscopy. *Opt. Express*, *10*(9), 405-412.

Roorda, A., & Williams, D. R. (1999). The arrangement of the three cone classes in the living human eye. *Nature*, *397*, 520-522.

Rushton, W. A. H. (1963). Cone pigment kinetics in the protanope. *J. Physiol.*, *168*(2), 374-388.

Rushton, W. A. H. (1965). Cone pigment kinetics in the deuteranope. *J. Physiol.*, *176*(1), 38-45.

Rushton, W. A. H. (1972). Pigments and signals in colour vision. *J. Physiol.*, *220*(3), 1-31P.

Rushton, W. A. H., & Henry, G. H. (1968). Bleaching and regeneration of cone pigments in man. *Vision Res.*, *8*(6), 617-631.

Sabesan, R., Hofer, H., & Roorda, A. (2015). Characterizing the human cone photoreceptor mosaic via dynamic photopigment densitometry. *PLOS ONE*, *10*(12), e0144891.

Sabesan, R., Schmidt, B. P., Tuten, W. S., & Roorda, A. (2016). The elementary representation of spatial and color vision in the human retina. *Sci. Adv.*, *2*(9), e1600797.

Schnapf, J. L., Kraft, T. W., & Baylor, D. A. (1987). Spectral sensitivity of human cone photoreceptors. *Nature*, *325*, 439-441.

Schrödinger, E. (1920/1970). Outline of a theory of color measurement for daylight vision. In D. L. MacAdam (Ed.), *Sources of Color Science* (p. 134-182). Cambridge, MA: MIT Press.

Shapley, R., Kaplan, E., & Purpura, E. (1993). Contrast sensitivity and light adaptation in photoreceptors or in the retinal network. In R. Shapley & D. M.-K. Lam (Eds.), *Contrast sensitivity* (p. 103-116). Cambridge, MA: MIT Press.

Sharpe, L. T., Stockman, A., Jagla, W., & Jägle, H. (2005). A luminous efficiency

function, $V^*(\lambda)$, for daylight adaptation. *J. Vision.*, *5*(11), 948-968.

Sharpe, L. T., Stockman, A., Knau, H., & Jägle, H. (1998). Macular pigment densities derived from central and peripheral spectral sensitivity differences. *Vision Res.*, *38*(21), 3233-3239.

Shepard, T. G., Swanson, E. A., McCarthy, C. L., & Eskew, R. T. (2016). A model of selective masking in chromatic detection. *J. Vis.*, *16*(9), 3.

Shevell, S. K. (1978). The dual role of chromatic backgrounds in color perception. *Vision Res.*, *18*(12), 1649-1661.

Shevell, S. K. (1980). Unambiguous evidence for the additive effect in chromatic adaptation. *Vision Res.*, *20*(7), 637-639.

Shevell, S. K. (Ed.). (2003). *The science of color* (2nd ed.). Netherlands: Elsevier.

Smith, V. C., & Pokorny, J. (1975). Spectral sensitivity of the foveal cone photopigments between 400 and 500 nm. *Vision Res.*, *15*(2), 161-171.

Smith, V. C., Pokorny, J., & van Norren, D. (1983). Densitometric measurement of human cone photopigment kinetics. *Vision Res.*, *23*(5), 517-524.

Sperling, H. G., & Harwerth, R. S. (1971). Red-green cone interactions in the increment-threshold spectral sensitivity of primates. *Science*, *172*(3979), 180-184.

Stevens, W. L. (1937). Significance of grouping. *Ann. Eugenic.*, *8*(1), 57-69.

Stiles, W. S. (1964). A modified Helmholtz line-element in brightness-colour space. *Proc. Phys. Soc. Lond.*, *58*(1), 87-117.

Stockman, A. (2016). Cone fundamentals. In M. R. Luo (Ed.), *Encyclopedia of Color Science and Technology* (p. 541-546). Elsevier.

Stockman, A., & Brainard, D. H. (2010). Color vision mechanisms. In M. Bass (Ed.), *the osa handbook of optics* (3rd ed., p. 11.1-11.104). NY: McGraw-Hill.

Stockman, A., MacLeod, D. I. A., & Johnson, N. (1993). Spectral sensitivities of the human cones. *J. Opt. Soc. Am. A*, *10*(12), 2491-2521.

Stockman, A., & Sharpe, L. T. (2000a). Cone spectral sensitivities and color matching. In K. Gegenfurtner & L. T. Sharpe (Eds.), *Color vision: from genes to perception* (p. 53-87). NY: Cambridge University Press.

Stockman, A., & Sharpe, L. T. (2000b). The spectral sensitivities of the middle- and long-wavelength-sensitive cones derived from measurements in observers of known genotype. *Vision Res.*, *40*(13), 1711-1737.

Stockman, A., Sharpe, L. T., & Fach, C. C. (1999). The spectral sensitivity of the human short-wavelength cones. *Vision Res.*, *39*(17), 2901-2927.

Stockman, A., Sharpe, T. S., Merbs, S., & Nathans, J. (2000). [42] spectral sensitivities of human cone visual pigments determined in vivo and in vitro. In *Vertebrate Phototransduction and the Visual Cycle, Part B* (Vol. 316, p. 626-650). Academic Press.

Stromeyer, C. F., Cole, G. R., & Kronauer, R. E. (1985). Second-site adaptation in the red-green chromatic pathways. *Vision Res.*, *25*(2), 219-237.

Stromeyer, C. F., Lee, J., & Eskew, R. T. (1992). Peripheral chromatic sensitivity for flashes: A post-receptoral red-green asymmetry. *Vision Res.*, *32*(10), 1865-1873.

Swinehart, D. F. (1962). The beer-lambert law. *J. Chem. Educ.*, *39*(7), 333-335.

Teich, M. C., R., P. P., Vannucci, G., & Breton M. E., W. J., McGill. (1982a). Multiplication noise in the human visual system at threshold: 1. quantum fluctuations and minimum detectable energy. *J. Opt. Soc. Am.*, *72*(4), 419-431.

Teich, M. C., R., P. P., Vannucci, G., & Breton M. E., W. J., McGill. (1982b). Multiplication noise in the human visual system at threshold. 3. the role of non-poisson quantum fluctuations. *Biol. Cybern.*, *44*(3), 157-165.

Thomson, L. C., & Trezona, P. W. (1951). The variations of hue discrimination with change of luminance level. *J. physiol.*, *114*(1-2), 98-106.

Trabka, E. A. (1968). On Stiles' line element in brightness–color space and the color power of the blue. *Vision Res.*, *8*(2), 113-134.

Trezona, P. W. (1983). Luminance level conversions to assist lighting engineers to use fundamental visual data. *Lighting Res. Technol.*, *15*(2), 83-88.

Tukey, J. W. (1949). Moments of random group size distributions. *Ann. Math. Statist.*, *20*(4), 523-539.

Valberg, A. (1974). Color induction: dependence on luminance, purity and dominant or complementary wavelength of inducing stimuli. *J. Opt. Soc. Am.*, *64*(11), 1531-1540.

van de Kraats, J., Berendschot, T. T. J. M., & van Norren, D. (1996). The pathways of light measured in fundus reflectometry. *Vision Res.*, *36*(15), 2229-2247.

van de Velden, A. (1946). The number of quanta necessary for the perception of light of the human eye. *Ophthalmologica*, *111*(6), 321-331.

van Norren, D., & Berendschot, T. T. J. M. (2004). Objective determination of the macular pigment optical density using fundus reflectance spectroscopy. *Arch. Biochem. Biophys.*, *430*(2), 149-155.

van Norren, D., & Vos, J. J. (1974). Spectral transmission of the human ocular media. *Vision Res.*, *14*(11), 1237-1244.

Vingrys, A. J., & Mahon, L. E. (1998). Color and luminance detection and discrimination asymmetries and interactions. *Vision Res.*, *38*(8), 1085-1095.

von Helmholtz, H. (1909/1962). *Handbook of physiological optics.* NY: Dover Publications, Inc. (English translation by Southall J. P. C., from the 3rd German edition, Handbuch der Physiologischen Optik , vol. 1. Voss: Hamburg, 1909)

von Kries, J. (1904). Die gesichtsempfindungen. In W. Nagal (Ed.), *Handbuch der physiologie der menschen* (Vol. 3, p. 109-282). Braunschweig: Druck und Verlag von Friedrich Vieweg und Sohn.

Vorobyev, M., & Osorio, D. (1998). Receptor noise as a determinant of color thresholds. *Proc. R. Soc. Lond. B*, *265*(1394), 351-358.

Vos, J. J. (1972). *Literature review of human macular absorption in the visible and its consequences for the cone receptor primaries.* TNO Report (IZF 1972-17), Institute for Perception, Soesterberg: The Netherlands.

Vos, J. J. (1978). Colorimetric and photometric properties of a 2^o fundamental observer. *Color Res. Appl.*, *3*(3), 125-128.

Vos, J. J., & Walraven, P. L. (1971). On the derivation of the foveal receptor primaries. *Vision Res.*, *11*(8), 799-818.

Wald, G. (1945). Human vision and the spectrum. *Science*, *101*(2635), 653-658.

Walraven, J. (1976). Discounting the background-the missing link in the explanation of chromatic induction. *Vision Res.*, *16*(3), 289-295.

Walraven, J. (1979). No additive effect of backgrounds in chromatic induction.

Vision Res., *19*(9), 1061-1063.

Walraven, P. L. (1966). The fluctuation theory of colour discrimination. In *Studies in perception: dedicated to M.A. Bouman* (p. 1-14). Soesterberg: Institute for Perception RVO–TNO.

Wandell, B. A. (1982). Measurement of small color differences. *Psychol. Rev.*, *89*(3), 281-302.

Wandell, B. A. (1985a). Color measurement and discrimination. *J. Opt. Soc. Am. A*, *2*(1), 62-71.

Wandell, B. A. (1985b, February). *Color measurement and discrimination* (NASA Contractor Report No. 3824). Stanford University.

Warrant, E. J., & Nilsson, D. E. (1998). Absorption of white light in photoreceptors. *Vision Res.*, *38*(2), 195-207.

Watson, A. B., & Yellott, J. I. (2012). A unified formula for light-adapted pupil size. *J. Vision*, *12*(10), 12.

Watterson, G. A. (1974). The sampling theory of selectively neutral alleles. *Adv. Appl. Probab.*, *6*(3), 463-488.

Weale, R. A. (1951). Hue-discrimination in para-central parts of the human retina measured at different luminance levels. *J. physiol.*, *113*(1), 115-122.

Weale, R. A. (1961). Notes on the photometric significance of the human crystalline lens. *Vision Res.*, *1*(1-2), 183-191.

Werner, J. S., & Walraven, J. (1982). Effect of chromatic adaptation on the achromatic locus: The role of contrast, luminance and background color. *Vision Res.*, *22*(8), 929-943.

Whittle, P. (2003). Contrast colors. In R. Mausfeld & D. Heyer (Eds.), *Color perception: Mind and the physical world* (p. 115-138). Oxford: Oxford University Press.

Williams, D. R., Sekiguchi, N., Haake, W., Brainard, D. H., & Packer, O. S. (1991). The cost of trichromacy for spatial vision. In A. Valberg & B. B. Lee (Eds.), *From pigments to perception: Advances in understanding visual processes* (p. 11-22). NY: Plenum Press.

Wright, W. D. (1928-1929). A re-determination of the trichromatic coefficients of the spectral colours. *Trans. of the Optical Society*, *30*, 141-146.

Wright, W. D. (1941). The sensitivity of the eye to small colour differences. *Proc. Phys. Soc.*, *35*(296), 93-112.

Wright, W. D. (1947). *Researches on normal and defective colour vision*. St. Louis: C.V. Mosby.

Wright, W. D., & Pitt, F. H. G. (1934). Hue-discrimination in normal colour-vision. *Proc. Phys. Soc.*, *46*(3), 459-473.

Wright, W. D., & Pitt, F. H. G. (1937). The saturation-discrimination of two trichromats. *Proc. Phys. Soc.*, *49*(4), 329-331.

Wyszecki, G., & Stiles, W. S. (1982). *Color science: Concepts and methods, quantitative data and formula*. NY: John Wiley & Sons.

Young, R. W. (1971). The renewal of rod and cone outer segments in the rhesus monkey. *J. Cell Biol.*, *49*(2), 303-318.

Young, T. (1802). On the theory of light and colors. *Trans. of the Royal Society of London*, *92*, 12-48.

Zhaoping, L., Geisler, W. S., & May, K. A. (2011). Human wavelength discrimination of monochromatic light explained by optimal wavelength decoding of light of unknown intensity. *PLOS ONE*, *6*(5), e19248.